Biblioteca Digital
F C E N - U B A

BIBLIOTECA CENTRAL LUIS F LELOIR
BIBLIOTECA CENTRAL LELOIR
FACULTAD DE CIENCIAS EXACTAS Y NATURALES UBA

Tesis Doctoral

Dinámica de osciladores móviles acoplados con retardos : un enfoque teórico de la formación de segmentos embrionarios

Petrungaro, Gabriela

2018-04-04

Este documento forma parte de la colección de tesis doctorales y de maestría de la Biblioteca Central Dr. Luis Federico Leloir, disponible en digital.bl.fcen.uba.ar. Su utilización debe ser acompañada por la cita bibliográfica con reconocimiento de la fuente.

This document is part of the doctoral theses collection of the Central Library Dr. Luis Federico Leloir, available in digital.bl.fcen.uba.ar. It should be used accompanied by the corresponding citation acknowledging the source.

Cita tipo APA:
Petrungaro, Gabriela. (2018-04-04). Dinámica de osciladores móviles acoplados con retardos : un enfoque teórico de la formación de segmentos embrionarios. Facultad de Ciencias Exactas y Naturales. Universidad de Buenos Aires.

Cita tipo Chicago:
Petrungaro, Gabriela. "Dinámica de osciladores móviles acoplados con retardos : un enfoque teórico de la formación de segmentos embrionarios". Facultad de Ciencias Exactas y Naturales. Universidad de Buenos Aires. 2018-04-04.

EXACTAS UBA
Facultad de Ciencias Exactas y Naturales

UBA
Universidad de Buenos Aires

Dirección: Biblioteca Central Dr. Luis F. Leloir, Facultad de Ciencias Exactas y Naturales, Universidad de Buenos Aires. Intendente Güiraldes 2160 - C1428EGA - Tel. (++54 +11) 4789-9293

Contacto: digital@bl.fcen.uba.ar

Universidad de Buenos Aires
Facultad de Ciencias Exactas y Naturales
Departamento de Física

Dinámica de osciladores móviles acoplados con retardos: un enfoque teórico de la formación de segmentos embrionarios

Tesis presentada para optar por el título de
Doctor de la Universidad de Buenos Aires en el área Ciencias Físicas
por Gabriela Petrungaro

Director de Tesis: Dr. Luis G. Morelli
Consejero de Estudios: Dr. Pablo Mininni
Lugar de trabajo: Instituto de Investigación en Biomedicina de Buenos Aires,
Consejo Nacional de Investigaciones Científicas y Técnicas,
Instituto Partner de la Sociedad Max Planck

Buenos Aires, 2018

Contents

1 Embryonic segment formation **9**

1.1 The vertebrate segmentation clock 11

1.2 Cell mobility in vertebrate segmentation 15

1.3 Coupling delays in Delta-Notch signaling 17

2 Theoretical description of synchronization **19**

2.1 Phase oscillators with instantaneous coupling 20

2.1.1 Mean-field coupling 22

2.1.2 Spatially extended systems 24

2.2 Mobile coupled phase oscilators 25

2.3 Phase oscillators with delays in the coupling 30

2.3.1 Time delays in the mean-field system 31

2.3.2 Spatially extended systems with coupling delays 33

3 Mobile delayed-coupled oscillators **41**

4 Synchronization dynamics of mobile delayed-coupled oscillators **49**

4.1 Spatial phase correlations 51

4.2 Characteristic relaxation time 54

4.3 Dynamical regimes 58

4.3.1 Non-mobile regime 61

4.3.2 Mobile regime 61

4.3.3 Mean-field regime 62

4.4 Discussion 65

5 A new method for the classification of dynamical states **69**

5.1 Distinguishing between states 69

5.2 Phase-difference motifs for classifying dynamical states 77

5.3 Discussion 80

6 Mobility-induced persistent chimera states 83
6.1 Brief intermission on chimera states 83
6.2 Chimera states in the system of mobile delayed-coupled oscillators 89
6.2.1 In-phase chimera states 89
6.2.2 Novel kinds of chimera states: antichimeras and dual-chimeras 91
6.2.3 Chimeras for periodic boundaries 93
6.3 Fraction of chimera states in time 93
6.4 Statistics for chimera states from random initial conditions 96
6.5 Statistics for chimera states from ordered initial conditions 98
6.6 Chimera states with the signal-sending delay 100
6.7 Discussion 101

7 Measures for synchronization timescales 107
7.1 Synchronization dynamics far away from synchrony 107
7.2 Different quantitative measures characterize different synchronization regimes 109
7.3 Effects of mobility on the different synchronization regimes 110
7.4 Relation between the different measures 112
7.5 Discussion 112

8 Summary and outlook 115

A Numerical methods 121

Bibliography 125

List of Figures

1.1 Zebrafish somitogenesis. 10
1.2 The vertebrate segmentation clock. 11
1.3 Delta-Notch coupling. 14
1.4 Local communication synchronizes the oscillations. 15
1.5 Cell mobility in the vertebrate segmentation clock. 16

2.1 Geometric interpretation of the Kuramoto order parameter. . . . 23
2.2 Typical time evolution of the order parameter for a mean-field system as it goes from an initially disordered state to reaching complete synchronization. 25
2.3 Different routes towards synchronization. 27
2.4 Parametric plot of the collective frequency Ω for different values of the coupling strength κ. 31
2.5 Parametric plots of the collective frequency Ω of the in-phase synchronized solutions and $\tilde{\Omega}$ of the antiphase synchronized solutions. 34
2.6 Illustration of the effects of coupling delays on the collective frequency. 35
2.7 Changes in segmentation period in zebrafish embryos are consistent with a delayed coupling theory. 37

3.1 Description of mobility in the one-dimensional lattice. 43
3.2 Description of delayed coupling: outgoing and incoming delays. . . 44
3.3 Illustration of mobile delayed-coupled oscillators in the lattice. . . 45

4.1 Sampled values of the outgoing coupling delay for which we explore synchronization dynamics, and the corresponding collective frequencies Ω. 52
4.2 Time evolution of the spatial phase correlations ρ_d. 53

4.3 Time evolution of the spatial phase correlations $1 - \rho_d$. 55
4.4 The function that determines the onset of non-local behavior $1/f(\kappa, \tau)$, together with $\cos(\Omega\tau)$. 58
4.5 Characteristic time T_c vs. mobility to coupling ratio λ/κ. 59
4.6 Characteristic time T_c vs. coupling delay τ. 60
4.7 Onset of mobile regime. 62
4.8 Onset of mean-field regime. 64
4.9 Order parameter shows erratic behavior in the presence of mobility and coupling delay. 67
4.10 A new route towards synchronization. 68

5.1 Examples of the variety of dynamical states that the system can visit depending on parameters. 70
5.2 Examples of how the strength of incoherence method works for states mixing in-phase and antiphase domains. 73
5.3 Examples of how the local curvature method works for different states. 75
5.4 Order and disorder are characterized by very different phase-difference motifs. 76
5.5 Typical disorder and order parts of the phase snapshots (top panel) and corresponding phase differences (bottom panel). 77
5.6 Phase-difference motifs. 78
5.7 phase-difference motifs allow to identify between a repertoire of dynamical states. 81

6.1 Chimera states 85
6.2 Chimera states with different shapes. 90
6.3 In-phase chimera states. 91
6.4 Anti-chimera and dual-chimera states. 92
6.5 Complete repertoire of dynamical states that the system can visit depending on parameters. 94
6.6 In-phase chimera state for periodic boundaries. 95
6.7 Transient and persistent in-phase chimera states. 95
6.8 Persistent antichimeras and dual-chimeras. 96
6.9 Fraction of dynamical states. 97
6.10 Prepared initial states without disorder. 99

6.11 Mobility induces chimera states from neighboring in-phase and antiphase domains. 100
6.12 Fraction of dynamical states. 102
6.13 Similarity of the statistics of chimera states for τ_{in} and τ_{out} 103

7.1 Definition of different timescales of synchronization. 109
7.2 Dependence of the different measures of synchronization timescales with mobility. 111
7.3 Correlations between synchronization timescales. 112

Resumen

En los sistemas biológicos, las células forman tejidos capaces de realizar tareas complejas, tanto durante el desarrollo embrionario como en organismos multicelulares adultos. Durante el desarrollo, en particular, la formación de estructuras es el resultado de la coordinación de las actividades de muchas células. Un ejemplo paradigmático es el caso de la formación de los segmentos embrionarios precursores de las vertebras, costillas y músculos esqueléticos de la columna en los vertebrados. Estos segmentos se originan en forma secuencial -uno a uno- y periódica, con un ritmo muy preciso. Dicho ritmo está controlado por un reloj biológico, el reloj de segmentación, que depende de manera crucial de la coordinación de oscilaciones genéticas entre muchas células. Se cree que cada una de las células involucradas actúa como un oscilador genético autónomo. La coordinación de las oscilaciones genéticas entre las células se logra por un mecanismo de comunicación local por la vía de señalización Delta-Notch. La complejidad del mecanismo de comunicación, que involucra la síntesis y el transporte de macromoléculas desde y hacia el núcleo y la membrana celular, es muchas veces capturada en los modelos mediante la incorporación de retardos temporales explícitos en los términos de acoplamiento. Por otro lado, a pesar de que el mecanismo de comunicación es local, existe movilidad celular en el tejido que ocasiona que las células intercambien sus vecinos en el tiempo. Los efectos de los retardos temporales y de la mobilidad han sido alternativamente considerados por separado en modelos del reloj de segmentación, mostrando que tienen importantes efectos sobre la dinámica de la sincronización y la formación de los segmentos. Sin embargo, de qué manera la combinación de estos factores afecta a la organización de las células y al funcionamiento del reloj, es una pregunta que aún espera a ser contestada.

En esta Tesis nos enfocamos en el estudio de la interrelación entre la movilidad celular y los retardos temporales que introduce el mecanismo de comunicación, mediante un enfoque teórico basado en el estudio de sistemas de osciladores acoplados que incorporan estos dos elementos del sistema biológico. En una primera parte nos centramos en el análisis del tiempo que requiere el sistema para alcanzar un estado de sincronización global, en el que todos los osciladores evolucionan con la misma fase y frecuencia. Encontramos que la movilidad es capaz de acelerar la sincronización, aún cuando el acoplamiento es retardado. Mostramos que la movilidad junto con los retardos temporales deter-

minan distintos regímenes dinámicos que gobiernan la evolución del sistema en su camino hacia la sincronización. En una segunda parte, estudiamos patrones espaciotemporales intrigantes que aparecen espontáneamente en el sistema estudiado. Dichos patrones, conocidos como Estados Chimera, consisten en uno o más grupos de osciladores sincronizados que coexisten en el mismo estado con otros que evolucionan asincrónicamente. Al ocurrir en sistemas de osciladores idénticos, representan un ejemplo paradigmático de ruptura de simetría. A pesar de la diversidad de sistemas en los que aparecen, comprender los mecanismos por los cuales se forman los estados Chimera resulta uno de los grandes desafíos actuales en el campo de los sistemas dinámicos. En este trabajo encontramos un mecanismo novedoso de formación de estados Chimera, como consecuencia de la interacción entre la movilidad de los osciladores y los retardos temporales en el acoplamiento. Desarrollamos un método capaz de distinguir estos estados frente a una variedad de otros estados dinámicos del sistema y lo utilizamos para caracterizar los estados observados. El método desarrollado permite identificar otros tipos de estados chimera que no habían sido reportados hasta el momento. Nuestros hallazgos sugieren que los estados chimera podrían ser observados en sistemas naturales donde la movilidad de los osciladores y los retardos temporales en la comunicación ocurren conjuntamente como por ejemplo el reloj de segmentación.

Dynamics of mobile delayed-coupled oscillators: a theoretical approach to embryonic segment formation

Abstract

In biological systems, cells form tissues that can perform complex functions both during development and in adult multicellular organisms. During embryonic development, in particular, pattern formation relies on the coordination of the activities of many cells. A paradigmatic example is the formation of the repetitive and segmented structures characteristic of vertebrates body axis. These structures form during embryonic development one by one, with a very precise rhythm. The rhythm is controlled by a biological clock, known as the *vertebrate segmentation clock*, which relies on the synchronization of cellular oscillators. It is thought that each cell in the tissue acts as an autonomous genetic oscillator. A local cell-cell communication mechanism couples the dynamics of neighbouring cells and gives rise to synchronization. The complexity of the local communication mechanism, which involves synthesis and transport of signalling macromolecules, can be captured in theoretical models by including coupling delays in the equations. Interestingly, although communication is local, cells move through the tissue and thus exchange neighbours over time. Although it is known that delays in communication and mobility distinctly affect oscillatory dynamics, it is not know in which way the interplay between these two features is affecting synchronization and pattern formation.

In this Thesis we address this question through a theoretical approach, consid-

ering a description based on coupled oscillators that includes both coupling delays and mobility of the oscillators. We present the theoretical description in Chapter 3, after introducing the key elements of the biological system in Chapter 1 and its theoretical counterparts in Chapter 2. We develop numerical methods to find solutions to the problem of mobile oscillators in the presence of coupling delays. The development of these methods constitutes an important part of this work and could be potentially employed to solve similar problems.

We analyse different aspects of the dynamics of the system of mobile delayed-coupled oscillators. When possible, we combine numerical simulations with analytical calculations. We first focus on the dynamics of the system near synchronized solutions, Chapter 4. We find that mobility can speed up synchronization in the presence of coupling delays, driving the system into distinct dynamical regimes that are modulated by the coupling delay. We next study intriguing spatiotemporal patterns that spontaneously arise in the system with coupling delays and mobility, Chapters 5 and 6. These complex patterns, known as *Chimera states*, consist of domains of synchronized oscillators that coexist with other domains of asynchronous oscillators within the same state. Despite the diversity of systems where they appear, understanding the mechanisms of formation of chimera states represents one of the current challenges in the field of dynamical systems. Our findings provide a new mechanism for their formation as a result of the interplay between mobility and coupling delays. We find that the system exhibits a wide repertoire of dynamical states in addition to chimera states and develop a method capable of distinguishing between them. The devised method allows to identify novel kinds of chimera states previously unreported. To finish with, we go back to synchronization dynamics and timescales in Chapter 7.

Agradecimientos

A Luis, por todos estos años de infinito trabajo y aprendizaje. Por la confianza y las oportunidades brindadas. Por transmitirme su forma de pensar y encarar los problemas. Por contagiarme su admiración y motivación por la biología. Por su enorme calidad humana.

To Koichiro, for his huge commitment and dedication to the work we do together, for always being available and being so kind, for keeping awake late for our Skype meetings.

A Cherno, que dirigió mi beca los primeros años, por el apoyo y la oportunidad brindada.

A Pablo, por ser mi consejero de estudios y tomarse ese rol en serio, estando siempre disponible para charlar.

A las y los *Morellis* (nunca pudimos ponerle otro nombre al grupo), Diego, Sol, Fiore e Ivan, porque simplemente no podría pedir mejores compañeros y porque hoy son grandes amigos. Un agradecimiento especial para Ivancho, con quien compartimos el doctorado desde el día 0, y a quien le debo muchos "20 pesitos". A Nati, que no es del grupo pero casi, por los cronogramas que tanto ayudaron en esta última etapa. A Gaby, Dani, Martín, Lu, Cora, Atto, Tomi y Walter, y al resto de los que hacen ese gran lugar llamado *Becarios*. A toda la comunidad del IBioBA, que además de tener excelentes científicos tiene excelentes personas, que hacen que el Instituto sea un lugar en el que es lindo trabajar.

A los docentes del área de los que aprendí mucho, en especial a Gabo Mindlin, Alberto Kornblihtt y Fernando Peruani.

Al Centro de Simulación Computacional para Aplicaciones Tecnológicas (CSC) y a la supercomputadora TUPAC[1], donde corrieron la mayor parte de las simulaciones de esta Tesis.

[1] http://www.csc-conicet.gob.ar/la-presidenta-de-la-nacion-inauguro-la-supercomputadora-tupac-en-el-csc/

Al CONICET y a todos los argentinos que pagaron mi beca doctoral.

A la Universidad pública y gratuita que me forma hace más de 10 años.

Al proyecto nacional $2003 - 2015$, por poner a la ciencia en el centro de la escena política y de la ciudad. Por el flamante Polo Científico y Tecnológico en el que pasé estos últimos años de doctorado. Porque ninguna actividad se desarrolla por fuera del contexto político en el que se enmarca. A la organización social y política *El Hormiguero*, y a la hermosa gente que la hace, porque con ellos aprendí a involucrarme en ese contexto.

A todos los que se subieron conmigo a la montaña rusa de emociones que fue el doctorado. Por hacer que las subidas sean más altas, las caídas menos empinadas y los rulos mucho más divertidos.

Empiezo por el historico y eterno *es-importante*, hermanos de la vida que siguen siendo lo mejor que me dio la física. A Nahue, Juli, Fede, Sabri, Mechi, Marian, NA, Mario, Ioni, PP, Fer, Ari, Vir, Alo. Por los asados y Giribones compartidos y por los futuros asados en todas las sedes del mundo.

A mis amigas, por existir. En especial a Caro, Virgi, Pau, Deby, Magu, Maru, Silvi, Estefi, Pau S.

A la vecindad de Superi, Dani, Sofi y Juan. Por trascender el vínculo meramente vecinal y estar en tantos momentos.

Al equipo de natación de Chacarita, donde descargué infinitos días cargados de doctorado para volver a alinear los patitos. A Edu. A Juli y a Jime. A Estefi otra vez. A Clelia, que me ayuda con los patitos que la natación no puede.

A mi familia, por todo el apoyo. A mi abuela, por las risas y la complicidad de siempre. Por las velitas prendidas desde el primer examen hasta el último. A Nico, mi Hermano, por estar siempre cerca. Por seguir creciendo juntos y compartiendo la vida. A mis viejos, por bancarme en todas. Por todo lo que hacen para que yo pueda hacer lo que me gusta. Porque todo lo que pueda decir es poco.

Glossary of terms

Variables and parameters

θ_i phase state of oscillator i

N total number of oscillators in the system

ω autonomous frequency for phase oscillators

Ω collective frequency for in-phase synchronization

$\tilde{\Omega}$ collective frequency for anti-phase synchronization

Abbreviations

PSM Pre-somitic Mesoderm

NICD Notch Intracellular Domain

MF Mean-field

NN Nearest-neighbors

ODE Ordinary differential equation

DDE Delayed differential equation

Chapter 1

Embryonic segment formation

The vertebrate body is endowed with a repetitive structure of segments. The best example of such structure is the vertebral column, composed by many segments that can range from about ten vertebrae in frogs to more than three hundred in snakes [1]. Vertebrate segments originate during embryonic development in a rhythmic and sequential way, in a process termed somitogenesis [2]. The formed segments are called somites, and are composed of packed mesodermal cells that will later give place to vertebrae, ribs and skeletal muscle. Somites are formed one by one, from the anterior tip of an unsegmented tissue called the presomitic mesoderm (PSM), while the tissue elongates, Figure 1.1. Defects in somitogenesis lead to congenital birth defects [3, 4].

Somites are formed with a very precise rhythm. This rhythm varies between species, ranging from about 25 minutes in zebrafish [5] to five hours in humans [6]. Rhythmic somite formation naturally introduces the idea of a biological clock. A paradigmatic conceptual scheme for translating the temporal rhythm into a spatial pattern of structures was proposed by Cooke and Zeeman in 1976 [7]. In this scheme, a clock of unspecified nature operates in the cells of the PSM in a coordinated manner to generate coherent oscillations at the tissue level. While these oscillations take place, a wavefront travels across the tissue from anterior to posterior with a velocity v. The wavefront freezes the oscillations generated by the clock as it passes by, leaving behind a fixed periodic pattern in space formed by the state of the oscillations at different time points. This pattern can be thought to precede the pattern of segments. Biochemical processes would then read the pattern and determine the somite boundaries from it [8, 9]. The relationship

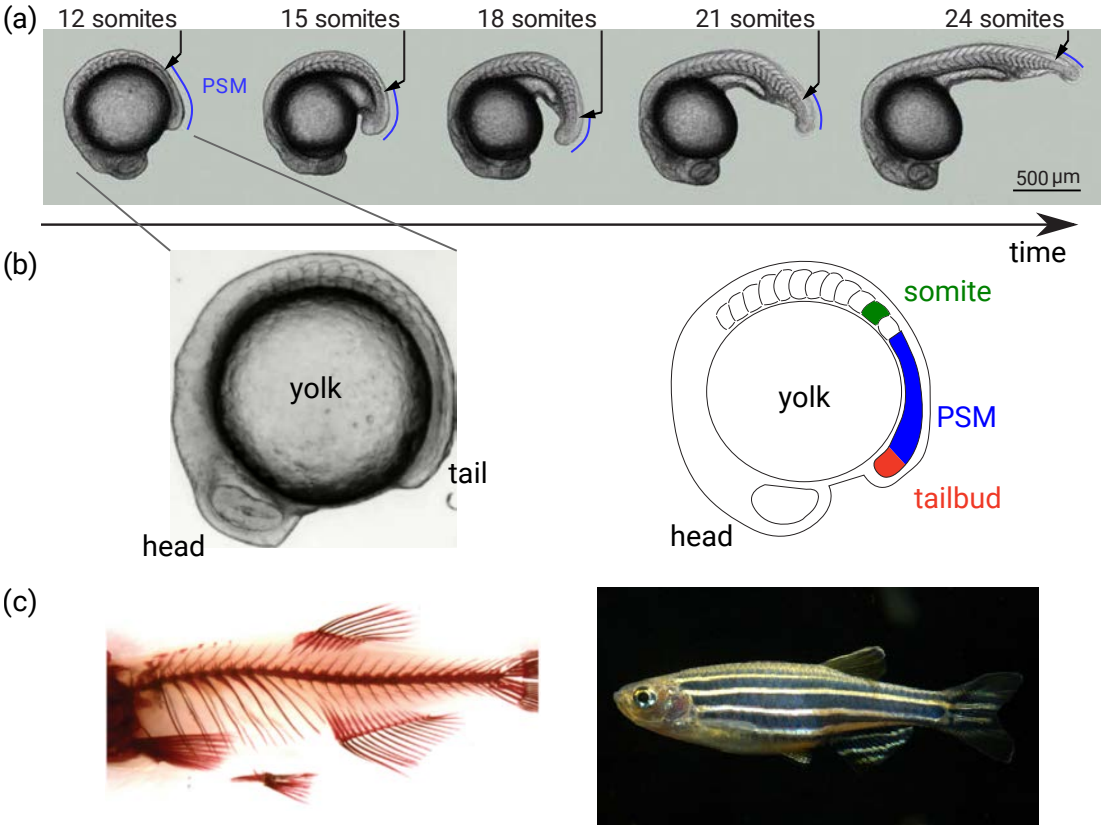

Figure 1.1: (a) Lateral view of zebrafish somitogenesis. Somites form sequentially from the anterior tip of the presomitic mesoderm (PSM, blue) with a very precise rhythm. (b) Zoom of the embryo laying on top of the yolk of the egg (left panel), and a drawing of it (right panel). In the drawing, one of the formed somites is marked in green, PSM is blue and the most posterior part of the PSM (tailbud) is marked red. (c) An adult zebrafish. The adult body has a segmented structure (left panel) and measures about 3cm (right panel). Figure adapted from several references of A. Oates lab.

between the characteristic timescales of the clock and the wavefront sets the size of the segments $S = vT$. Thus, according to this scheme the period of the clock T has the functional relevance of determining key morphological properties of the forming embryo, like the number of segments and their size [1]. For example, for a fixed wavefront velocity, a slow clock with a larger period results in larger segments while a fast clock determines smaller segments [1]. But what is this clock and what generates its rhythm?

Whatever the properties of the clock are, it needs to attain precision, as the morphological properties of the embryos are properly conserved among individ-

[1] Simulation of the Clock and Wavefront mechanism. https://youtu.be/gwtLL29bfnE

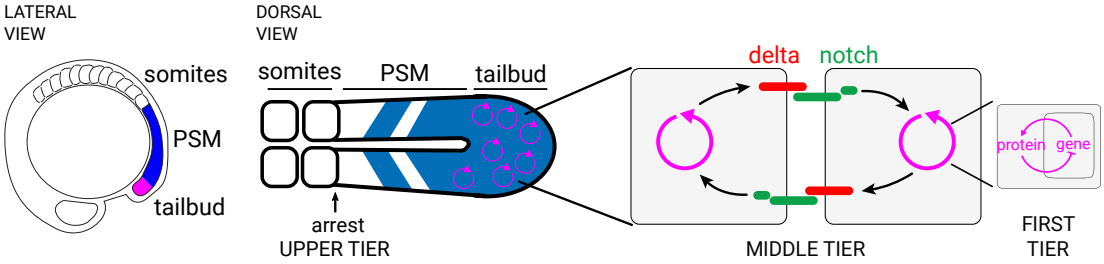

Figure 1.2: The vertebrate segmentation clock. From right to left: the three levels of organization. Each cell in the zebrafish PSM acts as an autonomous genetic oscillator. Genetic oscillations in neighboring cells are synchronized by Delta-Notch coupling. Oscillations are arrested at the anterior tip of the PSM where somites are formed. Figure adapted from [10] and [18].

uals in each species. To these days, there is huge experimental evidence that supports the idea of a real biological clock working in the PSM. This clock, known as the vertebrate segmentation clock, consists of a complex network of oscillating genes that can generate and sustain a collective rhythm at the tissue level [4, 6, 10–12].

In the remaining of this chapter, we introduce the key elements from the biology of the vertebrate segmentation clock that motivate this Thesis. Next, in Chapter 2, we will explain how these elements can be incorporated in theoretical descriptions of the biological clock.

1.1 The vertebrate segmentation clock

Oscillating gene expression within the PSM has been observed during somitogenesis in several species, first by *in-situ* hybridization experiments [13] and more recently by live-imaging with fluorescent reporters [14–17]. These molecular oscillations at the tissue level have the same rhythm as somite formation, suggesting that they regulate the period of somitogenesis [17]. In the PSM, molecular oscillations form waves of gene expression that travel from posterior to anterior. In the most posterior part of the tissue, called the tailbud, uniform synchronized oscillations are observed [17].

The vertebrate segmentation clock is thought to be a population of coupled genetic oscillators that locally synchronize their oscillations by means of intercellular communication [10]. In all species examined, oscillating genes include genes from the Hes/Her family [19]. Proteins of the Hes/Her family regulate their own

production by inhibiting their own transcription. This negative feedback loop at the transcription level strongly suggest that there are autonomous oscillations at the single cell level [20–23]. In zebrafish, autonomous oscillations in single cells have recently been observed experimentally [24]. In this experiment, individual cells belonging to the tailbud of a transgenic reporter line for the cyclic transcription factor Her1 were isolated and recorded in vitro. Single cells were observed to sustain autonomous oscillations in the protein concentration for several periods. Nevertheless, oscillations at the single cell level are noisy and their period does not coincide with the period of segment formation. This highlights the importance of intercellular communication for setting the precise collective period of the clock, as uncoupled single cell oscillations are not sufficient.

The current knowledge of the vertebrate segmentation clock can be organized in a framework of three levels of organization or *tiers* [10]. In a first tier, autonomous oscillations are produced in each cell in the PSM. In a middle tier, oscillations are coupled by intercellular communication. In an upper tier, arrest of the oscillations at the anterior tip of the PSM is thought to be controlled by long-length scale gradients of growth factors such as FGF and Wnt [25–27]. A schematic representation of this current knowledge about the vertebrate segmentation clock organization in zebrafish is shown in Figure 1.2. In this Thesis we focus on the dynamics of the cells in the tailbud. In that region, oscillations are homogeneous among the cells, without travelling waves, and in addition there is high cell mobility, see Section 1.2. We are interested in the interplay between intercellular communication, the middle tier, and cell mobility within that region. We will not consider arrest of the oscillations at the anterior nor the details of autonomous oscillations in individual cells in our descriptions.

Intercellular communication between PSM cells occurs through Delta-Notch signaling [28, 29]. Delta-Notch signalling is a well-studied cell-cell communication pathway, with many functions in development and disease [30, 31]. Depending on the context, this signalling pathway can attain very different functions [30]. For example, it plays a role in stem cells [32, 33] and in determining cell fate via *lateral inhibition* [34, 35]. In vertebrate segmentation, Delta-Notch pathway plays a different role [28, 29], as we describe below. The key elements of the pathway are Delta and Notch transmembrane proteins, that allow signaling between neighboring cells when they bind. In brief, intercellular communication via Delta-Notch pathway occurs as illustrated in Figure 1.3. Before the interaction,

ligands need to be synthesized and exported to the cell membrane. Importantly, Delta ligands are encoded by genes that are repressed by the same transcription factors that control the autonomous oscillator feedback loop. Delta is transcribed in the nucleus of the cell and the mRNA is exported to the cytoplasm, where it is translated. The protein is then subjected to post-translational modifications and exported to the cell membrane, where it shows up as an active ligand for Notch receptors in the neighboring cell. When Delta ligands in the membrane of this signal-sending cell contact Notch receptors in the membrane of a close cell, a cascade of signaling events starts. Pretty amazingly, endocytosis of the Delta ligand in the signal-sending cell mechanically pulls from the bound Notch receptor, exposing a site in the receptor for its cleavage. The Notch intracellular domain (NICD) is thus cleaved and translocates to the nucleus where it positively regulates the transcription of target genes from the autonomous oscillator such as Hes/Her. Notch is not required for the basal production of Her/Hes genes but it does influence their transcription. In this way, the oscillator in each PSM cell drives the activation of the Notch pathway in the neighboring cells, and this activation in turn affects the autonomous oscillator in these neighboring cells. Thus, Notch signaling couples the dynamics of the autonomous oscillators in neighboring cells.

It is known that coupling in systems of noisy oscillators can lead to synchronization [36]. Indeed, there is very strong evidence indicating that the essential function of Delta-Notch signaling in somitogenesis is to locally synchronize the oscillations [10, 37–41]. For example, the mentioned experiments with live-imaging and single-cell resolution that show local in-phase synchronization for neighboring cells in wildtype embryos, show desynchronized oscillations in mutants with loss-of-function of Notch signalling [16]. Besides, synchronization provides a collective rhythm at the tissue level that is less noisy than the oscillations in single cells [24].

The key role of Notch signaling in keeping synchronized the noisy single cell oscillations can be tested by perturbing the coupling. Experiments that temporary inhibit Notch pathway with chemicals consistently show that inhibition at the beginning of segmentation leads to a gradual loss of coherence reflected in defects in the segments. Coherence and correct pattern formation can be rescued by washing out the inhibiting chemicals [38]. The timescales of synchronization and desynchronization can be translated into positional information

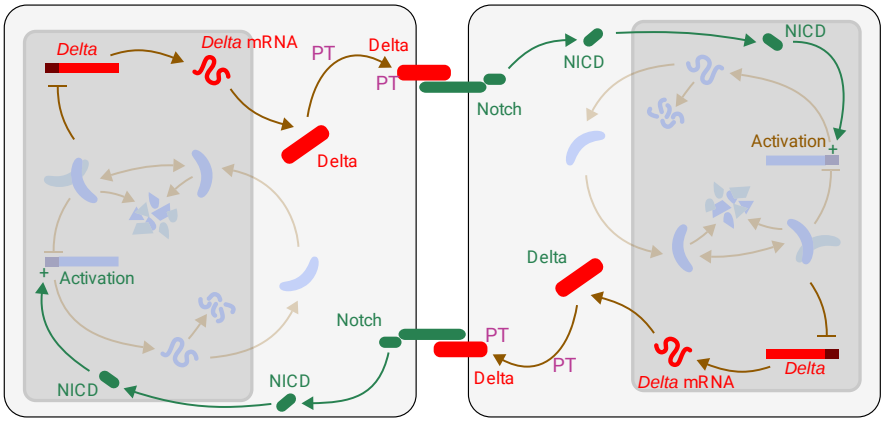

Figure 1.3: Delta-Notch coupling. Delta proteins are synthesized and transported to the cell membrane, where after the post-translational modifications (PT) act as active ligands to Notch receptors. Transcription of Delta genes is repressed by the same transcription factors that control de autonomous oscillator feedback loop (dimmed in figure). In the receiving cell, Notch intracellular domain (NICD) is cleaved and transported to the nucleus, where it activates transciption of genes involved in the autonomous oscillator. Figure adapted from [10].

along the axis of correctly ordered segments vs. disordered segments with broken boundaries [38, 40, 42]. Blocking Notch coupling and observing how oscillations in the PSM gradually loose synchrony gives information about the amount of noise present in the system. Conversely, re-activating the coupling and looking at the time that the system needs to recover synchrony provides information about the strength of the coupling. However, to quantitatively estimate these features, experiments have to be combined with theoretical models of coupled oscillators [38]. Combining experiments with these theories, it is possible to relate the loss of synchrony and recovery with a trajectory of the system in a phase diagram determined by the strength of the coupling between the oscillators κ and an order parameter r that measures the degree of synchronization in the system, Figure 1.4.

Taken together, these previous studies provide evidence that the segmentation clock behaves as a system of coupled oscillators where intercellular coupling via Delta-Notch signaling is essential to synchronize the oscillations among neighboring cells, thus generating the collective rhythm.

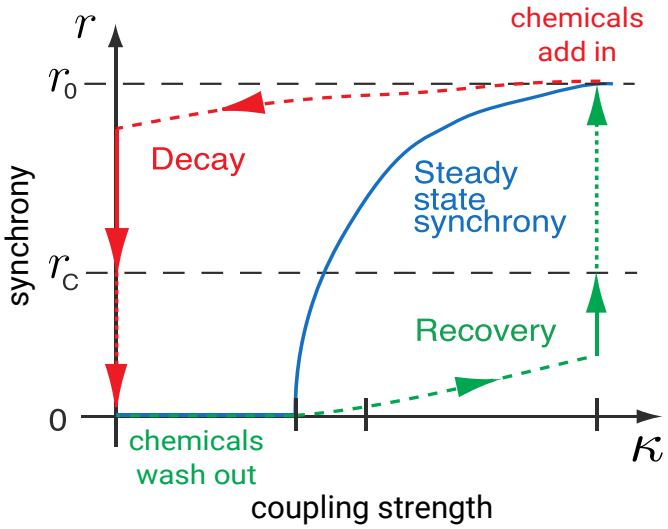

Figure 1.4: Local communication synchronizes the oscillations. Phase diagram determined by the degree of synchrony r and the coupling strength κ in a theory of coupled oscillators. Synchronization is disturbed experimentally by inhibiting coupling with added chemicals that block Delta-Notch signalling (DAPT). When the chemicals are washed out, the system recovers synchrony, describing a trajectory in this phase space. Figure adapted from [38].

1.2 Cell mobility in vertebrate segmentation

It has been observed that cells with the autonomous oscillators move within the PSM tissue, Figure 1.5. There is clear evidence of a posterior-to-anterior gradient of cell mobility and directionality in the PSM, with extensive cell mixing at the tailbud. Increasing mobility of cells from anterior to posterior has been observed in multiple experiments in zebrafish and chick embryos [42–45] and has also been recently quantified [18, 46]. Graduation in mobility along the PSM is thought to be controlled by molecular gradients of signaling molecules such as FGF [43,44]. Variability in the direction of movement between cells also increases anterior-to-posterior. In the anterior PSM, slow mobility of individual cells show some correlation in their direction of movement [44,45]. In contrast, random-walk diffusive cell movement is observed at the tailbud [42–45]. This leads to extensive cell mixing in that zone. Random movement in the tailbud causes cells to change their relative positions, exchanging neighbors over time. At first glance, this could disturb local synchronization because the change in the relative positions between oscillators can cause that an oscillator with a different phase to slip in between two neighboring synchronized oscillators, Figure 1.5(b). We already mentioned

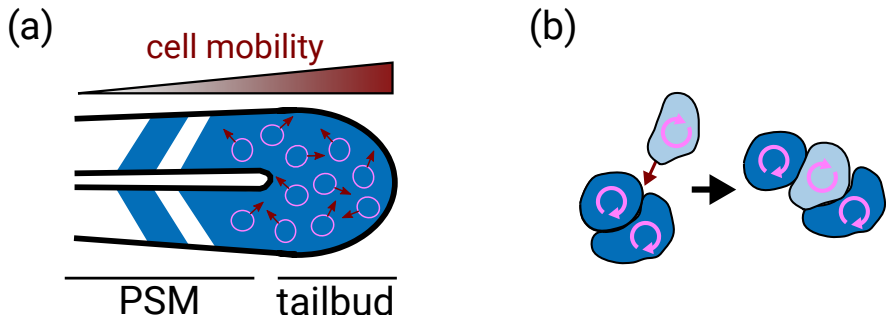

Figure 1.5: Cell mobility in the vertebrate segmentation clock. (a) A gradient of cell mobility in the PSM tissue is observed. (b) High mobility in the tailbud rearranges cell relative positions and could disturb local synchronization. Figure adapted from [18].

that local synchronization is crucial for correct pattern formation by the segmentation clock, and experiments that show that perturbations to synchrony in the segmentation clock has an effect on the forming segments. Thus, mobility could have a negative effect on patterning. In contrast to this first intuition of mobility disturbing locally synchronized patterns, Figure 1.5(b), theoretical models have shown that random cell mobility promotes synchronization in the segmentation clock [47, 48]. We will address theoretical models carefully in Chapter 2.

To understand whether mobility has an impact on signaling that can affect synchronization and patterning, the timescales of signaling and mobility have to be compared [18]. This entails the difficulty of reliably quantifying these timescales in time-lapse experiments, related to the need of tracking cells in elongating tissues, on the one hand, and to defining good observables that can reflect the real timescale of mobility, on the other. Recently, a framework for quantification of cell mixing in the segmentation clock was developed and statistical measures were proposed [18, 46]. Using these measures, the timescale for changing relative positions was compared with that of signaling, showing that mobility is expected to affect information flow in the tissue and pattern formation [18]. We explained that the vertebrate segmentation clock behaves as a population of autonomous oscillators in the PSM cells, that are locally synchronized by Delta-Notch coupling. Because Delta-Notch requires cell-cell contact for communication, the spatial organization of the cells defines which oscillators communicate and which ones do not, determining how information is propagated through the tissue.

1.3 Coupling delays in Delta-Notch signaling

As already explained, Delta-Notch communication involves a cascade of complex events that include synthesis and transport of signaling macromolecules. This cascade of complex events can introduce communication delays both for sending and processing signals. For instance, sending signals requires that Delta molecules are synthesized, subjected to post-translational modifications and transported to the cell membrane in order to be available there as active ligands for Notch. Delays arising from Delta synthesis and trafficking have been estimated to be in the range of tens of minutes in cell culture [49]. Similarly, Notch receptor needs to be first cleaved and then its intracellular domain transported to the nucleus to allow for a cell to receive a signal from its neighbor. Only when the NICD reaches its target genes regulatory sites, the signal can affect the autonomous oscillator in the receiving cell. Therefore, cleavage and translocation of NICD to the nucleus could introduce time delays for processing signals.

Communication delays have been shown to alter collective dynamics and patterning, both with theoretical models of coupled oscillators and by combining these with experiments in zebrafish embryos [50–53]. Perturbations to the biological system combined with theory including coupling delays allow for experimental tests on how delays in intercelular communication affect segmentation. Theories that include coupling delays will be addressed in detail in Chapter 2. Importantly, as we explain there, theories based on delayed-coupled phase oscillators show that delays change the collective period of the synchronized oscillation with respect to individual periods. Delays in the coupling can make collective oscillations slower than autonomous ones or even faster, Figure 2.4. Consistently, loss-of-function mutants in several genes involved in Delta-Notch coupling have been observed to increase the period of segmentation [51], Figure 2.7. More recently, transgenic zebrafish lines that overexpress Delta ligands have shown to reduce the period [53]. Disruption of the Delta-Notch pathway in zebrafish also alter the segment length and the wave pattern of cyclic gene expression in the PSM, consistent with a change in the period of segmentation [51]. Coupling delays can also explain the longer period in mouse with respect to zebrafish [50, 54]. Taken together these works show that a phase description in terms of coupled phase oscillators with delayed coupling is sufficient to compute the overall spatiotemporal patterns of gene expression and the collective period of the oscillations.

Chapter 2

Theoretical description of synchronization

In the previous chapter we introduced the biological system that motivates this Thesis. We discussed evidence that supports the idea that the segmentation clock can be thought as a population of locally coupled oscillators where cell mobility occurs together with coupling delays. Descriptions of the segmentation clock in terms of coupled phase oscillators that include either mobility of the oscillators or delays in the coupling have been proposed, showing that they are a powerful tool for answering relevant biological questions such as how fast synchronization occurs or how does the collective period of the clock emerges. In this chapter we introduce phase oscillator models in a more general way and describe the main effects that mobility and delays have on the dynamics of coupled phase oscillators when addressed separately.

A phase oscillator is perhaps the most simple description of an oscillatory unit. In this description, the state of the oscillator is entirely given by a single variable: its phase. The phase variable ranges between 0 and 2π that indicates the fraction of the cycle undergone by the oscillatory unit. The dynamics of the phase represents the periodic motion of the unit along the cycle. In particular, an individual unit i with a uniform periodic motion of frequency ω_i evolves according to the equation

$$\dot{\theta}_i = \omega_i. \tag{2.1}$$

We call this unit i an *autonomous oscillator* with homogeneous autonomous frequency ω_i, that is, the frequency with which it oscillates in the absence of interactions and external forcing.

Despite of their simplicity, phase-oscillator descriptions can well represent the relevant dynamics of more complex systems [36, 55]. In terms of dynamical systems, phase oscillators describe the dynamics of a system along a limit cycle in the phase space. In many situations, limit cycles constitute strong attractors that the systems approach within a rapid timescale. After the rapid transient, the periodic motion along the limit cycle can be parametrized by the phase.

2.1 Phase oscillators with instantaneous coupling

Systems of interacting phase oscillators constitute a paradigm for studying the emergence of coherent collective behaviour and synchronization [36]. In their general form these can be written as

$$\dot{\theta}_i = \omega_i + \sum_{j=1}^{N} K_{ij}\, f(\theta_i, \theta_j), \quad i = 1, \ldots, N \tag{2.2}$$

where the first term is the autonomous oscillation described before and the subsequent terms describe pair interactions between the oscillators. Here, N is the total number of oscillators, f is a coupling function and the coupling topology is given by K_{ij}. The coupling topology K_{ij} indicates which pairs of oscillators are coupled and with which strength. In general

$$K_{ij} = \frac{\kappa_{ij}}{n_i}\, a_{ij},$$

where κ_{ij} is the strength in the coupling between oscillators i and j, $a_{ij} = 0$ if oscillators i and j are uncoupled and $a_{ij} = 1$ if they are coupled, and n_i is a normalization by the total number of coupling terms for oscillator i. In this Thesis we study systems of coupled phase oscillators where the coupling function is sinusoidal in the phase difference and the coupling strength κ is the same for

all pairs of interacting oscillators

$$\dot{\theta}_i(t) = \omega_i + \frac{\kappa}{n_i} \sum_{j=1}^{N} a_{ij} \sin\left(\theta_j(t) - \theta_i(t)\right). \tag{2.3}$$

If $\kappa = 0$, each unit i with $i = 1, \ldots, N$ oscillates with its own autonomous frequency ω_i. When $\kappa \neq 0$, the sinusoidal coupling in Eq. (2.3) means that each oscillator adjusts its frequency according to the difference between its own present phase and the phases of the other oscillators to which it is coupled. In the most simple case of two oscillators,

$$\dot{\theta}_1(t) = \omega_1 + \kappa \sin(\theta_2(t) - \theta_1(t)) \tag{2.4}$$

$$\dot{\theta}_2(t) = \omega_2 + \kappa \sin(\theta_1(t) - \theta_2(t)), \tag{2.5}$$

the sinusoidal coupling will make each of them to speed up or slow down depending on their phase difference. For $\kappa > 0$, this coupling is attractive and oscillators try to even out their phase difference. To gain intuition into what this sinusoidal coupling does, lets imagine as an example two runners in a circular running track. If the runners were uncoupled, each of them would make turns to the running track at its own speed ω_i with $i = 1, 2$. Instead, at each instant of time t, runner 1 sees where in the running track the other runner is, i.e. he looks at runner's 2 present phase $\theta_2(t)$, and compare it with his own phase $\theta_1(t)$. If runner 2 is ahead, $\theta_2(t) > \theta_1(t)$, then the coupling term in Eq. (2.4) is positive and runner 1 will try to speed up. In contrast, the coupling term in Eq. (2.5) would be negative in such case and runner 2 slows down. From this example it is now natural to imagine that, unless their natural speeds are so different that they cannot adjust them the sufficient amount, they will end up running together with a common speed $\Omega = \dfrac{\omega_1 + \omega_2}{2}$. Whether this synchronized state is reached or not, or how much time it takes for the runners to synchronize their motion will depend on $\Delta\omega = \omega_1 - \omega_2$ and κ. In the special case of identical oscillators, $\Delta\omega = 0$, synchronization is always reached for $\kappa > 0$ and the only possible situation is that the collective frequency is the same as the autonomous frequency of the oscillators $\Omega = \omega$. As we explain later, this situation is conceptually different from synchronization when the coupling is delayed, Section 2.3.

In the more general case of N oscillators, Eq. (2.3), the synchronization scenarios depend on the heterogeneity in the autonomous frequencies, the coupling

strength and the coupling topology. The dynamics of model (2.3) was first studied by Yoshiki Kuramoto for all-to-all coupling and frequencies drawn from a unimodal and symmetric distribution $g(\omega')$. He found that a synchronization transition takes place for a sufficiently large value of the coupling constant κ. To his nice surprise [1], the Kuramoto model for coupled phase oscillators has become the most paradigmatic description to study collective synchronization of interacting units [56,57] and has been addressed for multiple coupling topologies [58]. In the following, we describe the special cases of mean-field systems and spatially extended systems with local coupling within a certain range.

2.1.1 Mean-field coupling

In his original work, Kuramoto analysed an all-to-all coupling topology [59]

$$\dot{\theta}_i(t) = \omega_i + \frac{\kappa}{N}\sum_{j=1}^{N}\sin\left(\theta_j(t) - \theta_i(t)\right). \tag{2.6}$$

The degree of global synchronization in the system can be quantified by means of the Kuramoto order parameter

$$Z(t) = r(t)\, e^{i\psi(t)} = N^{-1}\sum_{j=1}^{N} e^{i\theta_j(t)}. \tag{2.7}$$

This complex order parameter is a macroscopic quantity used to describe the collective rhythm of the population rather than that of the individual elements. It is a vector in the complex plane whose magnitude r measures the average coherence between the phases of all the oscillators in the system. Its phase ψ is the average phase of the system, Figure 2.1. If all oscillators are synchronized, with the same phase evolving with a collective rhythm, then the modulus of the order parameter is $r \sim 1$. In contrast, if phases are scattered around the circle then $r \sim 0$ and the system behaves incoherently without an emerging collective rhythm.

The governing Eqs. (2.6) can be rewriten in terms of the Kuramoto order parameter, Eq. (2.7) as

$$\dot{\theta}_i = \omega_i + \kappa r \sin(\psi - \theta_i), \quad i = 1, \ldots, N. \tag{2.8}$$

[1] Kuramoto talks about the Kuramoto model. https://www.youtube.com/watch?v=lac4TxWyBOg

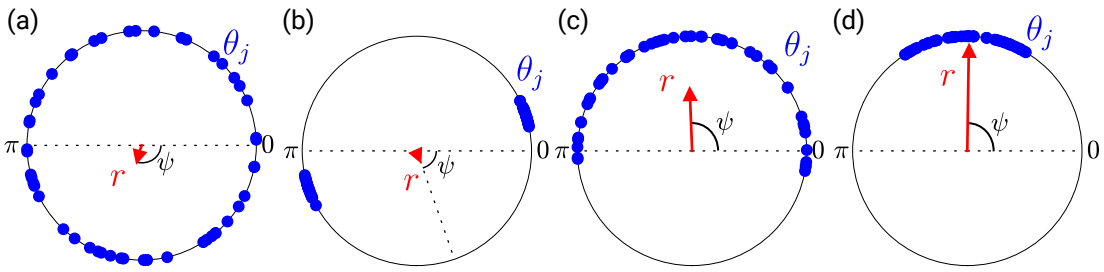

Figure 2.1: Geometric interpretation of the Kuramoto order parameter. (a) Randomly scattered phases over the circle, (b) Oscillators almost in antiphase, (c,d) Other examples. Note that the order parameter has small modulus for both (a) and (b). In (c) and (d) the complex order parameter has similar phase but the magnitude r is closer to $r \approx 1$ for smaller dispersion of the phases (d). Examples are shown for $N = 50$.

Written in this form, the mean-field (MF) character of the system becomes evident. The evolution equation for the phase of each oscillator seems to be decoupled from the others, being only coupled with them through a mean-field described by r and ψ. Looking at Eq. (2.8), each oscillator will speed up or slow down depending on how far its phase is from the mean phase ψ. Thus, the phase of each oscillator θ_i is attracted to the averaged phase ψ instead of to any particular phase from other oscillator θ_j. This is an important feature characterizing mean-field systems. It makes the transient dynamics of the MF system qualitatively different from the dynamics of spatially extended systems with short-range coupling topology, where oscillators are attracted only by their local neighbors. We will come back to this difference later in this Thesis.

In the original model studied by Kuramoto, where the frequencies ω_i are drawn from a unimodal and symmetric distribution $g(\omega')$ such that $g(\omega') = g(-\omega')\,\forall\omega'$, a synchronization transition occurs for a critical coupling strength κ_C. For low values of the coupling strength $\kappa < \kappa_C$, oscillators act as if they were uncoupled. However, if the coupling strength is strong enough to overcome the heterogeneity in the frequencies $\kappa > \kappa_C$, the system displays partially synchronized solutions. In such cases, after a transient time oscillators split in two groups. In one group oscillators are capable to follow the mean-field and synchronize, oscillating with a collective frequency equal to the mean frequency ω of the distribution $g(\omega')$. In the other group, oscillators with frequencies in the tails of the distribution are not capable to synchronize and their phases, scattered around the circle, keep drifting incoherently. Importantly, the splitting of the population into two groups

here comes from the fact that oscillators are heterogeneous: their frequencies are drawn from a distribution $g(\omega')$. The critical value of the coupling strength κ_C at which the synchronization transition occurs depends on the frequency distribution $g(\omega')$ and is smaller for sharper frequency distributions. In the same way, in this partially synchronized solutions, the asymptotic value of the order parameter r_∞ is closer to one as more oscillators belong to the synchronized group. In particular, in the most simple case where oscillators are identical $\omega_i = \omega \; \forall i$, the frequency distribution is a delta and the system achieves complete synchronization with $r_\infty \approx 1$. In this state, all the oscillators evolve with a common frequency Ω that is the same as the natural frequency of the oscillators, $\theta_i(t) = \Omega t \; \forall i$ with $\Omega = \omega$. This state of complete synchronization is achieved by the system of identical oscillators for any value of $\kappa > 0$, and regardless of their initial phase differences.

We are interested in the dynamics of the system of coupled oscillators as it goes from an incoherent state to the completely synchronized state, that is, we are interested on how order spontaneously emerges out of disorder. In the reminder of this Thesis, we will only consider identical oscillators. We can track the macroscopic evolution of a system of coupled phase oscillators that starts from a disordered state and ends up in a state of complete synchronization by looking at the time evolution of the order parameter as it grows from $r \sim 0$ to $r \sim 1$. A typical such behavior for the mean-field system of identical oscillators is shown in Figure 2.2. Importantly, in the system of identical oscillators with mean field coupling, the rate at which the system approaches synchronization is determined only by the coupling strength κ; oscillators will synchronize faster for stronger coupling. In more complex coupling schemes, the speed of synchronization will also depend on other parameters of the system as we show later.

2.1.2 Spatially extended systems

Motivated by local communication mechanisms in biology and in particular in the vertebrate segmentation clock, we study spatially extended systems where coupling has a certain range ξ. These systems correspond to assigning in Eqs. (2.3),

$$a_{ij} = \begin{cases} 1 & \text{if } j \epsilon V_i \\ 0 & \text{otherwise} \end{cases}$$

where V_i is the neighborhood of oscillator i within a range ξ. Thus, for each oscillator i the summation only runs over oscillators j belonging to its neighborhood

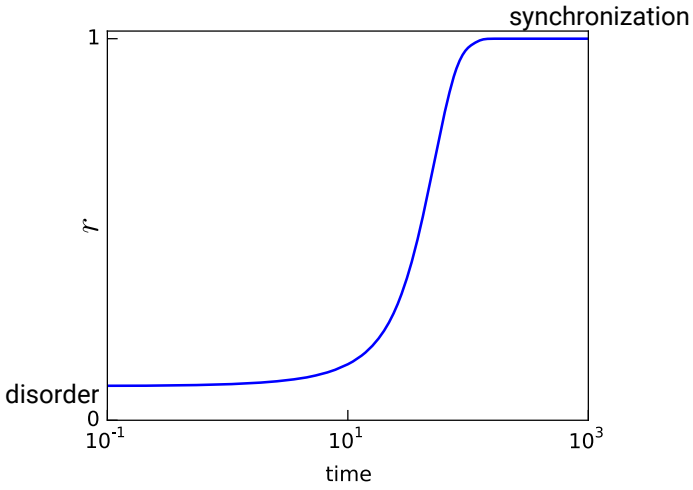

Figure 2.2: Typical time evolution of the order parameter for a mean-field system as it goes from an initially disordered state to reaching complete synchronization. Parameters are: $N = 100$, $\omega = 1$, $\kappa = 0.1$.

V_i

$$\dot{\theta}_i(t) = \omega + \frac{\kappa}{n_i} \sum_{j \epsilon V_i} \sin\left(\theta_j(t) - \theta_i(t)\right). \tag{2.9}$$

We assumed identical oscillators with autonomous frequency ω and n_i the number of neighbors of oscillator i. We will focus in particular in systems of oscillators placed on a one dimensional lattice where each oscillator stands on a lattice site. In such systems, the position of an oscillator i in the lattice is $x_i = k\,\Delta x$ where $k = 0, \ldots, N-1$ denotes the lattice site. The neighborhood of oscillator i within a range ξ in the lattice is defined by

$$V_i(t) = \{j \text{ such that } |x_j(t) - x_i(t)| \leq \xi\,\Delta x\}.$$

2.2 Mobile coupled phase oscilators

The effects of mobility on synchronization dynamics can be addressed by considering mobile oscillators in the lattice [47,60]. Mobility of oscillators sets the timescale for how often single oscillators exchange neighbors, which is particularly relevant in locally coupled systems. An advantage of the lattice model is that defining such a timescale for exchanging neighbors is straightforward. Moreover, this simplification of the physical geometry makes the model more tractable, while still capturing the relevant effects of mobility on the dynamics. Several

works have shown that similar results can be obtained for mobile oscillators off-the-lattice [61–63].

In the lattice model of mobile oscillators, the positions of the oscillators are constrained to the lattice sites as explained in Section 2.1.2, but oscillators can move through the lattice by stochastically exchanging positions with their nearest neighbours. This exchange events are described as a Poisson process, in which each pair of neighboring oscillators has a probability $\lambda/2$ of exchanging positions per unit time [47, 60, 63]. In between exchange events, phase dynamics obeys Eqs. (2.9)

$$\dot{\theta}_i(t) = \omega + \frac{\kappa}{n_i} \sum_{j \epsilon V_i} \sin\left(\theta_j(t) - \theta_i(t)\right). \tag{2.10}$$

with nearest-neighbors coupling

$$V_i(t) = \{j \text{ such that } |x_j(t) - x_i(t)| = 1\}.$$

and boundary conditions such that oscillators in the left and right ends of the lattice interact only with their right and left neighbors, respectively, and can only exchange positions with them. In this situation, the timescale for mobility is defined by λ^{-1}. The only other relevant timescales are those for the phase dynamics due to autonomous oscillations ω^{-1} and to coupling κ^{-1}. We could remove the dependence of ω in Eqs. (2.10) by changing to the rotating reference frame, but we keep it here for future comparison with the case of delayed coupling, where equations do not remain invariant if switching to the rotating reference frame. The relative weight of timescales, given by the mobility to coupling ratio λ/κ, determines the behavior of the system.

Like in the systems without mobility described above, identical mobile oscillators in the lattice always achieve complete synchronization, regardless of its initial phase differences. Thus, mobility does not change the steady state of the system. In contrast, mobility can significantly affect the transient dynamics towards synchronization and has been shown to reduce the time that the system needs to reach this state.

Starting from disordered states, two distinct routes towards a completely synchronized state are observed. For low mobility oscillators behave similarly to non-mobile. If mobility is small compared to the coupling strength, the dynamics of the system is dominated by coupling, which is local. The system first synchronizes locally, forming spatial patterns where oscillators that are close in the lattice

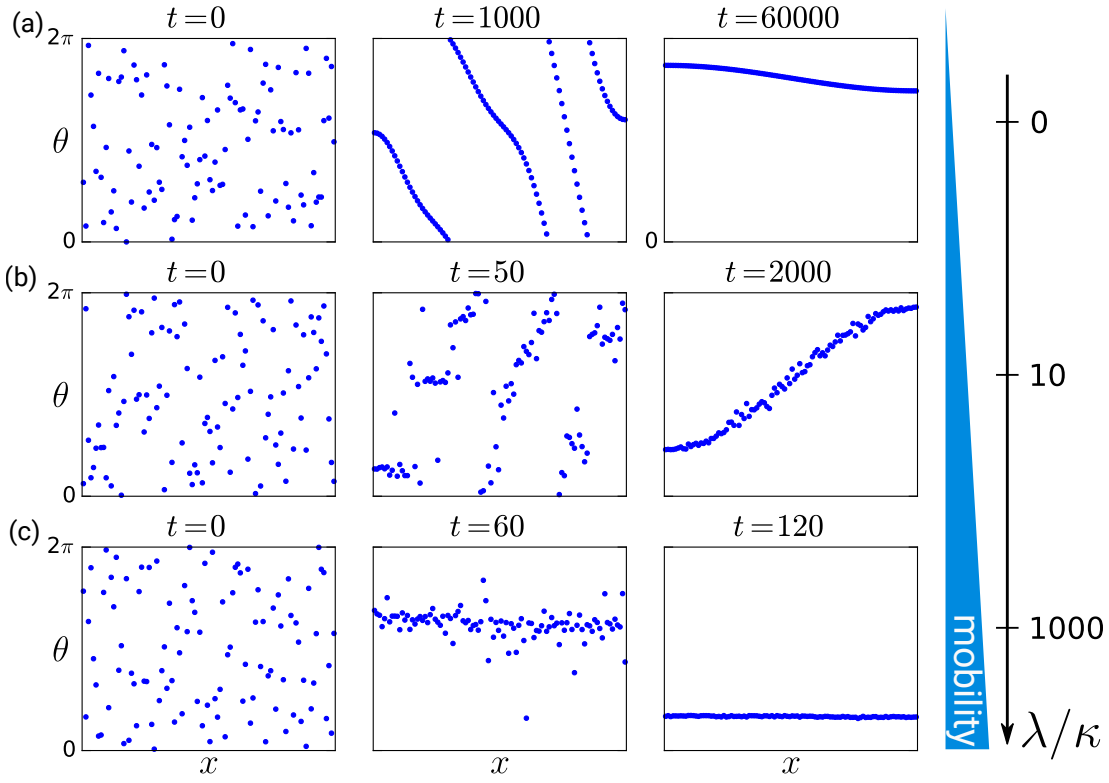

Figure 2.3: Different routes towards synchronization are observed in transient dynamics depending on mobility to coupling ratio. Panels show snapshots of the system state on its evolution from disorder to synchronization. (a) $\lambda/\kappa = 0$ (non-mobile), (b) $\lambda/\kappa = 10$ and (c) $\lambda/\kappa = 1000$. Other parameters are: $N = 100$, $\omega = 1$, $\kappa = 0.1$.

have similar phases while oscillators with distant positions can have large phase differences, Figure 2.3(a). In the other extreme, for very large mobility, the system behaves as a mean-field system where the phases are attracted to the mean phase of the population rather than to their close neighbors. Instead of forming locally ordered patterns, the phases are spread within an apparently disordered cloud of the size of the system that gradually reduces its phase dispersion, Figure 2.3(c). This is because the short interaction time with local neighbors before exchanging positions is not enough to synchronize their phases locally. The crossover between these two qualitatively different behaviors is determined by the mobility to coupling ratio λ/κ. For intermediate values of this ratio, $\lambda/\kappa = 10$, oscillators still form a spatial pattern with local phase correlations, but this pattern is characterized by longer wavelengths, Figure 2.3(b). Remarkably, synchronization occurs much faster for high mobility, by the mean-field route.

Local phase correlations in spatially extended systems cannot be captured by the Kuramoto order parameter Z introduced above. While this parameter properly describes the global state of the system, it averages equally over all the oscillators and has no spatial information. To study the transient dynamics towards synchronization of spatially extended systems, we introduce a spatial phase correlation between lattice sites

$$\rho_d(t) = \langle \cos\left[\vartheta_{k+d}(t) - \vartheta_k(t)\right] \rangle_k \tag{2.11}$$

where the phase $\vartheta_k(t)$ in site k is defined as the phase of the oscillator i such that $x_i(t) = k$, d is the dimensionless distance between lattice sites and $\langle \ldots \rangle_k$ indicates the average over sites k with $k = 0, ..., N-1-d$ [60]. If sites at distance d have similar phases on average, then $\rho \approx 1$. In contrast, if they are in antiphase on average, $\rho \approx -1$. If there is no correlation at this distance, $\rho \approx 0$.

In this Thesis we will refer to complete synchronization, global order, coherent state or completely synchronized state alternatively as synonyms to describe a state of the system where all the oscillators are oscillating with the same collective frequency and the same phase. When relevant, in spatially extended systems we call this state the in-phase synchronized state, to explicitly distinguish it from antiphase synchronization, where oscillators are frequency locked but neighboring oscillators maintain a fixed phase difference of $\Delta\theta \approx \pi$. In contrast, when phases of the oscillators drift around with different frequencies and their phases are spread over the circle, we will refer to an incoherent or disordered state. The completely synchronized state is then characterized by a value of the spatial correlations $\rho_d \approx 1$ for all distances d. Conversely, for the incoherent state $\rho_d \approx 0 \, \forall d$.

Note that the spatial phase correlation ρ_d can give information about local patterns, while the order parameter Z defined prevously can not. For example, $|\rho_1| \sim 1$ for in-phase and also for antiphase synchronization but can still distinguish between them as $\rho_1 \sim 1$ for in-phase and $\rho_1 \sim -1$ for antiphase synchronization. In contrast, the order parameter averages equally over the whole system and its modulus is small for many local patterns, making them indistinguishable. In particular, the order parameter cannot distinguish antiphase synchronization from incoherence. The two routes towards synchronization described above for the lattice model of mobile coupled phase oscillators are well reflected in the evolution of these spatial correlations ρ_d [60], see also Chapter 4.

Variations of the lattice model of mobile oscillators applied to the segmentation clock have shown similar results. In particular, models that describe the tailbud as a two-dimensional lattice of coupled phase oscillators that can exchange positions show that random cell mobility promotes synchronization in the segmentation clock [47, 48]. In [47] it is shown that synchronized oscillations can be sustained in the presence of random cell movement. This is consistent with the uniform expression of cyclic genes in the tailbud, where extensive cell mobility with a high variability in the directions of movement between cells is observed [42–45]. Moreover, when considering an initial pertubation to the synchronized state in the model, synchronization is restored much faster and for a wider range of parameters than the case without cell movement. This is consistent with the fast recovery observed in experiments that perturb synchronization [38, 40, 42]. In [48] the model includes an additional timescale for cells to recover the interaction with their neighbors after movement. Recovery is gradual, implemented by including a time dependence in the coupling strength between oscillators. They find that there is an optimal rate of mobility for which the system synchronizes fastest. In addition, there is a critical rate of mobility above which synchronization is not possible. This emphasizes the importance of comparing timescales between movement and signaling to understand how mobility affects information transfer and synchronization.

The influence of cell mobility on synchronization in the segmentation clock has also been addressed by a different approach [63]. Instead of considering a discrete lattice model, the PSM tissue is described as a Voronoi diagram where each region represents one cell. Movement is considered an active process, where cells are thought as self-propelled particles with intrinsic velocities. Additionally, repulsive forces between cells are included in the model. The dynamics of movement is thus governed by the balance of self-propelled and repulsive forces between cells. This description allows to consider correlations between the velocities of different cells reported for more anterior parts of the PSM tissue [45]. On top of this description of the tissue dynamics, oscillatory dynamics is described as a system of coupled phase oscillators with added noise. As well as in the lattice models, this continuous description of the PSM tissue also shows enhancement of synchronization by movement. Interestingly, short-range correlations in the velocities can enhance synchronization more than random cell movement.

Descriptions of the individual oscillations in single cells have also been con-

sidered in further detail [47]. In particular, the oscillatory dynamics of cyclic genes has been explicitly modeled, considering equations for her mRNA, Her protein in cytoplasm, Her protein in nucleus, and Delta protein. Importantly, similar results were obtained between these models and less detailed models of the individual oscillations like the one in [20] and models based on coupled phase oscillators [55]. This similarity strongly suggests that the enhancement of synchronization by random cell movement does not depend on the detailed modeling of molecular events. Thus, relevant questions about the impact of mobility on the collective oscillatory dynamics can be addressed with more tractable models based on phenomenological descriptions in terms of phase oscillators. These models permit to define macroscopic timescales such as κ^{-1} and ω^{-1} and to focus on the interplay between timescales, keeping the individual dynamics of single oscillators in a simple way.

2.3 Phase oscillators with delays in the coupling

Systems of coupled units are frequently subjected to delays in the coupling. We already mentioned that Delta-Notch coupling in the biological system that motivates this Thesis involves coupling delays that arise from the synthesis and trafficking of signaling macromolecules, Section 1.3. In general, coupling delays between a sending and a receiving unit could arise for three reasons. First, the sending element could require some time for preparing and sending the signal. Second, time could be needed for the signal to travel between units because of finite speed of propagation of the signal. Last, the receiving element could need time to process the signal that arrives. In particular, time delays associated to Delta-Notch coupling are related to the first and last reasons mentioned. Thus, later in this Thesis we will only consider delays due to sending and processing signals and we will not consider any delay due to finite speed propagation. In this section, however, we consider coupling delays in a general way that could in principle refer to any of the three reasons. We consider systems of coupled phase oscillators as introduced in Section 2.1 and consider coupling delays including a discrete delay τ in the sinusoidal function. The aim is to illustrate how the main effects of coupling delays on the collective dynamics of systems of coupled oscillators arise.

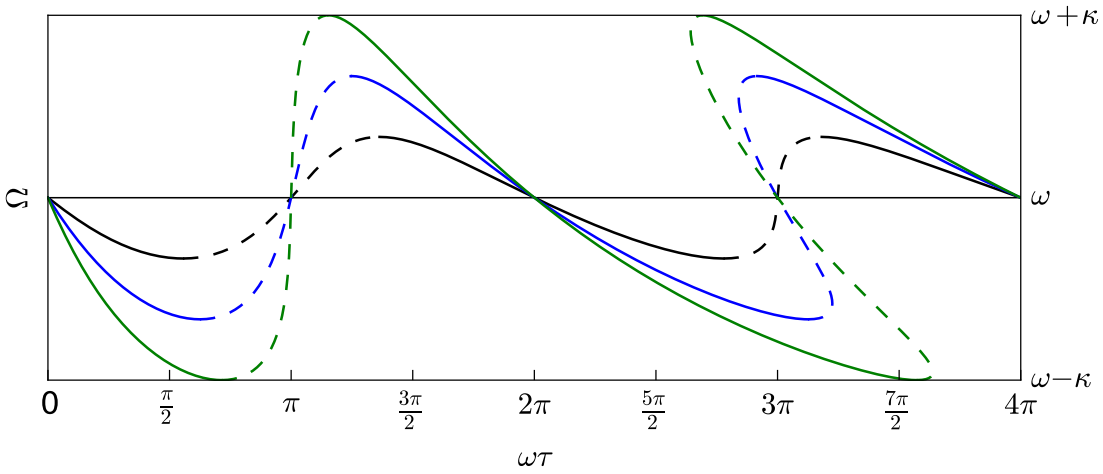

Figure 2.4: Parametric plot of the collective frequency Ω, Eq. (2.14), for $\kappa = 0.1$ (black), $\kappa = 0.2$ (blue) and $\kappa = 0.3$ (green). Solid lines indicate that the synchronized state is stable, Eq. (2.16). Larger values of κ tilt the curves, leading to more stable in-phase synchronized solutions for the same value of τ, i.e. larger multistability in Ω. Horizontal black line indicates the autonomous frequency ω of individual oscillators.

2.3.1 Time delays in the mean-field system

Consider the Kuramoto model for identical oscillators with mean-field coupling with a delay τ [64, 65]

$$\dot{\theta}_i(t) = \omega + \frac{\kappa}{N}\sum_{j=1}^{N}\sin\left(\theta_j(t-\tau) - \theta_i(t)\right) \quad \text{with } i = 1, \ldots, N \tag{2.12}$$

where ω is the autonomous frequency and the subsequent terms describe the interaction between the oscillators through a sinusoidal coupling function of the phase differences. The important thing here is that coupling is not instantaneous. The instantaneous frequency $\dot{\theta}_i(t)$, Eq. (2.12), depends on the state of the other oscillators at an earlier time $t - \tau$. As we show below, this delayed-coupling profoundly changes the dynamics with respect to the non-delayed case, Eq. (2.8).

Synchronized in-phase solutions of system (2.12)

$$\theta_i(t) = \Omega t \quad \forall i \tag{2.13}$$

always exist. Replacing the ansatz (2.13) in the Eqs. (2.12), we obtain a condition

for the collective frequency Ω of the synchronized state

$$\Omega = \omega - \kappa \sin(\Omega\tau). \tag{2.14}$$

This result has proven to be robust also for multiple other systems of delayed-coupled oscillators [50, 64, 66–68]. Eq. (2.14) is a trascendental equation for the collective frequency that cannot be solved in a closed-form. Thus, to understand its solutions it is useful to plot it parametrically in the (τ, Ω) plane defining the parameter $\psi \equiv \Omega\tau$, Figure 2.4

$$\begin{aligned} \Omega &= \omega - \kappa \sin\psi \\ \tau &= \frac{\psi}{\omega - \kappa \sin\psi}. \end{aligned} \tag{2.15}$$

Remarkably, in contrast to the case with no delay, the collective frequency Ω is in general different from the autonomous frequency of the oscillators ω. This is the first important effect of delayed coupling on synchronization: the value of the collective frequency is shifted by the delay in a non-trivial way given by the transcendental Eq. (2.14). There are solutions for which the collective frequency can be smaller than the natural frequency of the oscillators $\Omega < \omega$ (frequency depression [67]) and there can also exist other solutions where $\Omega > \omega$. According to a stability criterion by Earl and Strogatz [69], in-phase synchronized solutions given by Eq. (2.13) are stable when

$$\kappa \cos(\Omega\tau) > 0. \tag{2.16}$$

This defines multiple stable branches of solutions, that lie between

$$-\pi/2 + 2n\pi < \Omega\tau < \pi/2 + 2n\pi \tag{2.17}$$

with $n = 0, 1, \ldots$ and $\tau > 0$, solid lines in Figure 2.4. Looking at Figure 2.4, with increasing values of the coupling strength κ curves given by Eq. (2.14) become more tilted. This leads to the occurrence of multiple synchronized solutions with different collective frequencies Ω that can be simultaneously stable for the same value of the delay τ. Therefore, the presence of coupling delays can also give rise to multistability of in-phase synchronized solutions with different collective frequencies. This is the second important effect of delayed coupling on the collective

dynamics of coupled oscillators. In contrast to the case of instantaneous coupling where the coupling strength κ determines how fast the system approaches synchronization, Section 2.1, here κ also determines how many synchronized solutions the system could reach and modifies the value of their collective frequency.

2.3.2 Spatially extended systems with coupling delays

In-phase synchronized solutions given by Eqs. (2.13) and (2.14) and the stability criteria (2.16) are valid for almost any coupling topology [50,64,66–69]. For nearest-neighbor coupling

$$\dot{\theta}_i(t) = \omega + \frac{\kappa}{n_i} \sum_{j \epsilon V_i} \sin\left(\theta_j(t-\tau) - \theta_i(t)\right), \tag{2.18}$$

in addition to in-phase synchronization the system could also exhibit antiphase synchronized solutions where neighboring oscillators have a phase lag of π

$$\begin{aligned} \theta_i(t) &= \tilde{\Omega} t, \\ \theta_{i+1}(t) &= \tilde{\Omega} t + \pi. \end{aligned} \tag{2.19}$$

Antiphase solutions satisfy

$$\tilde{\Omega} = \omega + \kappa \sin(\tilde{\Omega}\tau) \tag{2.20}$$

and are stable when [69–71]

$$\kappa \cos(\tilde{\Omega}\tau) < 0. \tag{2.21}$$

Stable branches for the antiphase solution lie between

$$-\pi/2 + 2n\pi < \tilde{\Omega}\tau < \pi/2 + 2n\pi \tag{2.22}$$

Note that $\Omega \neq \tilde{\Omega}$ and the stability boundaries for the in-phase and antiphase solutions do not coincide. A parametric plot of in-phase and antiphase collective frequencies together is shown in Figure 2.5. We choose a rather small value of the coupling strength $\kappa = 0.1$ that has a small tilt in the parametric plot of collective frequency, Figure 2.4, and thus exhibits multistability of in-phase synchronized solutions only for large time delays, outside the range of the plot. We highlight

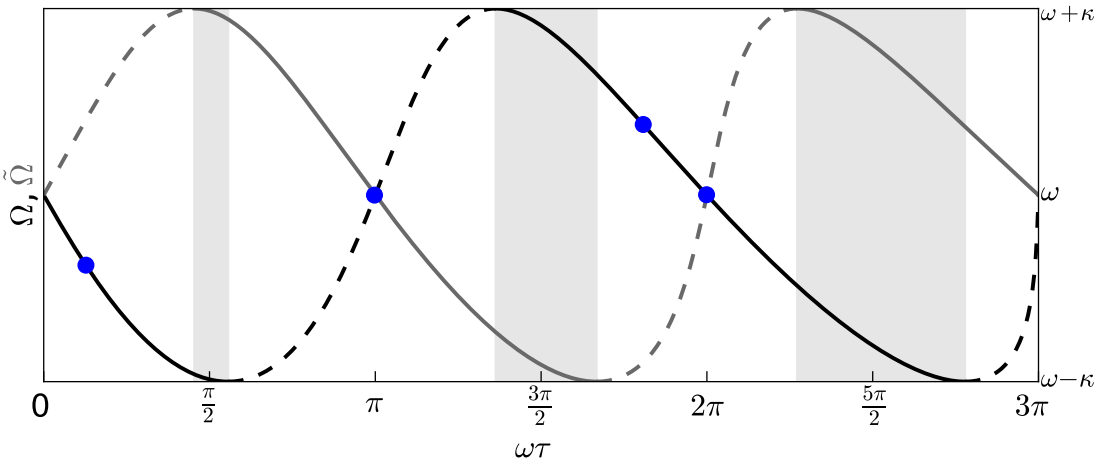

Figure 2.5: Parametric plots of the collective frequency Ω of the in-phase synchronized solutions (black) and of the collective frquency $\tilde{\Omega}$ of the antiphase synchronized solutions (gray), Eqs. (2.14) and (2.20), for $\omega = 1$ y $\kappa = 0.1$. Shadowed regions indicate bi-stability between in-phase and antiphase solutions. Blue dots show example delay values to illustrate four different situations explained in the text: (i) $\Omega < \omega$, (ii) $\tilde{\Omega} = \omega$, (iii) $\Omega > \omega$ and (iv) $\Omega = \omega$.

that even in this case, bistability is observed between in-phase and antiphase solutions, shadows in Figure 2.5.

To understand the frequency shift shown in Figure 2.5 more intuitively, lets imagine two autonomous oscillators like the two runners in the circular running track described in Section 2.1, but with a delayed coupling [66]

$$\dot{\theta}_1(t) = \omega + \kappa \sin(\theta_2(t-\tau) - \theta_1(t)) \tag{2.23}$$

$$\dot{\theta}_2(t) = \omega + \kappa \sin(\theta_1(t-\tau) - \theta_2(t)) \quad . \tag{2.24}$$

As in the case of eqs. (2.4) and (2.5), for $\kappa > 0$ each oscillator tries to adjust its frequency according to how similar it is to the phase of the other. The important difference is that at each instant of time t, a runner $\theta_i(t)$ does not see the current state of the other, $\theta_j(t)$, but its state at an earlier time $\theta_j(t-\tau)$. [2] Thus, in contrast to the case of instantaneous coupling, each oscillator is now attracted by the *ghost* of the state of the other at a time point in the past. Lets imagine that the state of the system at time $t-\tau$ is the one depicted in Figure 2.6(a). In

[2] This situation is hard to imagine with real runners in one running track. For instance, we can imagine that the running track is as big as the galaxy, in such a way that light needs a time τ to travel between the two runners.

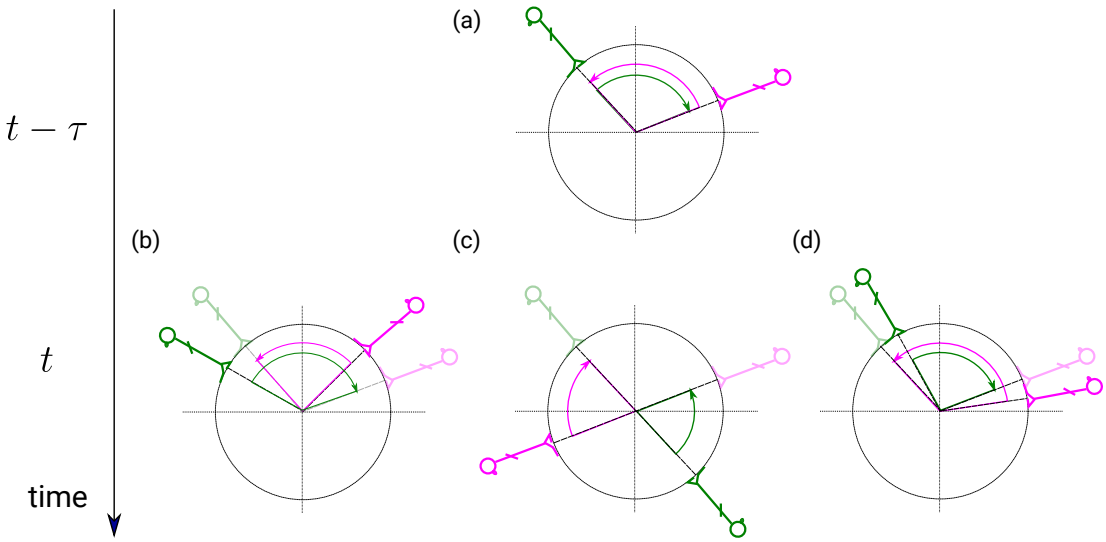

Figure 2.6: Two runners on a circular running track that are coupled with a delay in the coupling τ. (a) State of the runners at time $t-\tau$. This state is repeated in dim colors in the subsequent panels. (b-d) At time t, each runner is attracted to the *ghost* of the state of the other at time $t-\tau$. This leads to a shift in the collective frequency Ω of the synchronized state with respect to the individual frequency ω. The different panels illustrate different situations, for different values of the delay τ: (b) delay is small $\tau \ll 2\pi/\omega$ and leads to a frequency depression $\Omega < \omega$, (c) delay is similar to half the autonomous period $\tau \sim \pi/\omega$ and the oscillators end up in antiphase, (d) delay is similar to the autonomous period but smaller $\tau \lesssim 2\pi/\omega$ and leads to synchronization with larger frequency $\Omega > \omega$.

that situation, if the coupling were instantaneous, runner 1 (pink) would speed up and runner 2 (green) would slow down. For delayed coupling, we can imagine four different situations depending on the value of τ, Figure 2.6 and blue dots in Figure 2.5. In the first case, the delay is small $\tau \ll 2\pi/\omega$ and when the signal arrives at time t each runner is just a small angle $\delta \sim \omega\tau$ ahead of its state at $t-\tau$, Figure 2.6(b). As a consequence, runner 1 still speeds up as in the non-delayed case but he adjust his speed in a smaller amount because his phase difference with the ghost of runner 2 is smaller than if he receives the signal instantaneously at time $t-\tau$. Conversely, runner 2 still slows down as in the case of instantaneous coupling but in a bigger amount because his phase difference with the ghost of runner 1 is bigger. This leads to frequency depression $\Omega < \omega$. With increasing delay, one can imagine a situation where the delay is half the autonomous period $\tau = \pi/\omega$. In such situation, runners have moved forward almost half a period when the signal arrives and the coupling to the ghost state

turns repulsive: runner 1 will try to slow down to get closer to the ghost of runner 1, actually increasing the current phase differences, Figure 2.6(c). Oscillators can end up frequency locked at $\tilde{\Omega} = \omega$ but in antiphase. In a third situation, when the delay is a bit smaller than the autonomous period $\tau \lesssim 2\pi/\omega$, the runners will adjust their speeds in the same directions as if the coupling was instantaneous, but the one speeding up will do it by a bigger amount and the one slowing down will decrease its speed less than in the non-delayed case, Figure 2.6(d). This leads to an increased collective frequency of synchronization $\Omega > \omega$. Finally, if the delay is an integer multiple of the autonomous period $\tau = 2\pi/\omega$, at time t the state of the system is almost the same as in $t - \tau$, as each oscillator performed a complete cycle. As a result, the collective frequency of synchronization is not shifted $\Omega = \omega$.

In 2009, Morelli et al. proposed a delayed coupling theory (DCT) of vertebrate segmentation. The theory is based in a phase representation of cellular oscillators, where each oscillator has a fixed position in a lattice that spans the PSM. The model includes four key ingredients: a frequency profile of oscillators, slowing across the PSM form posterior to anterior; a moving boundary describing embryonic axis elongation; coupling between neighboring oscillators; and delay in the coupling. The frequency profile is included as a phenomenological description of the arrest of the oscillations at the anterior end of the PSM, that was linked to a spatial dependence of the autonomous frequency of the individual oscillators [1, 13, 72, 73]. The moving boundary accounts for tissue elongation and it is incorporated in the model such that the number of oscillators is fixed: the arrest front and the moving boundary move at the same velocity. They used a sinusoidal coupling function between neighboring oscillators and included a discrete delay in it, in the same way as in the models described above. The main result from the DCT of vertebrate segmentation is that the collective period of the segmentation clock $T = 2\pi/\Omega$ depends on the delay in the coupling τ

$$\Omega = \omega_{\mathrm{L}} - \kappa \sin(\Omega\tau). \tag{2.25}$$

where ω_{L} is the frequency of the oscillators at the most posterior part of the tissue. As explained above, the dependence of the collective frequency on coupling delays is an important feature of systems of delayed-coupled oscillators [64–66]. Eq. (2.25) shows that the collective period of the clock composed by multiple cellular oscillators emerges as a self-organized property and depends not only on

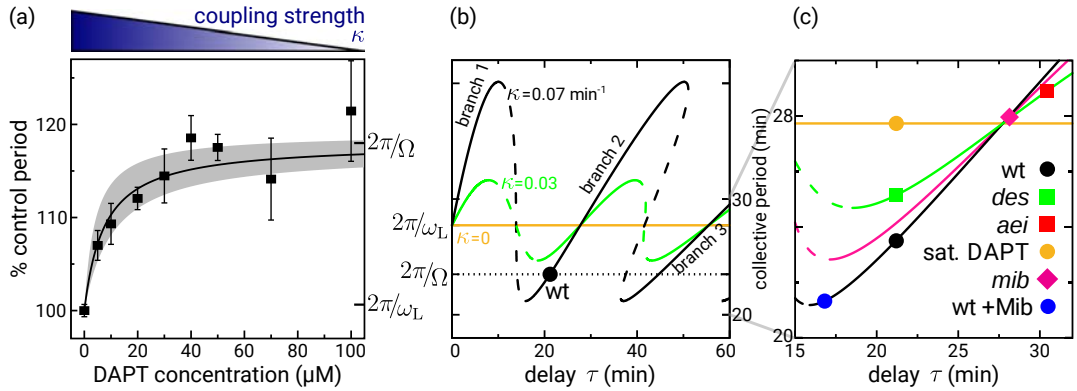

Figure 2.7: (a) Segmentation clock period can be tuned by changing the coupling strength with chemicals (DAPT). (b,c) This is consistent with a theory that includes coupling delays, Eq. (2.25). Panel (c) is a closer look at (b) where the wild type and different Notch mutants have been placed on the curves given by the theory from fitting the DCT to experimental data from zebrafish embryos [50, 51]. Figure adapted from [51].

the intrinsic frequency of individual cells, but also on the coupling strength and the time delay. Thus, time delays are biologically relevant as they determine the period of somitogenesis and, with it, the length of the formed segments. The delayed coupling theory of vertebrate segmentation can be fitted to experimental data from zebrafish embryos to quantitatively estimate relevant parameters of the biological system [50, 51].

Besides, Eq. (2.25) indicates that the collective period does not depend on the specific shape of the frequency profile included in this model, but only on the uniform phase cell population at the tailbud with frequency ω_L. It might be possible that the synchronized population of cells at the tailbud plays an important role for the period of segmentation.

From a mathematical point of view, Eqs. (2.12) and (2.18) are delayed differential equations (DDE) [74–76]. Delay makes the equations harder to solve for several reasons. First, it turns the equations to be infinite dimensional: to integrate one step, we need to know not only the initial condition at t_0 but all the history in the whole interval $[t_0 - \tau, t_0]$. To see this consider for example

$$\dot{x}(t) = f(x(t), x(t-\tau)). \tag{2.26}$$

To make a first infinitesimal step of integration, from $t = 0$ to $t = dt$, it is necessary that we know $x(t = 0)$ (initial condition) and $x(t = -\tau)$. With only this two values we can obtain $x(dt)$. Now, if we want to do a next integration step and go from $x(dt)$ to $x(2dt)$, then we need to know $x(dt)$ that we just calculate but also $x(dt - \tau)$. Thus, to provide the initial conditions completely, we need to provide the whole history of $x(t)$ in the past times belonging to the interval $[-\tau, 0]$. Second, providing this history as a predefined function of time $x(t) = g(t)$ for $t < 0$ usually leads to a discontinuity in the derivative that propagates on further derivatives and needs to be kept in mind when solving this equations numerically [77]. Usually, to get this discontinuities localized in numerical integration, time delays in the equations are chosen as integer multiples of the time step of integration.

Another important feature of DDEs is that the characteristic functions are not polynomials (as in the case of ordinary differential equations ODEs without delays) but transcendental equations. For example, consider the simplest delayed differential equation

$$\dot{x}(t) = x(t - \tau) \tag{2.27}$$

If $\tau = 0$, the simplest ODE reads $\dot{x}(t) = x(t)$ and the canonical way to solve this is to propose an exponential function $x(t) = e^{\alpha t}$ and solve the characteristic polynomial equation $P(\alpha) = 1 - \alpha = 0$ with the only solution $\alpha = 1$. However, if in this simple differential equation $\tau \neq 0$, the situation changes drastically. Proposing an exponential function $x(t) = e^{\alpha t}$ and replacing it in Eq. (2.27) gives

$$\alpha x(t) = x(t - \tau) = e^{\alpha(t-\tau)} = e^{-\alpha\tau} x(t), \tag{2.28}$$

which means that in order to get α, it is necessary to solve a trascendental equation $P(\alpha) = \alpha - e^{-\alpha\tau}$.

In conclusion, delayed differential equations entail their difficulties and constitute a field of research by themselves. Despite their technical difficulties, theories based on DDEs have the huge advantage of the economy in the description, as they reduce a complex chain of events to only one parameter, the time delay τ. In the following, we just take from this field of research some of the known elements to be able to solve the equations that govern the dynamics of the system of mobile delayed-coupled oscillators that we present in the next chapter. For more extensive descriptions of delayed systems we refer the reader to the litera-

ture: for a mathematical treatment of delayed equations [74, 78, 79], for numerical methods for solving delayed differential equations [77], for examples of works on complex systems that include time delays [80] and for time delays in biological systems [75, 76].

Chapter 3

Phase-oscillator description of mobile delayed-coupled genetic oscillators

As described in the previous chapters, the vertebrate segmentation clock is thought to be a population of coupled genetic oscillators working in each cell in the PSM. Oscillators are coupled through Delta-Notch intercellular communication mechanism, which requires cell-cell contact and involves synthesis and transport of signaling macromolecules within each cell. These characteristics of Delta-Notch coupling can be included in theoretical descriptions by considering local coupling with coupling delays. Besides this delayed local coupling, cells move within the PSM, with high random mobility occurring at the tailbud. In the last chapter we describe theories that include either mobility or coupling delays, and showed that these have important effects on the dynamics of coupled oscillators. Although both elements are present in the biological system, theories that incorporate both coupling delays and mobility of the oscillators are lacking. In this chapter we propose a general theory that brings together these two key ingredients of the biological system. In the following chapters we consider particular cases of this theory and study different aspects of the dynamics.

We consider a phase-oscillator description based on the Kuramoto model in the lattice, Chapter 2. As already explained, these descriptions provide a paradigmatic framework to study collective dynamics and in particular synchronization.

In our model, each phase oscillator is thought to describe the autonomous oscillator contained in each individual cell. We consider that the biochemical details of how these individual oscillations are sustained are superfluous for the question we ask, where the relevant components are the timescales of synchronization, mobility and coupling delays. We thus describe the cyclic protein levels in one cell only with a phase. In this scenario, cells with similar protein levels have similar phases. Over this basis we incorporate the two features of the biological system whose interplay we are interested in studying: mobility of the oscillators and delayed coupling. Mobility is introduced as a stochastic exchange of positions of nearest-neighbor oscillators in the lattice, Section 2.2. We already mentioned that for instantaneous coupling lattice models in terms of phase oscillators can capture the effects of mobility on collective dynamics, showing similar results than off-lattice models and than models with more detailed descriptions of the individual oscillations in the segmentation clock. Delayed coupling is addressed through explicit delayed evaluation of the phases in the coupling terms, as described in Section 2.3. Previous results show that a phase description in terms of coupled phase oscillators with delayed coupling is sufficient to address the effects of delayed coupling on patterning and on synchronization in a more general way, Sections 1.3 and 2.3. Taken together, these previous results suggest that a description as the one presented in this section should capture the effects that mobility and coupling delays have on the oscillatory dynamics when considered together.

Description of mobility. We consider a system of N identical phase oscillators, placed on a one-dimensional lattice of N sites. Each phase oscillator with phase θ_i has a position x_i that is constrained to the position of a lattice site $x_i = k\,\Delta x$ with $k = 0, \ldots, N-1$. The lattice spacing Δx can be thought to be proportional to the cell diameter but does not play a role in the dynamics. In the following we set $\Delta x = 1$ without loss of generality. Positions of the oscillators are thus constrained to integers $x_i = 0, \ldots, N-1$. Mobility is described by letting the oscillators exchange positions with their nearest-neighbors, Section 2.2. The stochastic exchange of positions is modeled as a Poisson process. Each pair of neighboring oscillators can exchange positions with a rate $\lambda/2$ per unit time, Figure 3.1. At each time point, only one exchange event can take place. Exchange events have a waiting time t_e that is drawn from the corresponding exponential

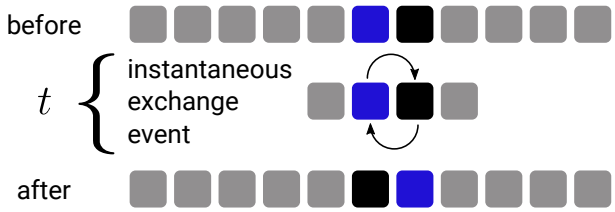

Figure 3.1: Mobility of oscillators in the one-dimensional lattice. Each pair of oscillators has a probability $\lambda/2$ of exchanging positions. Positions of the oscillators only change at random instants of time when an exchange event occurs.

distribution. The average waiting time is proportional to the inverse of the mobility rate λ^{-1}, see Appendix A. The state of oscillator i, with $i = 1, \ldots, N$, is described by its phase $\theta_i(t)$ and its position $x_i(t)$ in the lattice. The position $x_i(t)$ is piecewise-constant: the value of $x_i(t)$ changes only when oscillator i exchanges its position. As a result of the stochastic exchange of positions each oscillator performs a random walk in the lattice and after a sufficient amount of time it could be sitting at any site.

Description of delayed communication. As already explained, the complexity of molecular events taking place in Delta-Notch signaling, Figure 3.2(a), can be captured in theoretical models by including discrete delays in the coupling function. Delta-Notch coupling involves two conceptually different processes that could lead to delays in the interaction. On the one hand, the cell sending the signal needs to synthesize and transport Delta molecules form the nucleus to the membrane and make the necessary modifications for them to become active ligands for Notch receptors, red pathway in Figure 3.2(a). On the other hand, once the interaction takes place, the cell receiving the signal needs to process this signal. This processing requires cleavage and transport of the NICD from the membrane to the nucleus, where it affects transcription of the target oscillating genes, green pathway in Figure 3.2(a). To capture this complexity of Delta-Notch signaling in the context with mobility we split the delayed interaction into two explicit time delays, τ_{out} and τ_{in} , Figure 3.2(b). The *outgoing* or *signal-sending* delay τ_{out} accounts for the time it takes to the cell to prepare and export the signal. Differently, the *incoming* or *signal-processing* delay τ_{in} accounts for the time the cell needs to process the received signal, after the interaction takes place. With these considerations, the total time delay in the interaction is $\tau = \tau_{\text{out}} + \tau_{\text{in}}$. Considering such a description in terms of a delayed interaction has a cost,

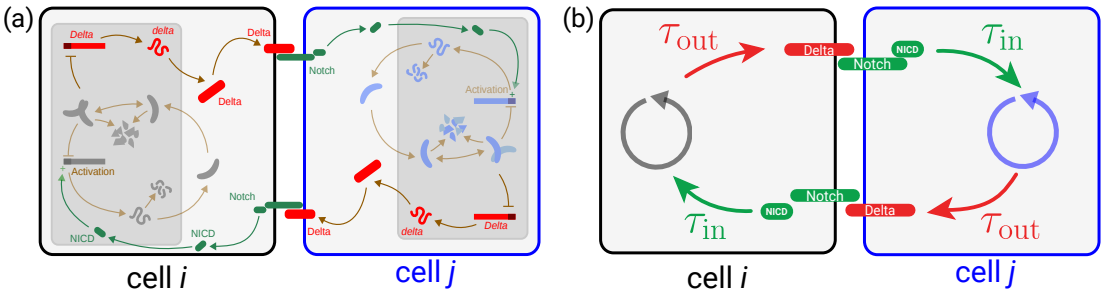

Figure 3.2: Schematic representation of the coupling between neighboring oscillators. The complexity of the communication mechanism (a) is captured in the model (b) by considering two different time delays τ_{out} and τ_{in} , which account for preparing the signal to send and processing the signal received, respectively.

as we explained in Section 2.3, as it involves solving harder, infinite-dimensional equations. However, this description has the great advantage of reducing the complexity of the communication mechanism to only two parameters, the time delays τ_{out} and τ_{in} , which set well defined timescales. This allows as to focus on the question we aim to address, which is how the interplay between the different timescales present in the system affects the collective dynamics of the coupled oscillators.

In summary, in between the exchange events caused by mobility, the phase dynamics is governed by

$$\dot{\theta}_i(t) = \omega + \frac{\kappa}{n_i} \sum_{j \in V_i(t-\tau_{\text{in}})} \sin\left(\theta_j(t - \tau_{\text{in}} - \tau_{\text{out}}) - \theta_i(t)\right) \tag{3.1}$$

where ω is the autonomous frequency of the oscillators, considered identical, and

$$V_i(t) = \{j \text{ such that } |x_j(t) - x_i(t)| = 1\}$$

is the neighborhood of oscillator i, which only includes nearest-neighbors. Communication between oscillators is described by the sinusoidal coupling term. In the equations, κ is the coupling strength and n_i is the number of neighbors of oscillator i. In the biological system, the coupling strength can be related to the amount of ligands and receptors that are available at the cell membrane [38,51,53]. The n_i neighbors of cell i would be the cells that are close enough to interact with it via the Delta-Notch pathway. The coupling includes a summation over the neighborhood at the time of the interaction $V_i(t - \tau_{\text{in}})$ that is not considered in the models introduced in previous sections. This is because mobility can provoke

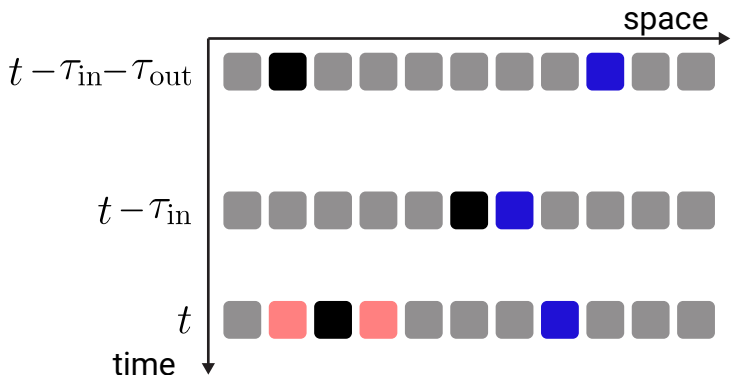

Figure 3.3: Mobile delayed-coupled oscillators. The phase evolution of an oscillator at time t, black square, is affected by the signals that it receives from the oscillators that were its neighbors at an earlier time $t-\tau_{\text{in}}$. One of these is marked blue. In contrast, neighbors of the black oscillator at time t are painted pink. to illustrate that it could not be a neighbor of the black oscillator at time t, due to mobility. Note that neighborhoods change because oscillators move, exchanging neighbors over time. In addition, the signal sent by the blue oscillator at time $t-\tau_{\text{in}}$ has information about its phase at an earlier time $t-\tau_{\text{in}}-\tau_{\text{out}}$.

the neighborhood of one oscillator at time $t-\tau_{\text{in}}$ to be different from the one at present time t. We use open boundary conditions: the oscillators at both ends of the lattice interact only with their single left or right neighbors respectively and can only exchange positions with them. This choice of open boundary conditions is a better description of the conditions in the segmentation clock tissue than periodic boundary conditions and at the same time prevents the formation of stable twisted states that may appear for periodic boundaries [61, 81].

Altogether, the phase dynamics in the system with mobility and coupling delays can be understood as schemed in Figure 3.3. Consider an arbitrary oscillator i that at time t is in position x_i in the lattice, black square in the bottom row. This oscillator changes its phase according to the equation for $\dot{\theta}_i(t)$, Eq. (3.1), which includes coupling terms that consider the signal received from neighboring oscillators. However, because there is a time delay due to the time τ_{in} that the cell needs to process the received signals, the received signals at time t had been sent at a previous time $t-\tau_{\text{in}}$. Thus, the change in phase of oscillator i at time t is affected by the signals sent at a previous time $t-\tau_{\text{in}}$. The oscillators that sent the signals were neighbors of oscillator i at that previous time, for example the blue square in the middle row. Due to mobility, a neighbor of oscillator i sending a signal at time $t-\tau_{\text{in}}$, blue square, can differ from the neighbors of oscillator i at the current time t, pink squares in bottom row. Thus, in the differential equations

for the phase evolution, neigborhoods V_i need to be evaluated at time $t-\tau_{\text{in}}$. In addition to this, the signals sent by these neighboring cells need to be prepared a time τ_{out} before the interaction, because cells need a time τ_{out} to export the signal. Then, the neighbors phases θ_j in the coupling terms are evaluated at an earlier time $t - \tau_{\text{in}} - \tau_{\text{out}}$ in Eqs. (3.1).

In summary, the general model presented incorporates mobility together with coupling delays, combining an stochastic exchange of positions with the evolution of the phases given by the set of delayed coupled differential equations (3.1). The total delay τ usually considered in the delayed coupling theories here has two contributions $\tau = \tau_{\text{in}} + \tau_{\text{out}}$, to consider delays in the mobile context. This brings the necessity to include a delayed neighborhood to account for mobility together with processing times. This delayed neighborhood is a novel feature of this theory and is not present in previous models of non-mobile oscillators with delayed coupling, as in those models neighbors do not change.

Our description includes five independent timescales related to phase dynamics ω^{-1} and κ^{-1}, mobility λ^{-1}, and coupling delays τ_{out} and τ_{in} . The dynamics of the system will result from the interplay between these timescales. We are interested in studying the interplay between mobility and coupling delays. To this end and for simplicity, in the remainder of this Thesis we fix the other parameters. We define the units of time such that the autonomous frequency $\omega = 1$ for all the oscillators, which sets the autonomous period to $T = 2\pi$. The interplay of mobility and phase dynamics due to coupling is characterized by the ratio λ/κ. In the following, we fix $\kappa = 0.1$ and only vary λ. The chosen relatively small value of κ avoids an otherwise larger tilt in the collective frequency curves which would provide more multistability in the synchronized solutions, see Figure 2.4. This is consistent with previous estimations of the coupling strength [38, 51]. We set the system size $N = 100$, which is of the order of magnitude of the linear dimensions of the tailbud.

Results presented in the next chapters are obtained from numerical simulations and, when possible, also from analytical calculations. To perform numerical simulations of the system of mobile delayed-coupled oscillators just described, we developed an algorithm that combines numerical integration of the delayed coupled differential equations (3.1) with the stochastic exchange of positions. Within each simulation, numerical integration of the delayed differential equations is carried out with an integration scheme with fixed time step. Time delay values are

always fixed to integer multiples of the time step of integration. The stochastic exchange of positions is implemented using an approximation of the Gillespie algorithm for discrete time intervals [48,82]. Exchange events always occur at time points that are integer multiples of the integration step. A detailed explanation of the numerical methods is provided in appendix A. In brief, the algorithm iterates the following steps:

1. Obtain the amount of time steps until the next exchange event n_e as explained in apprendix A, and also randomly choose which pair of oscillators will exchange positions at that time point.

2. Integrate n_e time steps of Eq. (3.1), with fixed positions for all the oscillators in the lattice.

3. Update positions and neighborhoods affected by the exchange event and go back to step 1.

In the next chapters, we study different particular cases of the general theory presented here. We explore different mobility scenarios and different values of the delay timescales. For simplicity, we consider only one or the other contribution to the time delay τ_{out} or τ_{in} but not both together. A characterization of the general system with both delays should be interesting but complex if the effects of each delay is not addressed separately first. We leave this for future work. We start considering only the outgoing time delay τ_{out} in Chapter 4. This corresponds to setting $\tau_{\text{in}} = 0$ in Eqs. (3.1). There are two reasons why we start with this situation. First, this simplified model does not include a delayed neighborhood and thus it is more accessible as a first step to compare our delayed-coupled model for mobile oscillators with usual delayed-coupled models without mobility. Second, it was indicated that sending-signals timescales in the vertebrate segmentation clock are larger than those of processing signals, $\tau_{\text{out}} \gg \tau_{\text{in}}$ [51]. With the biological system as the main motivation, in Chapter 4 we explore this time delay in specific ranges within the first and second stable branches for synchronization, Figure 4.1. We focus on the dynamics of the system as it approaches the synchronized solutions, what from now on we call synchronization dynamics.

We next explore a wider range of delay values in chapters 5 and 6 both for τ_{in} and τ_{out} alternatively. When further exploring parameter space, we encounter that the system of mobile delayed-coupled oscillators can exhibit a wide repertoire of distinct dynamical states on its way to synchronization. Remarkably,

this repertoire includes complex spatio-temporal patterns where groups of synchronized oscillators coexist with other incoherent groups within the same state. These patterns in which order and disorder coexist in systems of identical oscillators are known as chimera states and represent a paradigm of dynamical symmetry breaking of great interest in the field of dynamical systems. Because of the wide variety of different patterns that the system shows together with chimera states, we find the necessity of distinguishing and classifying between these states. Because of the mixed nature of chimera states, reliable detection and classification of chimera states posses a challenge. In Chapter 5 we develop a classification method for dynamical states that is capable of distinguishing chimera states from the variety of other states that the system of mobile delayed-coupled oscillators exhibits. With this tool at hand, in Chapter 6 we make an exhaustive analysis of these states and their occurrence in parameter space.

In Chapter 7 we go back to the dynamics of the system as it approaches synchronization addressed in Chapter 4. In Chapter 4 we address synchronization dynamics mostly in the linear regime, where the system is already close to synchronization. In Chapter 7 we ask to what extent results obtained in a linear regime can be used to analyse also the nonlinear regimes, where the system is far from synchronization.

Chapter 4

Synchronization dynamics of mobile oscillators in the presence of coupling delays

In this chapter we focus on the dynamics of the system of mobile, delayed-coupled oscillators close to complete synchronization. The effects of mobility and coupling delays on synchronization dynamics of coupled phase oscillators have been addressed separately in previous sections. Here we study how mobility affects synchronization dynamics in the presence of coupling delays. Results presented in this chapter are summarized in a manuscript that is currently in preparation and will be sent for publication soon.

In the previous chapter we introduced a general description of mobile delayed-coupled oscillators. As we discussed there, due to mobility, the delay in the coupling τ has a double contribution given by an outgoing delay τ_{out} and an incoming delay τ_{in} , $\tau = \tau_{\text{out}} + \tau_{\text{in}}$

$$\dot{\theta}_i(t) = \omega + \frac{\kappa}{n_i} \sum_{j \in V_i(t-\tau_{\text{in}})} \sin\left(\theta_j(t - \tau_{\text{in}} - \tau_{\text{out}}) - \theta_i(t)\right). \tag{4.1}$$

The outgoing contribution τ_{out} accounts for the time that an oscillator needs to prepare and export the signal to send to its neighbor. In the vertebrate segmentation clock, this represents the time that a cell needs to synthesize Delta ligands

and export them to the cell membrane, and is thought to be the main contribution to time delays in communication in the biological system [50,51], Figure 3.2. In this chapter we consider the dynamics of system (4.1) in the presence of only this outgoing contribution to the coupling delay $\tau = \tau_{\text{out}}$, with $\tau_{\text{in}} = 0$

$$\dot{\theta}_i(t) = \omega + \frac{\kappa}{n_i} \sum_{j \in V_i(t)} \sin\left(\theta_j(t-\tau) - \theta_i(t)\right) \tag{4.2}$$

with

$$V_i(t) = \{j \text{ such that } |x_j(t) - x_i(t)| = 1\}\,.$$

One way to examine the underpinnings of the collective organization of the segmentation clock is to perturb coupling and observe the dynamics away from the synchronized state [38,39,51], Section 1. Here we analyse the dynamics of system (4.2) as it approaches in-phase synchronized solutions. Eqs. (4.2) include coupling delay in the usual way, where oscillators are coupled to the state of their neighbors at a past time $t - \tau$ but the neighborhoods V_i are evaluated at the present time t, Section 2.3. However, because there is mobility, these neighborhoods could be different from those at past times. Thus, the presence of mobility together with coupling delays implies that each oscillator tries to synchronize to the ghost of its neighbors at a past time in which they may not have been neighbors.

In-phase synchronized solutions of system (4.2)

$$\theta_i(t) = \Omega t \quad \forall i \tag{4.3}$$

always exist, as can be confirmed by taking the time derivative of the ansatz (4.3) and inserting it in Eq. (4.2)

$$\Omega = \omega + \frac{\kappa}{n_i} \sum_{j \in V_i(t)} \sin\left(\Omega t - \Omega\tau - \Omega t\right), \tag{4.4}$$

which leads to the trascendental equation for the collective frequency of these in-phase synchronized solutions, Eq. (2.14)

$$\Omega = \omega - \kappa \sin(\Omega\tau). \tag{4.5}$$

For non-mobile oscillators we saw in Section 2.3 that a stability criterion defines

multiple stable branches of solutions for in-phase synchronized states. These stable branches correspond to delay values such that $\kappa \cos(\Omega\tau) > 0$, Eq. (2.16). Because mobility is described in our model as an exchange of positions between neighboring oscillators, it has no effect on the in-phase synchronized solutions once they are reached. Thus, we expect similar stability conditions for these solutions as those for non-mobile oscillators, Figure 4.1. In contrast, antiphase solutions are not expected, as the exchange of positions between neighboring oscillators could destabilize those patterns.

We already mentioned a delayed coupling theory of vertebrate segmentation that was fitted to experimental data in zebrafish embryos [51]. Somitogenesis period measurements from different mutants of Delta-Notch pathway is consistent with the presence of coupling delays, Figure 2.7. The theory together with the experimental data, pointed the coupling delay value in the second branch of stability for synchronized solutions, Figure 2.7(b,c). Here we explore a range of values of the coupling delay τ in the first and the second stable branches, Figure 4.1. For non-mobile oscillators there are regions of bistability where the antiphase solutions are also stable. For the moment we avoid delay values that fall inside those bistability regions, for reasons that will become clear later.

4.1 Spatial phase correlations

The effects of mobility on synchronization dynamics of phase oscillators can be captured by the spatial phase correlations introduced in Section 2.1

$$\rho_d(t) = \langle \cos\left[\vartheta_{k+d}(t) - \vartheta_k(t)\right] \rangle_k \tag{4.6}$$

where $\vartheta_k(t)$ is the phase at site k of the lattice at time t, d is the dimensionless distance between lattice sites and $\langle ... \rangle_k$ indicates the average over sites k with $k = 0, ..., N - 1 - d$. Correlations ρ_d take values near $\rho_d \approx 1$ when sites at distance d have similar phases on average, $\rho_d \approx -1$ when sites at distance d are in antiphase and $\rho_d \approx 0$ if phases of d-distant sites are uncorrelated. The completely synchronized state is thus characterized by a value of correlations $\rho_d \approx 1$ for all distances d.

In Figure 4.2 we show the evolution of spatial correlations for three different values of the mobility to coupling ratio λ/κ (columns) and three different

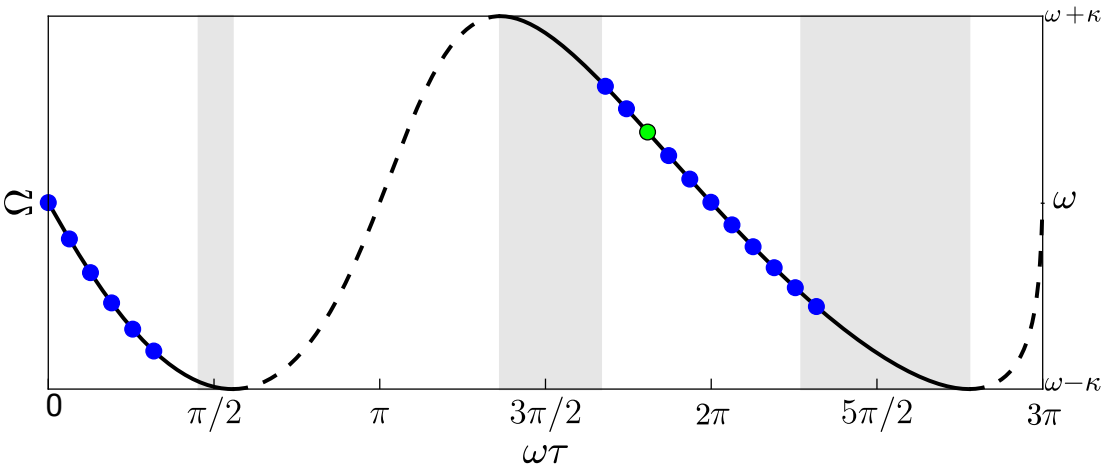

Figure 4.1: Sampled values of the coupling delay for which we explore synchronization dynamics. Values are indicated with dots over the parametric plot of the collective frequency for in-phase synchronized solutions. Solid lines indicate expected stable solutions while dashed lines indicate unstable ones. All values of the time delay explored lay in the first and second stable branches for the in-phase synchronized solutions. The green dot indicates the sampled value that is closest to the value indicated for the biological system $\tau \sim 0.9\,(2\pi/\omega)$ [51]. Shadowed regions indicate the regions of bi-stability between the in-phase and the antiphase solutions for non-mobile oscillators. For the moment we avoid sampling delay values in those regions.

values of the delay τ (rows). In all cases we start with disordered states composed of randomly distributed phases. Comparing columns in Figure 4.2 we see that synchronization occurs earlier for larger mobility. For zero and low mobility, correlations between close sites increase faster than correlations between distant sites, first two columns in Figure 4.2. This difference between short and long range correlations indicates that the system forms local ordered patterns in which close sites have similar phases while distant sites do not. For larger values of mobility all correlations increase simultaneously indicating that local ordered patterns do not occur, last column in Figure 4.2. In this latter case, the time for which all correlations approach $\rho_d(t) \approx 1\ \forall d$ is shorter, see reference line at $t = 300$ in Figure 4.2. In addition, comparing rows in Figure 4.2 we see that this qualitative behavior is also observed with increasing coupling delays. Taken together, these results show that mobility can speed up synchronization even in the presence of coupling delays. Given that both mobility and delays are present in the vertebrate segmentation clock, it is important to know that mobility has an effect on synchronization even when coupling delays are present.

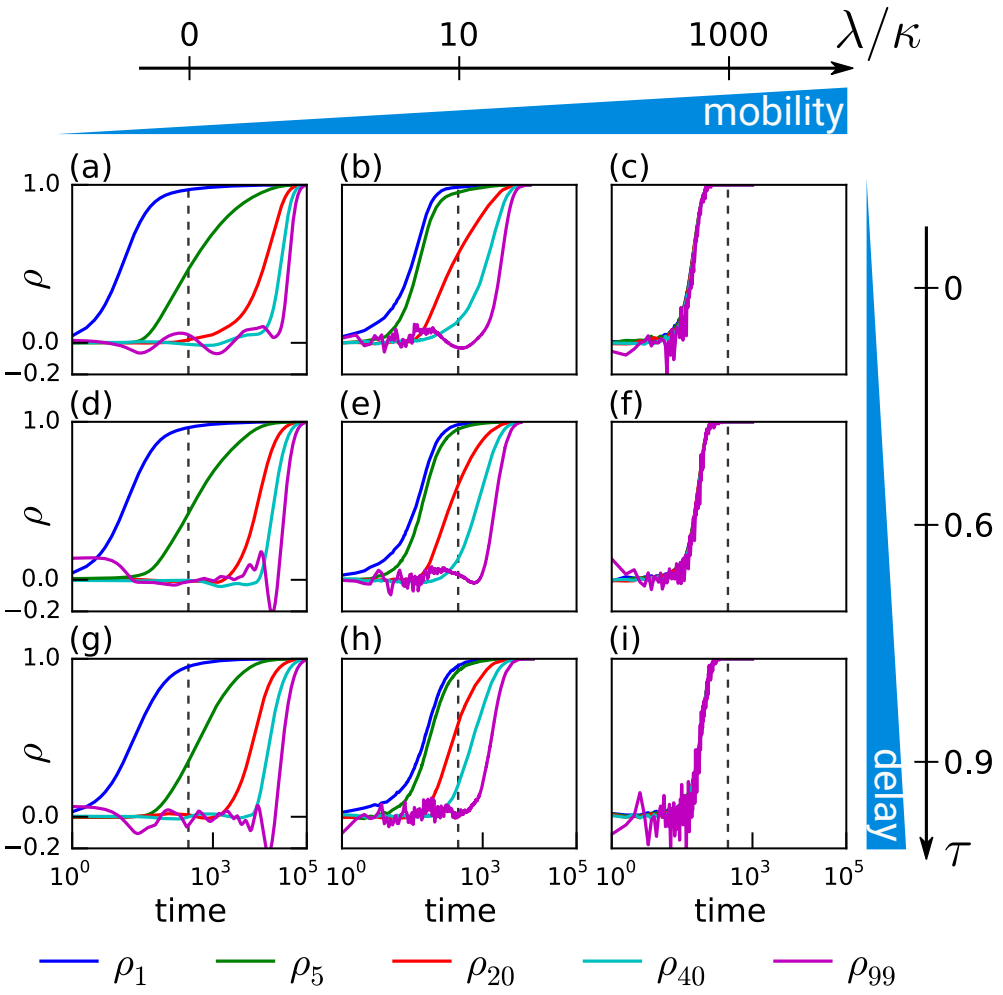

Figure 4.2: Time evolution of the spatial phase correlations between lattice sites, for different mobility rates (columns) and different delay values (rows). (a) $\lambda/\kappa = 0$, $\tau = 0$, (b) $\lambda/\kappa = 10$, $\tau = 0$, (c) $\lambda/\kappa = 100$, $\tau = 0$, (d) $\lambda/\kappa = 0$, $\tau = 0.6$, (e) $\lambda/\kappa = 10$, $\tau = 0.6$, (f) $\lambda/\kappa = 100$, $\tau = 0.6$, (g) $\lambda/\kappa = 0$, $\tau = 0.9$, (h) $\lambda/\kappa = 10$, $\tau = 0.9$, (i) $\lambda/\kappa = 100$, $\tau = 0.9$. A dashed vertical line is drawn at $t = 300$ in all panels for reference. We show the averaged evolution over 64 realizations.

4.2 Characteristic relaxation time

We aim to quantify the effects of mobility on the time the system needs to reach synchronization, and to compare these effects with those of the non-delayed case previously analyzed in [60], Figure 4.2(a-c). To this end, we look at the characteristic time T_c of the late exponential relaxation of the system [60]. This relaxation is better observed in the behavior of $1-\rho$, Figure 4.3. We observe that after a transient, all correlations enter an exponential regime characterized by $1-\rho \propto e^{-t/Tc}$. This behavior is observed for all values of the coupling delay studied.

Looking at the first two columns in Figure 4.3, the evolution of the correlations for different lengths d only differ in the early evolution. Once they enter the exponential regime, the characteristic time T_c is the same for all correlation lengths d. However, short correlations enter this exponential regime earlier than long range correlations. This reflects the fact that the different spatial modes in the local order patterns have different lifetimes. When modes with shorter wavelengths have disappeared, the relaxation of the system is dominated by the longest spatial mode. The characteristic time T_c reflects the relaxation time of the longest spatial mode.

For non-mobile oscillators with open boundary conditions, the longest spatial mode has a sinusoidal shape $\sim \cos(\pi x/N)$. The relationship between the eigenvalue σ that dictates the relaxation of this mode and the characteristic time T_c has a factor 2 due to the expansion of the cosine in the definition of the correlations, Eq. (4.6)

$$T_c^{-1} = 2\sigma. \tag{4.7}$$

This relationship can be obtained considering a small perturbation to the synchronized state $\varphi_k(t)$, solution of the linearized equations, written as the longest spatial mode with a decaying amplitude $\propto e^{-\sigma t}$.

For mobile oscillators, the relationship between σ and T_c is

$$T_c^{-1} = 2\sigma + \pi^2\lambda/N^2. \tag{4.8}$$

This expression for T_c can be derived considering how a single exchange event affects relaxation of the longest spatial mode [60]. The first steps of the derivation consist in expanding a perturbation $\varphi_k(t)$ of the synchronized solution in the basis

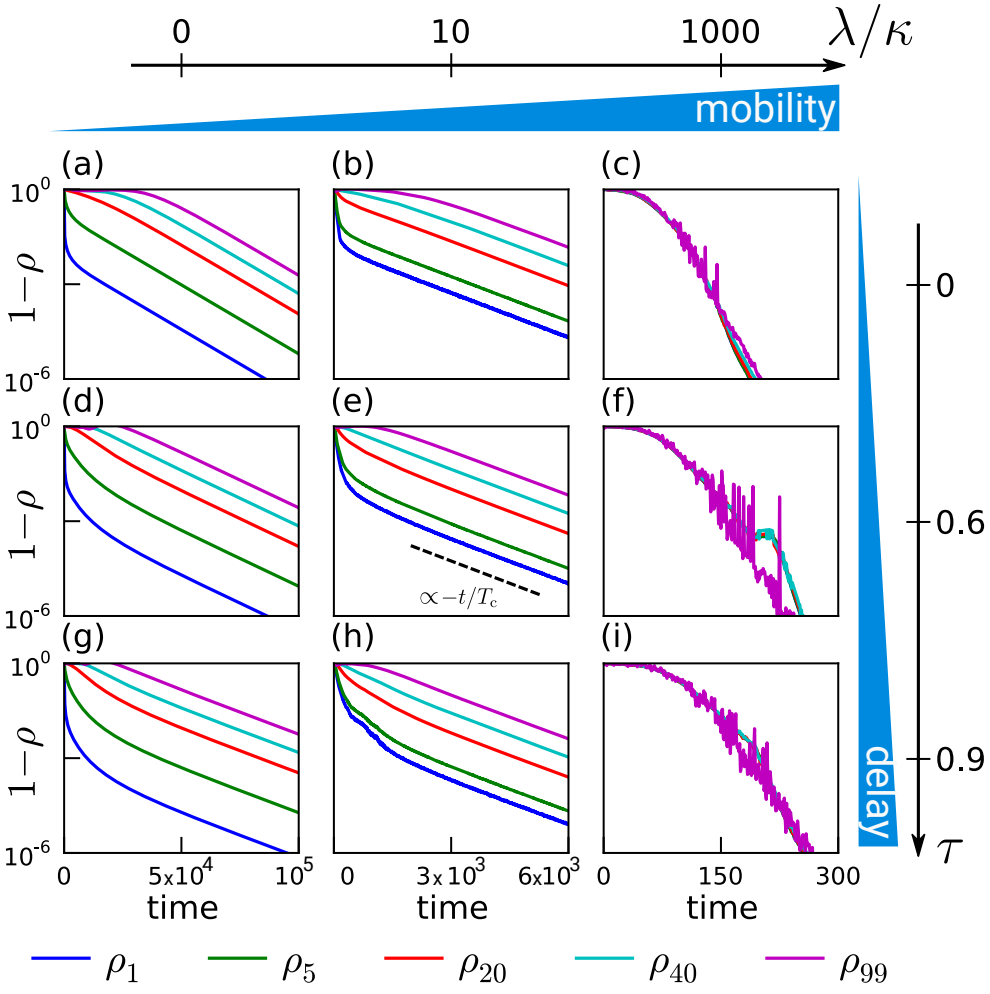

Figure 4.3: Time evolution of $1-\rho$, for the same mobility and delay parameters as in Figure 4.2. The characteristic time T_c is defined as the slope at the late exponential regime.

of eigenvectors of the linearized system. The effects of the exchange event can be encompassed in the time dependence of the coefficients in this expansion. These time dependent coefficients can be then obtained writing the perturbation due to the single exchange event in the basis of eigenvectors of spatial modes. This derivation of Eq. (4.8) relies on the fact that the shortest spatial mode induced by the exchange of positions between oscillators relaxes much quicker than the longest spatial mode.

For instantaneous coupling $\tau = 0$, the relaxation rate σ depends on the coupling strength and system size as $\sigma \approx \kappa\pi^2/2N^2$. Substituting this in Eq. (4.8) gives

$$T_c \approx \frac{N^2}{\pi^2\,\kappa}\,\frac{1}{1+\lambda/\kappa}. \tag{4.9}$$

Expression (4.9) suggests that the onset of the effects of mobility on T_c occur for $\lambda/\kappa \sim 1$. These effects are present up to the onset of mean-field behavior at $\lambda/\kappa \sim 2N^2/\pi^2$. Above this mean-field onset, each oscillator can effectively interact with every other oscillator in the lattice before its phase changes significantly [60].

Below we derive an analytical expression for the characteristic time T_c for delayed nearest-neighbors coupling. We hypothesize that relaxation of the longest spatial mode is affected by single exchange events in the same way as in the absence of coupling delays, that is Eq. (4.8) is still valid. In contrast, the relaxation due to coupling is modulated by delay. To extend Eq. (4.9) for delayed coupling, we need to compute the relaxation rate σ of the slowest spatial mode for coupled phase oscillators with delayed coupling. In the absence of mobility, the characteristic equation is

$$\gamma - \sigma = \gamma u e^{\sigma\tau} \tag{4.10}$$

where u is the eigenvalue of the slowest spatial mode [68].

The relaxation rate for the longest spatial mode σ should become small for a large system size N. Then, for sufficiently small delay $\sigma\tau \ll 1$, we expand the exponential function in Eq. (4.10) and neglect terms of order $O\left(\sigma^2\tau^2\right)$

$$\gamma - \sigma \approx \gamma u\left(1+\sigma\tau\right). \tag{4.11}$$

Solving this equation with respect to σ we obtain the relaxation rate of the longest

spatial mode

$$\sigma \approx \frac{\gamma\,(1-u)}{1+\gamma u\tau}. \tag{4.12}$$

Substituting expression (4.12) in (4.8),

$$T_{\mathrm{c}} = \frac{N^2}{\pi^2}\frac{1}{\dfrac{2N^2}{\pi^2}\dfrac{\gamma\,(1-u)}{1+\gamma u\tau}+\lambda}. \tag{4.13}$$

Here u is the eigenvalue of the longest cosine mode for 1D lattice with open boundary. For $N \gg 1$ it can be approximated as $u \approx 1-\pi^2/2N^2$. Replacing this in Eq. (4.13) and rearranging terms,

$$T_{\mathrm{c}} = \frac{N^2}{\pi^2\kappa_e}\frac{1}{1+\lambda/\kappa_e}, \tag{4.14}$$

with

$$\kappa_e \equiv \frac{\gamma}{1+\gamma u\tau}. \tag{4.15}$$

Eq. (4.14) looks similar to Eq. (4.9) for non-delayed coupling except that the coupling constant κ is replaced by κ_e. Replacing the values of u and γ in (4.15) and neglecting higher order $O(N^2)$ terms,

$$\kappa_e \approx \frac{\kappa\cos(\Omega\tau)}{1+\tau\kappa\cos(\Omega\tau)}. \tag{4.16}$$

Thus, delayed coupling alters synchronization dynamics by renormalizing the coupling strength κ to an effective coupling strength κ_e, which is a function of the coupling delay, Eq. (4.16).

Finally, by inserting this expression in (4.14) and defining

$$f(\kappa,\tau) \equiv \frac{\kappa}{\kappa_e} = \frac{1+\tau\kappa\cos(\Omega\tau)}{\cos(\Omega\tau)} \tag{4.17}$$

we arrive to an analytical expression for the characteristic relaxation time in the presence of mobility and coupling delay

$$T_{\mathrm{c}}(\lambda,\tau) = \frac{N^2}{\pi^2\kappa}\frac{1}{1/f(\kappa,\tau)+\lambda/\kappa}. \tag{4.18}$$

Comparing this result with Eq. (4.9) explicitly shows that the effect of coupling

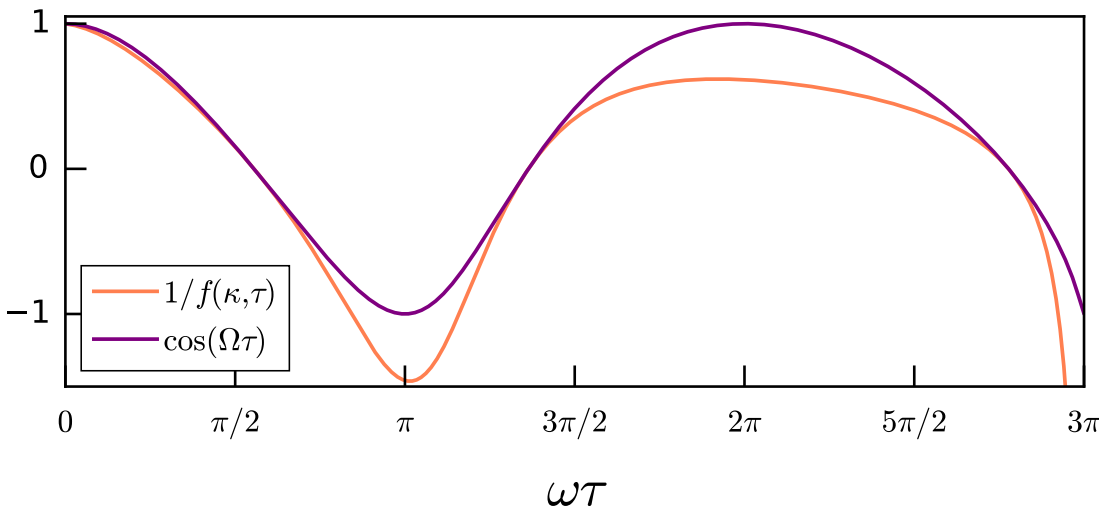

Figure 4.4: The function that determines the onset of non-local behavior, $1/f(\kappa,\tau)$ in Eq. (4.17), together with $\cos(\Omega\tau)$.

delays can also be interpreted as a shift in the onset of the effects of mobility determined by $1/f(\kappa,\tau)$, Figure 4.4.

To assess the validity of this analytical result, we obtain numerical values of T_c performing a linear fit of the long-term behavior of the evolution of $1-\rho_d$ in log-linear scale, see Figure 4.3. This long-term behavior corresponds to times greater than a value of $t=t_L$ for which we are sure that the system has entered the exponential relaxation. For each combination of parameters, we choose this time as $t_L = 0.85t_f$, where t_f is such that $1-|Z(t_f)| \leq 10^{-10}$ in most simulations and $t_f = 10^5$ in the long simulations with very low or zero mobility. For each value of the mobility and delay explored, we fit each of the average correlations shown and then averaged the value of T_c for the five values of d shown in the figure. As we show in Figures 4.5 and 4.6, numerical simulations are in very good agreement with the analytical result, Eq. (4.18).

4.3 Dynamical regimes

Considering Eq. (4.18), different dynamical regimes can be identified for different mobility to coupling ratios λ/κ. Below, we explore the λ/κ axis and classify the different dynamical regimes.

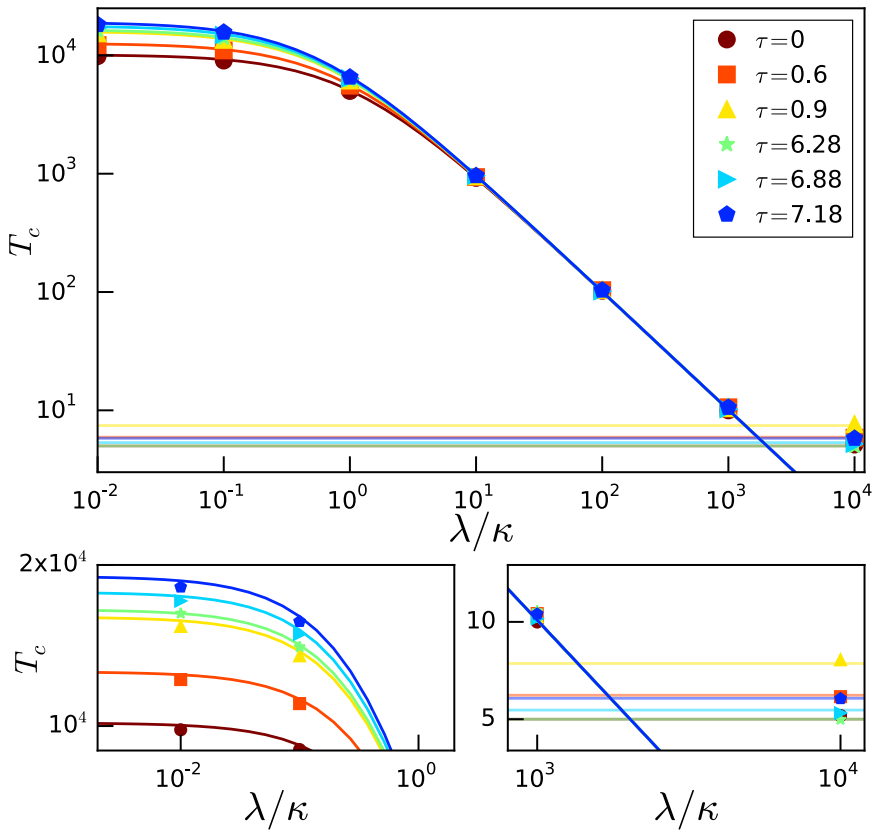

Figure 4.5: Characteristic time T_c vs. mobility to coupling ratio λ/κ, for six different delay values: $\tau = 0$ bordeaux, $\tau = 0.6$ red, $\tau = 0.9$ yellow, $\tau = 6.28$ green, $\tau = 6.88$ light blue and $\tau = 7.18$ blue. Color markers are numerical simulations and solid lines are theoretical values, Eq. (4.18). Horizontal lines correspond to theoretical values of T_c for large mobility in the mean-field regime Eq. (4.30). Left and right bottom panels display zoom-ins for small and large mobility respectively, to emphasize the dependence on delay values.

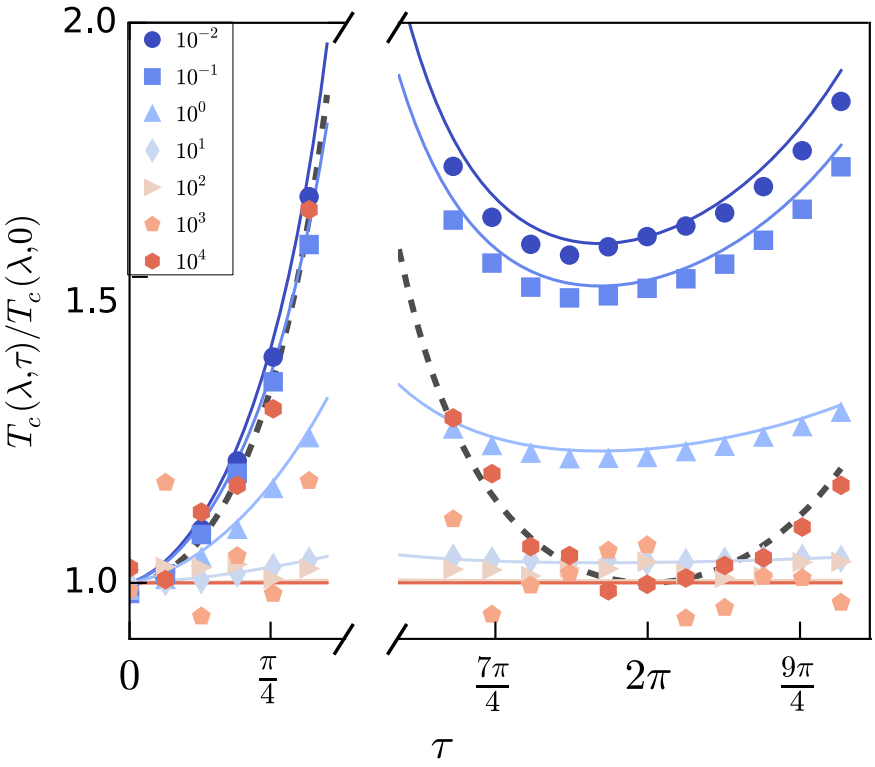

Figure 4.6: Characteristic time T_c vs. coupling delay τ, for different mobility regimes. Color markers are numerical simulations, solid lines are analytical values from Eq. (4.18) before the onset of mean-field behavior and dashed lines are analytical values for mean field behavior, Eq. (4.30). Symbols correspond to different values of λ/κ as indicated in the plot legend.

4.3.1 Non-mobile regime

Equation (4.18) suggests that mobility does not affect synchronization dynamics in the non-mobile regime defined by $\lambda/\kappa \ll 1/f(\kappa,\tau)$. In contrast, coupling delay strongly affects the relaxation time T_c in this regime, bottom left panel in Figure 4.5. The relative characteristic time $T_c(\lambda,\tau)/T_c(\lambda,0)$ reveals the fold change values of T_c as a function of τ, Figure 4.6. In this non-mobile regime, T_c significantly increases with increasing delay, almost duplicating its value at $\tau = 0$ for delays near the stability boundaries, blues in Figure 4.6. Simulations are in good agreement with the analytical result Eq. (4.18), solid coloured lines in Figure 4.6. In this non-mobile regime we can approximate T_c as

$$T_{co}(0,\tau) = \frac{N^2}{\pi^2\kappa} f(\kappa,\tau). \tag{4.19}$$

A rescaling of T_c in Eq. (4.18) by Eq. (4.19),

$$T_{c|co}(\lambda,\tau) \equiv \frac{T_c(\lambda,\tau)}{T_{co}(0,\tau)} = \frac{1}{1+(\lambda/\kappa)f(\kappa,\tau)}, \tag{4.20}$$

collapses the curves in Fig. 4.5 within this regime, Figure 4.7(a).

The effects of mobility become appreciable when

$$\lambda/\kappa \sim 1/f(\kappa,\tau) \tag{4.21}$$

in Eq. (4.18), marking the end of the non-mobile regime. The onset of the effects of mobility on synchronization is modulated by the coupling delay through the function $1/f(\kappa,\tau)$, Figure 4.4. The mobility rate that can produce a non-local behavior depends on the value of the coupling delay, dashed vertical lines in Figure 4.7(a). The curves for different delay values, together with the dashed vertical lines that mark the onset of mobility, collapse if we plot $T_{c|co}$ as a function of $(\lambda/\kappa)f(\kappa,\tau)$, Figure 4.7(b).

4.3.2 Mobile regime

For mobile oscillators with an intermediate mobility rate $\lambda/\kappa > 1/f(\kappa,\tau)$, relaxation time T_c significantly decreases with increasing mobility, Figure 4.5. Within this intermediate range, the curves for T_c vs. λ/κ for the different delay values collapse, indicating that T_c is independent of the delay value. Taking

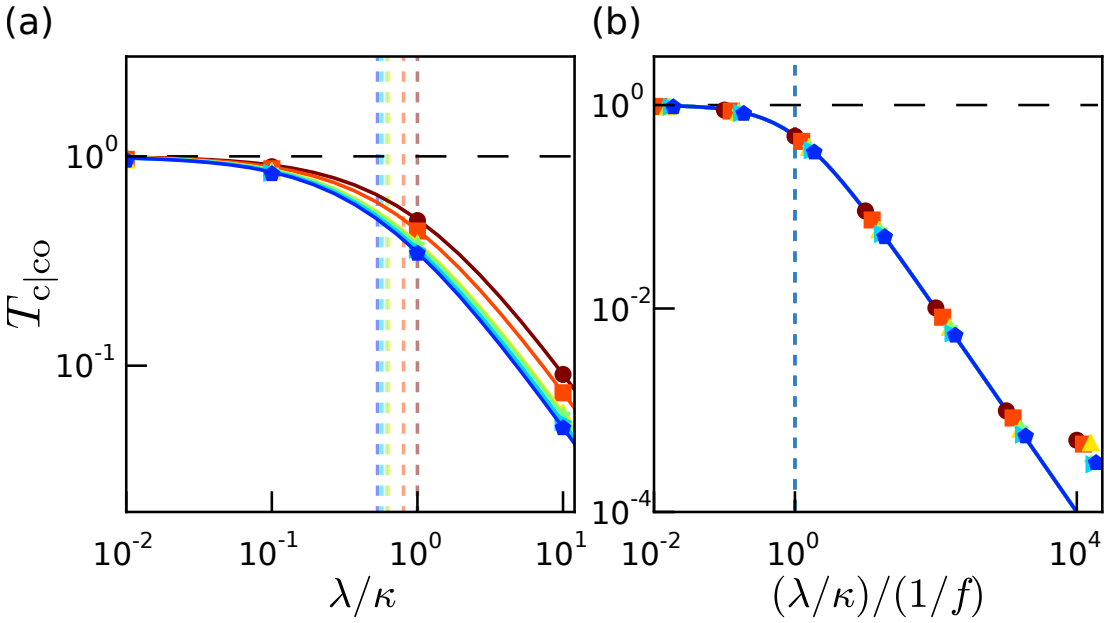

Figure 4.7: Onset of mobile regime. (a) Rescaled characteristic time $T_{c|co}$ as a function of mobility to coupling ratio λ/κ and (b) $T_{c|co}$ as a function of $(\lambda/\kappa)f(\kappa,\tau)$. Dashed vertical lines mark the onset of mobile regime, Eq. (4.21), and their collapse in (b). Delay values are the same as in Figure 4.5: $\tau = 0$ bordeaux, $\tau = 0.6$ red, $\tau = 0.9$ yellow, $\tau = 6.28$ green, $\tau = 6.88$ light blue and $\tau = 7.18$ blue.

$\lambda/\kappa \gg 1/f(\kappa,\tau)$ in Eq. (4.18),

$$T_c \approx \frac{N^2}{\pi^2}\frac{1}{\lambda} \tag{4.22}$$

that is independent of the delay. Numerical results are consistent with this expectation from the theory, see light orange symbols in Figure 4.6.

4.3.3 Mean-field regime

The effect of mobility on the characteristic time T_c saturates for sufficiently large mobility, bottom right panel Figure 4.5. This occurs when oscillators are moving so fast that they are effectively behaving as a mean-field system, and T_c is independent of mobility. However, the characteristic time T_c does depend on coupling delays, dark orange hexagons in Figure 4.6.

An estimation of a mean-field characteristic time T_{cmf} can be obtained con-

sidering the mean-field approximation

$$\dot{\theta}_i(t) = \omega + \frac{\kappa}{N}\sum_{j=1}^{N}\sin\left(\theta_j(t-\tau) - \theta_i(t)\right). \tag{4.23}$$

We introduce a small perturbation $\eta_i(t)$ to the synchronized state, $\theta_i(t) = \Omega t + \eta_i(t)$ with $|\eta_i(t)| \ll 1$. Expanding the sine around $-\Omega\tau$ and using the expression for the collective frequency

$$\Omega = \omega - \kappa\sin(\Omega\tau), \tag{4.24}$$

we can linearize Eq. (4.23):

$$\dot{\eta}_i(t) = \kappa\cos(\Omega\tau)\left(\frac{1}{N}\sum_{j=1}^{N}\eta_j(t-\tau) - \eta_i(t)\right). \tag{4.25}$$

For large N we can approximate

$$\frac{1}{N}\sum_{j=1}^{N}\eta_j(t-\tau) \ll |\eta_i|\,\forall i \tag{4.26}$$

and neglect the average perturbation term, so

$$\dot{\eta}_i(t) \approx -\kappa\cos(\Omega\tau)\,\eta_i(t). \tag{4.27}$$

Solutions to Eq. (4.27) have the form

$$\eta_i(t) \sim e^{-\kappa\cos(\Omega\tau)t}. \tag{4.28}$$

Therefore, relaxation of spatial correlations follows

$$\rho(t) \sim e^{-2\kappa\cos(\Omega\tau)t}, \tag{4.29}$$

and we can define a mean-field characteristic time

$$T_{\mathrm{cmf}} = \frac{1}{2\kappa\cos(\Omega\tau)}. \tag{4.30}$$

This expression is in very good agreement with numerical simulations, Figure 4.5

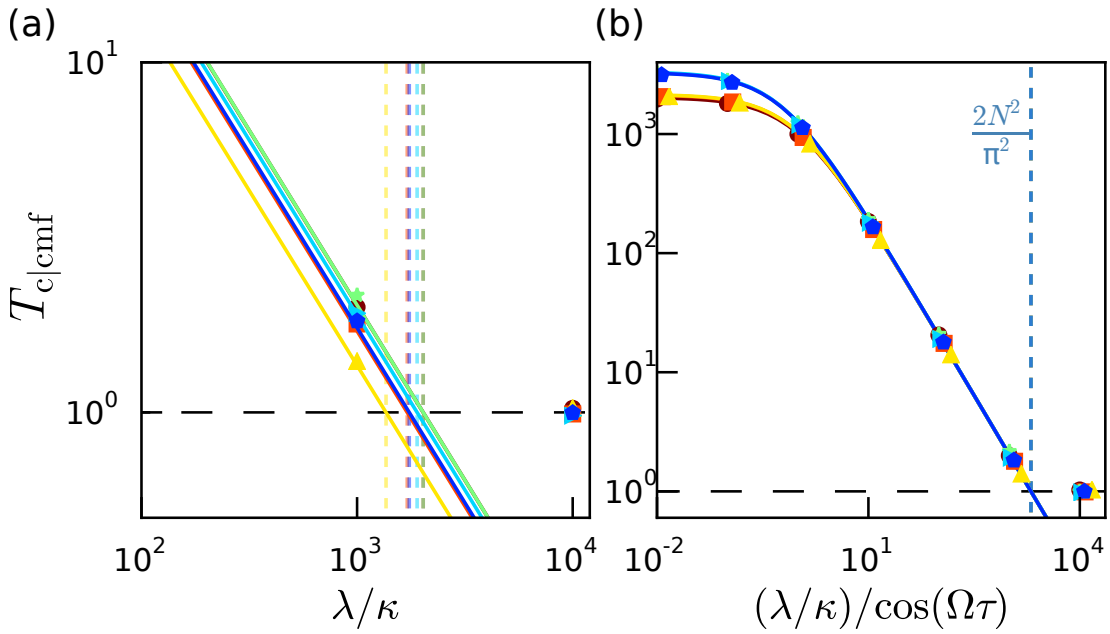

Figure 4.8: Onset of mean-field regime. (a) Rescaled characteristic time $T_{c|cmf}$ as a function of mobility to coupling ratio λ/κ and (b) $T_{c|cmf}$ as a function of $(\lambda/\kappa)/\cos(\Omega\tau)$. Dashed color lines indicate the onset of mean-field regime for each delay value, Eq. (4.32). Delay values are the same as in Figure 4.5: $\tau = 0$ bordeaux, $\tau = 0.6$ red, $\tau = 0.9$ yellow, $\tau = 6.28$ green, $\tau = 6.88$ light blue and $\tau = 7.18$ blue.

and 4.6, confirming that in this regime oscillators behave as if coupled with all the others.

Rescaling of T_c by T_{cmf}

$$T_{c|cmf}(\lambda, \tau) = \frac{T_c(\lambda, \tau)}{T_{cmf}} \tag{4.31}$$

collapses the data points for different delays in this regime, Figure 4.8.

The onset of mean-field dynamic regime is defined by the intersection of the mobile regime described by Eq. (4.18) and the mean-field regime where $T_c = T_{cmf}$, Figure (4.5). To determine this onset we evaluate $T_{cmf} = T_c(\lambda, \tau)$ equating Eq. (4.30) with Eq. (4.18)

$$\lambda/\kappa \approx \frac{2N^2}{\pi^2}\cos(\Omega\tau). \tag{4.32}$$

Similar to the onset of mobile regime, the onset of mean-field regime is modulated by coupling delays, dashed vertical lines in Figure 4.8(a). There is a stronger de-

pendence of the mean-field onset on delay compared with the mobile regime onset, despite the similarity between Figures 4.7(a) and 4.8(a) because of logarithmic scale. In the first stable branch, the increase in τ reduces the onset of mean-field behavior, Figure 4.4. In contrast, the onset becomes larger in the second stable branch as τ increases. These changes are almost in parallel with the changes in the effective coupling strength $1/f(\kappa,\tau)$. Rescaling the mobility to coupling ratio according to Eq. (4.32) together with T_c rescaling Eq. (4.31), the mean-field onset for different delay values collapse, Figure 4.8(b).

In summary, the mobility to coupling ratio determines synchronization dynamics of mobile oscillators in the presence of coupling delays. Delays modulate the onset of the different dynamical regimes

1. non-mobile dynamics, $\lambda/\kappa \lesssim 1/f(\kappa,\tau)$,
2. mobile dynamics, $1/f(\kappa,\tau) \ll \lambda/\kappa < \frac{2N^2}{\pi^2}\cos(\Omega\tau)$
3. mean-field dynamics $\lambda/\kappa > \frac{2N^2}{\pi^2}\cos(\Omega\tau)$.

4.4 Discussion

In this chapter we analyzed the system of phase oscillators with delayed coupling in a linear regime, where oscillators are very close to complete synchronization. We extended previous calculations [60] to include coupling delays and obtained an analytical expression of the characteristic relaxation time in the linear regime, Eq. (4.18). This characteristic relaxation time reveals the onset of non-local behavior and that of mean-field dynamics. Whether these hold in the nonlinear regime, where oscillators are far from complete synchronization, remains an interesting open question. We address this question in Chapter 7.

The segmentation clock features intercellular communication through Notch signaling [16, 37–39]. Mutants of the Notch signaling pathway display changes to segmentation period [51]. Furthermore, segmentation clock period can be tuned by gradually changing the strength of Notch signaling with chemicals [51], Figure 2.7(a). These experiments are consistent with a delayed coupling theory that describes the dynamics of pattern formation in the segmentation clock [50, 51]. A fit of the theory to experimental data results in coupling delays that are somewhere within the left part of the second stable branch of solutions, see Figure 4.1.

A recent study quantified cell mixing in the zebrafish PSM and tailbud to determine its impact on synchronization of genetic oscillators [46]. A phase oscillator model without coupling delays was adopted to simulate the effect of measured cell mixing on synchronization. Cell mixing reproduced by a physical model enhanced synchronization of the phase oscillators in simulations. A key result of our current study reveals that inclusion of coupling delays reduces the onset of non-local behavior to lower mobility values. Given the presence of time delays in Notch signaling [51], our present results further strengthen the possibility that cell mixing influences synchronization in the zebrafish tissue.

Zebrafish segmentation clock cells can behave as autonomous genetic oscillators [24]. In contrast, in the mouse it is thought that single cells behave as excitable systems [83]. It remains an interesting open question how mobility affects synchronization in this kind of coupled system.

In Figure 4.2 we show the time evolution of spatial correlations $\rho_d(t)$ as the system goes from disorder to complete synchronization. For all the values of the coupling delay τ explored, the system reaches complete synchronization and the entire evolution towards synchronization is faster for larger mobility. In terms of the of the Kuramoto order parameter that measures global synchronization $Z(t) = N^{-1}\sum_{j=1}^{N} e^{i\theta_j(t)}$, Eq. (2.7), this implies that the asymptotic value of $|Z| \sim 1$ is reached faster for larger mobility, Figure 4.9(a). So far, we have only examined the behavior of mobile delayed-coupled oscillators for some values of the coupling delay, corresponding to the first and second stable branches of synchronization. Intriguingly, when further exploring parameter space for delays near the stability boundaries, we find that $|Z|$ exhibits erratic behavior, Figure 4.9(b). This behaviour could eventually evolve into complete synchronization, Figure 4.9(b) blue line, or persist in time, green line. The erratic behavior of the order parameter suggests that for some values of the coupling delay, mobility induces a state that differs from the known local patterns and from the mean-field behavior. However, from this behavior of the order parameter we are not able to understand what is going on at the microscopic state of the system. Looking closer at the phase dynamics, the observed behavior of the order parameter is indicating the presence of complex patterns with coexisting domains of order and disorder, Figures 4.9(c). This kind of patterns were first observed in systems with non-local coupling [84] and are known as *chimera states* [85].

The occurrence of chimera states in the system of mobile oscillators with

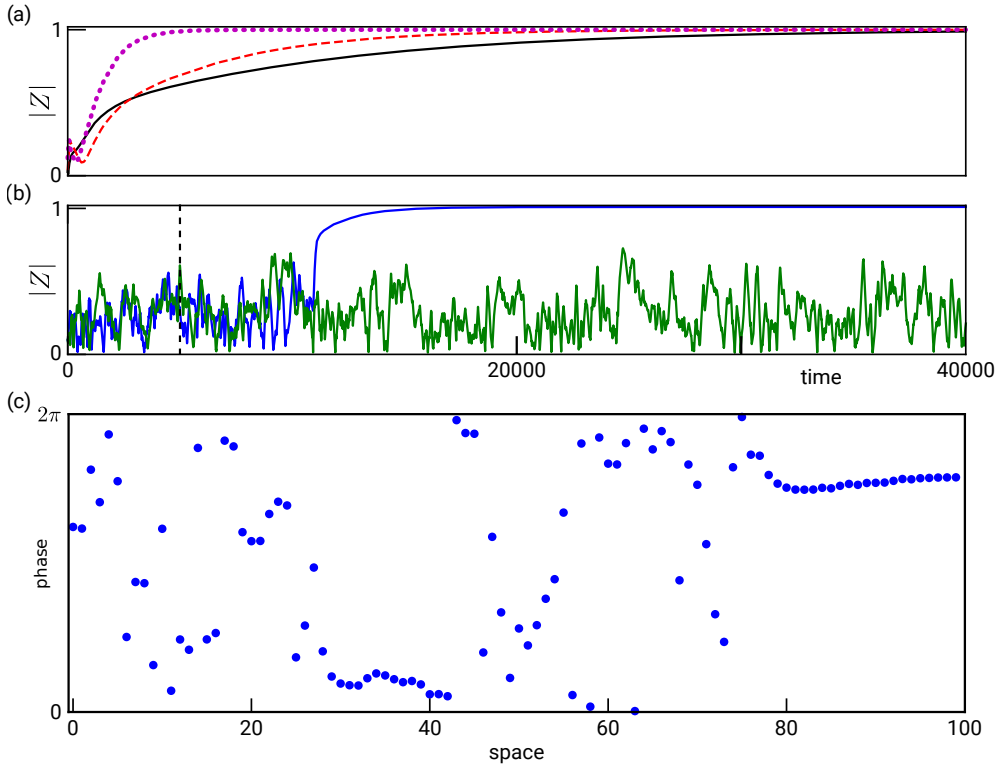

Figure 4.9: Order parameter shows erratic behavior in the presence of mobility and coupling delay. The modulus $|Z|$ of the order parameter as a function of time in simulations of Eq. (4.2) with (a) $\tau_{\text{out}} = 0$ and $\lambda/\kappa = 0$ (solid black line), $\lambda/\kappa = 1$ (dashed red line) and $\lambda/\kappa = 10$ (dotted magenta line), and (b) $\tau_{\text{out}} = 1.2$ and $\lambda/\kappa = 1$. Green and blue curves are two realizations for the same parameters. In both panels $\omega = 1$, $N = 100$. (c) Snapshot of the system state at time $t = 5000$ (dashed black line) for the simulation in blue in panel (b). The erratic behaviour of $|Z|$ reflects the presence of chimera states.

coupling delays was unexpected, and constitutes a new route towards synchronization, Figure 4.10, that differs from the know routes for the system without coupling delays, Figure 2.3.

We find chimera states occurring in the more general system of mobile delayed-coupled oscillators, Eq. (3.1), both for $\tau_{\text{in}} = 0$ and $\tau_{\text{out}} \neq 0$ and for $\tau_{\text{in}} \neq 0$ and $\tau_{\text{out}} = 0$. A detailed analysis of chimera states for this system and their dependence on parameters will be addressed in Chapter 6. First, in the next chapter we address the problem of classification of dynamical states that arises from the necessity of distinguishing between chimera states and a variety of other dynamical states that the system exhibits. Because of the mixed nature of chimera states, ensemble averaged quantities such as the order parameter or the spatial

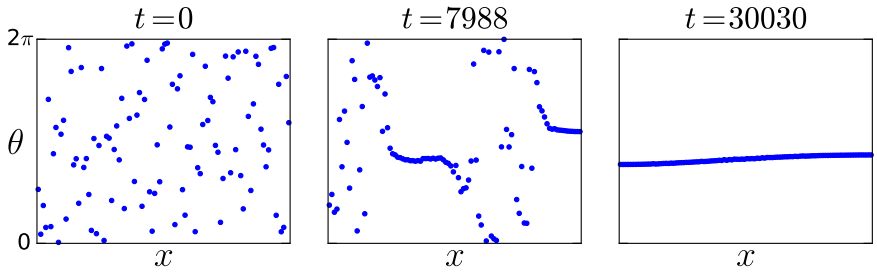

Figure 4.10: A new route towards synchronization. When mobility is present together with coupling delays, the system could reach synchronization through a different route: after forming long-lived chimera states. Mobility to coupling ratio and delay values are $\lambda/\kappa = 1$ and $\tau = 1.2$. Other parameters are: $N = 100$, $\omega = 1$, $\kappa = 0.1$.

correlations fail to reflect the local attributes of these more complex dynamical states. How to define measures that are informative of the complexity of chimera states is not yet clear. Thus, the necessity of developing tools for characterizing these states arises.

Chapter 5

A new method for the classification of dynamical states

As we next show, when varying mobility rate and coupling delay values, a rich variety of dynamical states appear in the system together with the in-phase synchronized state to which we devoted the previous chapters. In particular, chimera states with coexisting domains of order and disorder appear. Because of the mixed nature of chimeras and their different characteristics depending on parameters, identifying their occurrence might be difficult. In this chapter we introduce a computational method capable of systematically identifying the occurrence of chimera states. The method is developed because of the necessity of having a tool for telling apart chimera states form the variety of other dynamical states that appear in the system. In the next chapter, we employ this method to make a statistical analysis of the results. Some of the results reported in this chapter have been included in the article *Mobility-induced persistent chimera states*, recently published in Phys. Rev. E [86]. Here we additionally review other classification methods previously proposed in the literature and show conditions in which they fail to reliably distinguish between states.

5.1 Distinguishing between states

We have shown in previous chapters that mobility can drive the system of coupled oscillators into complete synchronization through different routes. Roughly, the system can either form locally ordered patterns and then relax these patterns

or behave like a mean-field system where the whole population is attracted to the mean phase, Figure 2.3. However, for some values of the coupling delay and the mobility rate, the system can also visit more complex spatio-temporal patterns on its way to synchronization. For non-mobile oscillators, these patterns can include states of mixed nature, combining domains of in-phase and anti-phase order, Figure 5.1(c). Remarkably, when mobility is present together with coupling delays, the system can also form long-lived chimera states, with coexisting domains of order and disorder, Figure 5.1(d). Thus, even after a long transient the

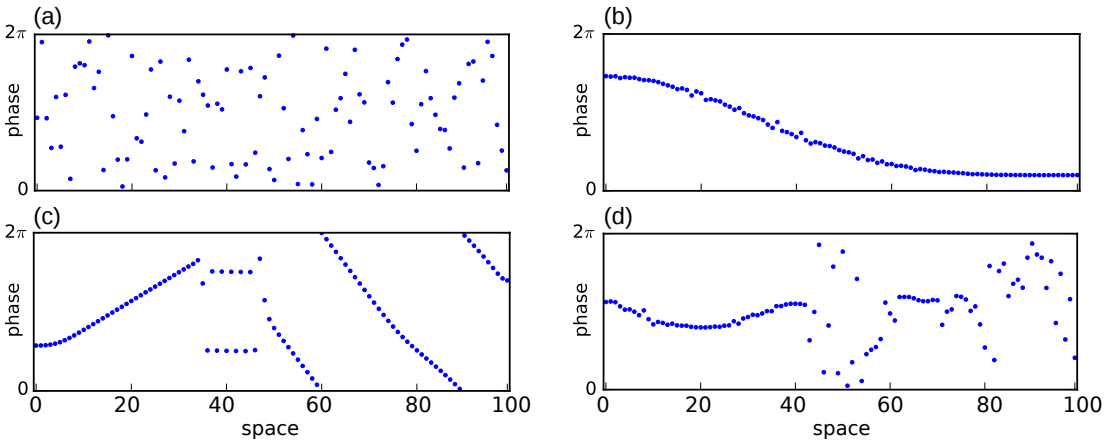

Figure 5.1: Examples of the variety of dynamical states that the system can visit depending on parameters. An accurate classification method should distinguish between them. (a) disorder, $\lambda/\kappa = 10^2$ and $\tau_{\text{in}} = 2.2$; (b) local order, $\lambda/\kappa = 1$, $\tau_{\text{in}} = 6.16$; (c) coexistence of in-phase and antiphase domains, $\lambda/\kappa = 0$, $\tau_{\text{in}} = 1.36$; (d) chimera state, $\lambda/\kappa = 1$ and $\tau_{\text{in}} = 4.88$. Other parameters: $\tau_{\text{out}} = 0$, $N = 100$, $\omega = 1$. All snapshots are taken after a sufficiently long transient $t > 5000$.

system can exhibit a wide diversity of dynamical states, depending on parameters, Figure 5.1. To further understand the dynamics of coupled oscillators in the presence of mobility and coupling delays it is therefore important to characterize these variety of states. Specifically, we seek a method capable of systematically distinguish between the different dynamical states that appear and, in particular, between chimera states and the other non-chimera states.

Reliable detection and classification of chimera states poses a challenge. As we discuss below in Section 6.1, dynamical properties of chimera states differ between systems. As a result, different quantitative measures have been proposed to characterize chimeras [87–89]. The need for a universal systematic way of defining chimera states has motivated the development of different methods [90–92]. Although methods proposed in these works have demonstrated to be useful

in several systems, here we find the necessity of developing a different approach to distinguish chimera states from all the other dynamical states occurring in the system. The novel approach we develop in this Thesis is the consequence of the knowledge we got from an extensive study on how other methods work when applied to the states encountered in the system of mobile delayed-coupled oscillators, Figure 5.1. Before presenting our method in the next section, below we describe how the two methods that most reliably identify chimeras in a variety of systems fail to identify chimeras in some situations that are relevant for the mobile delayed-coupled system.

Chimera states are, by definition, states combining ordered and disordered groups of oscillators. Therefore, a successful method for identifying chimera states needs to be able to locally detect the presence of ordered and disordered parts of the system at the same time. For example, the method proposed in [91] is based on the idea of partitioning the system into several clusters of a fixed size and comparing the local coherence between the clusters. If all the clusters are locally coherent (incoherent), then the state as a whole is a coherent (incoherent) state. If on the contrary some clusters show local coherence while others do not, coexistence of coherence and incoherence is detected and the state is identified as a chimera state. Specifically, the method can be adapted to the one-dimensional lattice with mobile oscillators considered here as follows. First, the absolute values of the phase differences modulo 2π between lattice sites are considered instead of the original phase variables

$$\Delta\vartheta_k(t) = \min\left\{ \left|\vartheta_{k+1}(t) - \vartheta_k(t)\right|, 2\pi - \left|\vartheta_{k+1}(t) - \vartheta_k(t)\right| \right\}, \tag{5.1}$$

where $\vartheta_k(t)$ is the phase value at site k at the time t, with $k = 0, ..., N-2$. Next, the lattice is partitioned into M clusters of $n = N/M$ oscillators. Introducing the standard deviation σ_m and the mean value of the phase differences within each cluster $\langle\Delta\vartheta\rangle_m$, Eqs. (5.2) and (5.3)

$$\sigma_m(t) = \sqrt{\frac{1}{n}\sum_{j=n(m-1)+1}^{nm} \left(\Delta\vartheta_j - \langle\Delta\vartheta\rangle_m\right)^2} \tag{5.2}$$

$$\langle\Delta\vartheta\rangle_m = \frac{1}{n}\sum_{j=n(m-1)+1}^{nm} \Delta\vartheta_j(t) \qquad m = 1, \ldots, M, \tag{5.3}$$

the local coherence of a cluster is measured by comparing σ_m with a predefined noise threshold δ. If $\sigma_m < \delta$, cluster m is classified as a coherent cluster and assigned $c_m = 1$. Otherwise, $c_m = 0$. Then, the *strength of incoherence* $\mathcal{I}$ of the state defined as

$$\mathcal{I} = 1 - \sum_{m=1}^{M} c_m/M, \qquad c_m = \begin{cases} 1 & \text{if } \sigma_m < \delta \\ 0 & \text{if } \sigma_m \geq \delta \end{cases} \tag{5.4}$$

is a measure of the ratio between coherent and incoherent parts of the system: $\mathcal{I} = 1$ if all parts are incoherent (disorder), $\mathcal{I} = 0$ if every part is coherent (global order) and $0 < \mathcal{I} < 1$ if there is coexistence of coherent and incoherent parts (chimera state).

The success of this method in identifying chimera states depends on two parameters: the size of the clusters n and the threshold for noise δ. Even for suitable parameters, the difficulty of applying this method to the system considered here comes from the fact that there are states other than chimeras ($0 < \mathcal{I} < 1$), disorder ($\mathcal{I} = 1$) or global order ($\mathcal{I} = 0$). Besides, the method involves a predefined partitioning of the system into smaller clusters, which usually do not coincide with coherent domains. Splitting coherent domains with the predefined partitioning causes two problems. On the one hand, the method can miss some coherent domains because splitting them increases σ_m. This becomes particularly relevant when coherent domains are small, and causes a misclassification of chimera states as disorder states. On the other hand, and more frequent, the method fails to distinguish chimera states from states combining domains of in-phase and antiphase order. Even if the fixed clustering does not split coherent domains, the presence of domain walls at the interphase between in-phase and antiphase domains contributes to increasing σ_m, Figure 5.2. Some coherent clusters that include domain walls are then wrongly classified as incoherent clusters, causing the method to identify a chimera state where it is not. It is not easy to exclude domain walls by using this method.

More recently, a classification method was proposed for chimera states which does not need a predefined clustering of the system [90]. Instead, the relative amount of coherent regions in the system is measured by evaluating a probability density function g of what is defined as the *local curvature* D. For phase oscillators in the one-dimensional lattice, the local curvature at each point in space is defined

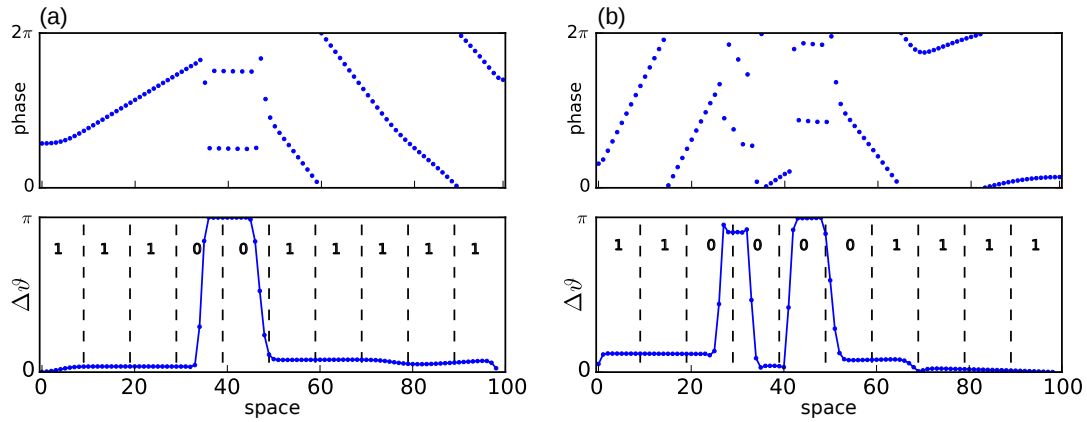

Figure 5.2: Examples of how the strength of incoherence method works for states mixing in-phase and antiphase domains. Dashed lines indicate the method's clustering for clusters of $n = 10$ oscillators. Bold black numbers indicate the value of c_m in each cluster for $\delta = 0.15\pi$. For both states $0 < \mathcal{I} < 1$.

as the discrete Laplacian

$$Df = \frac{f(x + \Delta x, t) - 2f(x, t) + f(x - \Delta x, t)}{\Delta x^2} \tag{5.5}$$

where $f(x, t) \equiv e^{i\theta(x,t)}$ and we fix $\Delta x = 1$. For left and right borders we use forward and backward schemes to compute the Laplacian, respectively. $|Df|$ is, for each time point, a transformation of the phase variables into new variables that account for phase differences in the circle, Figure 5.3(a-d) middle panels. For in-phase synchronization, $|D| = 0$ and the phases are projected into the x-axis through this transformation. In contrast, incoherent parts of the system have non-zero values of the curvature with pronounced fluctuations. Therefore, by considering the normalized probability density function $g(|D|)$, it is possible to measure the relative size of spatially coherent regions. For a fully in-phase synchronized state $g(0) = 1$, for a fully incoherent state $g(0) = 0$. A value between 0 and 1 of $g(0)$ means that some oscillators are synchronized in-phase since $g(0) > 0$ but not all of them since $g(0) < 1$. Thus, $0 < g(0) < 1$ indicates coexistence of synchrony and incoherence. To account for some degree of fluctuations for defining coherence, the degree of spatial synchronization in the system is measured as

$$g_0(t) \equiv \int_0^{\delta} g(t, |D|)\, d|D| \tag{5.6}$$

where δ is a noise threshold for defining coherence [90]. The threshold δ is a

parameter of the method and should be chosen relative to the maximum value of the curvature D_m, as a certain percentage of it. For example, a threshold of $\delta = 0.15D_m$ means that a point in space that has absolute local curvature less than 15% of the maximum curvature $D_m = 4$ is considered coherent, and incoherent otherwise. Then, if $g_0 = 1$ ($g_0 = 0$) the state has only coherent (incoherent) regions and is classified as an order (disorder) state. A value of $0 < g_0 < 1$ indicates coexistence between coherent and incoherent parts and the state is classified as a chimera state.

In the system considered here, dynamical states may present ordered but noisy regions because the exchange of positions between neighbouring oscillators with different phases disturbs local order, Figure 5.3(a,b). Moreover, and besides being noisy, some local order states may also present twists, Figure 5.3(b) top panel. Twisted local order should be consistently considered local order, although it presents higher values of the curvature, Figure 5.3(b) middle panel. Thus, the threshold δ needs to be high enough to account for these cases. However, such a permissive threshold fails between coexistent coherent but noisy domains and incoherent domains. This can lead to misidentifying disorder states as chimera states, Figure 5.3(c). After an extensive tuning of the parameter δ, we could not find a suitable value with which this method could distinguish between the variety of chimera states and other dynamical states that occur in the system for the whole range of mobility rates and delay values that we explore. Even if we could find accurate parameters, to successfully apply this method to the system considered here, we would still need to redefine the local curvature to account for antiphase order and domain walls.

So far, we reviewed how two of the methods proposed in the literature, which succeed in identifying chimeras in other systems, work for the repertoire of states that appear in the system of mobile delayed-coupled oscillators. There are other methods that we do not review here, that fail when applied to this system for different reasons. For example, measures based on looking at the microscopic state of the system are successful for small systems [89, 93] and local order parameters [88] and entropic measures [87] are reliable for community structured populations. In summary, while the proposed methods have proved to be successful in a variety of contexts, it is not clear how to adapt them to the context of mobile, delayed-coupled oscillators. We could not find a way to redefine the quantities such that these methods could reliably distinguish between the diver-

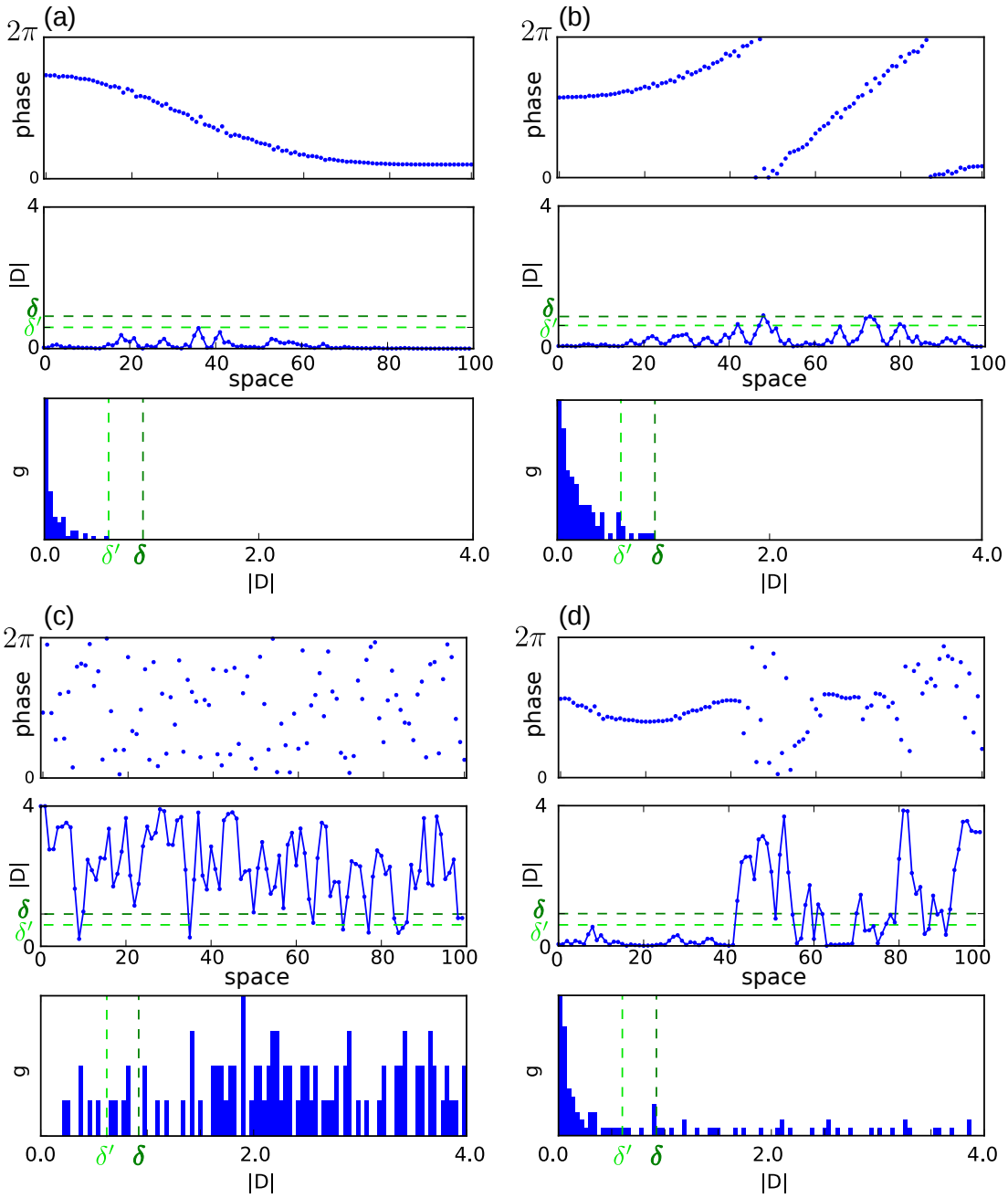

Figure 5.3: Examples of how the local curvature method works for different states. (a) Local order with fluctuations, (b) twisted local order, (c) disorder and (d) chimera state. Local order with fluctuations needs a high noise δ tolerance. Twisted local order needs even higher δ. In the examples $\delta' = 0.15D_m$, (light green) gives $g_0 = 1$ in (a) but $g_0 < 1$ in (b). A higher value of $\delta = 0.23D_m$ (dark green) gives $g_0 = 1$ for (a) and (b) but $g_0 > 0$ for (c).

sity of dynamical states that appear for the entire range of mobility rate and delay values. However, from analyzing how the described methods work for each

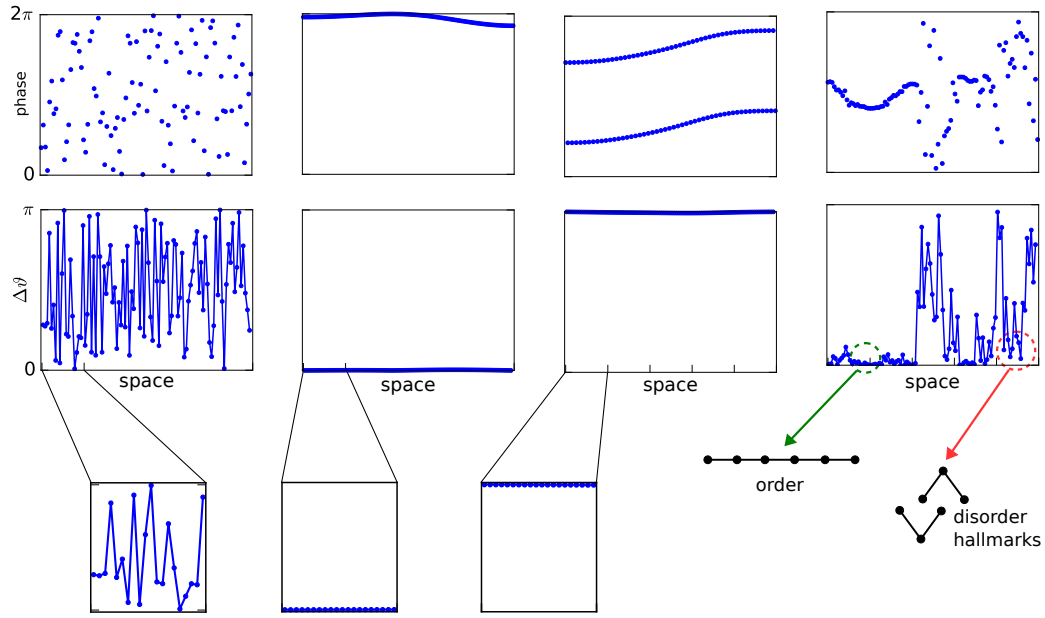

Figure 5.4: Order and disorder are characterized by very different phase-difference motifs.

of the dynamical states, we unveiled some aspects that an accurate classification method should consider. For example, we learnt that the successful measure should be able to identify order and disorder locally, should include a threshold parameter that accounts for fluctuations, should consider antiphase as another kind of local order and should tackle the difficulty posed by domain walls. In addition, it becomes evident that the method should be based on a transformation of variables that accounts for phase differences in the circle instead of on the original phase variables. From this basis, we develop a different approach that employs phase-difference motifs to locally distinguish order and disorder and succeeds in identifying between the variety of dynamical states mentioned. The main idea of our approach comes from the fact that order and disorder are composed of very different phase-difference motifs. While order is characterized by small phase differences, i.e. flat motifs, disorder in contrast shows peaked motifs with large amplitude in the phase differences, Figure 5.4. Thus, identifying these motifs within the dynamical states allows for locally distinguishing order from disorder.

5.2 Phase-difference motifs for classifying dynamical states

To distinguish between the variety of dynamical states that appear in the system of mobile delayed-coupled oscillators, Figure 5.1, we devise a classification method that introduces phase-difference motifs to identify ordered and disordered domains in the lattice. Given a snapshot at time t of the system state, our aim is to locally identify between parts of the system which are disordered and parts which are locally synchronized, either in-phase or in antiphase, Figure 5.5 top panels. With this purpose we first consider the absolute value of phase differences between first neighbours, modulo 2π

$$\Delta\vartheta_k(t) = \min\left\{ \left|\vartheta_{k+1}(t) - \vartheta_k(t)\right|, 2\pi - \left|\vartheta_{k+1}(t) - \vartheta_k(t)\right| \right\} \tag{5.7}$$

where $\vartheta_k(t)$ is the phase value at site k at the time t, with $k = 0, ..., N-2$, Figure 5.5 bottom panels. While disordered parts of the snapshots display variable

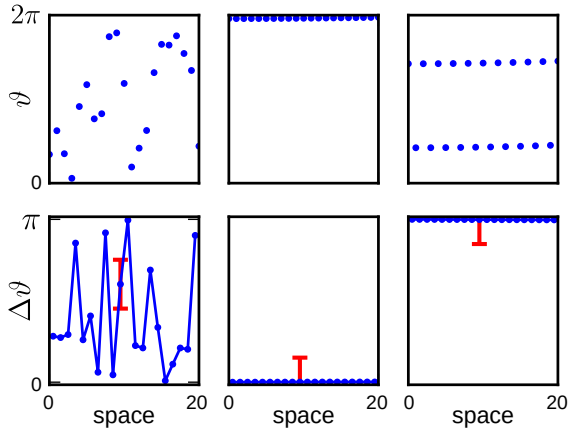

Figure 5.5: Typical disorder and order parts of the phase snapshots (top panel) and corresponding phase differences (bottom panel). Red error bars indicate the noise tolerance window defined by $\pm\delta$, here $\delta = 0.15\pi$. For ordered patterns all subsequent phase differences lay inside the noise tolerance window while most subsequent phase differences in the disordered pattern lay outside.

phase differences with large changes from one site to the next, phase differences for ordered parts remain almost constant, Figure 5.5. Therefore, we seek a way to identify whether consecutive phase differences change abruptly going up or down, or stay almost constant.

We introduce phase-difference motifs consisting of three nodes, corresponding to three consecutive phase differences, Figure 5.6(a). Motifs are labeled with

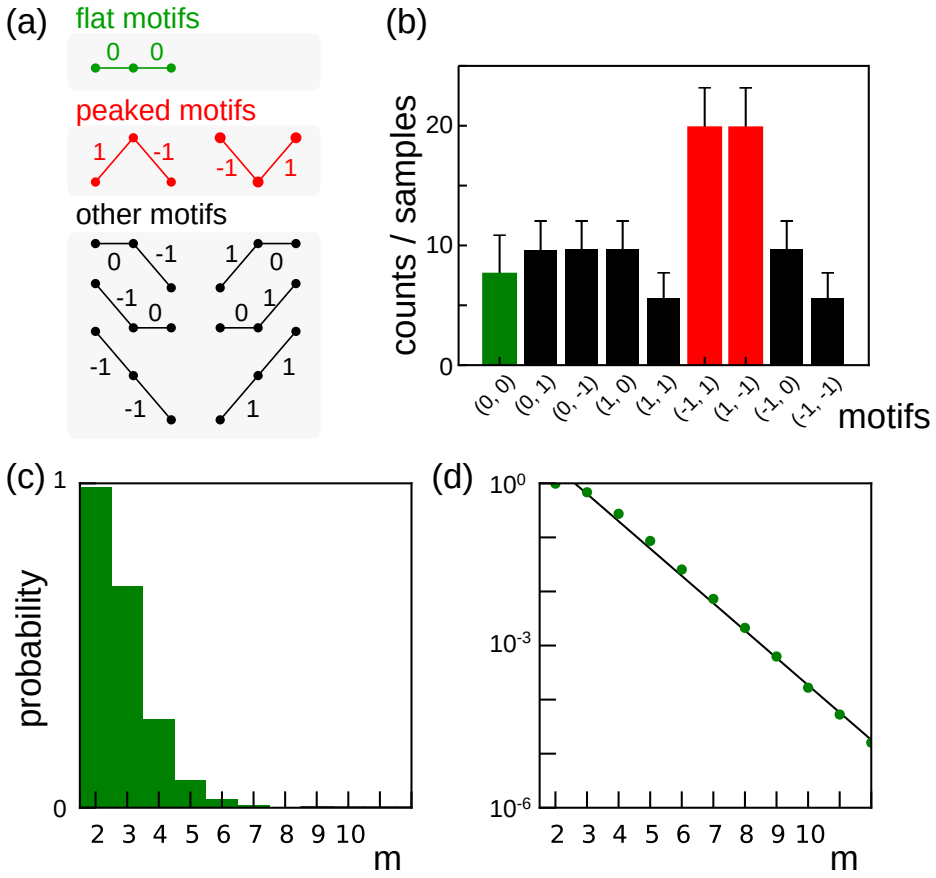

Figure 5.6: (a) Possible phase-difference motifs arranged to show the signatures of order (top) and disorder (middle). Other occurring motifs (bottom) are not used by our classification scheme. (b) Histogram of three-node motifs for disordered states. Green and red bars are flat and peaked motifs, respectively, black bars are all other motifs. Snapshots were prepared by taking $N = 100$ phases from a uniform distribution between $[0, 2\pi]$. Total sample snapshots considered: 5×10^5. (c, d) Probability of finding at least one domain of m consecutive zeros in a disordered state. Probability was computed over 10^6 sample disordered snapshots, with noise threshold $\delta = 0.15\pi$. Black line in right panel shows the exponential fit used to estimate the decay rate and to choose m_0.

two numbers, one for each of its two links. These numbers reflect how similar a phase difference $\Delta\vartheta_k$ is from the following $\Delta\vartheta_{k+1}$. We assign the labels to a link according to the following criteria, Figure 5.6(a):

- if $-\delta < \Delta\vartheta_{k+1} - \Delta\vartheta_k < \delta$, link value is 0

- if $\Delta\vartheta_{k+1} - \Delta\vartheta_k > \delta$, link value is 1
- if $\Delta\vartheta_{k+1} - \Delta\vartheta_k < -\delta$, link value is -1 .

The quantity δ determines the threshold of noise that we admit for defining order and is a parameter of our method. In the following we choose $\delta = 0.15\pi$, which is a 15% of the maximum possible value of the phase differences. This value of δ has proven to successfully reflect coherence while accounting for fluctuations to local order for almost every value of the mobility rate.

Figure 5.6(b) shows the distribution of motifs for a snapshot consisting of randomly chosen phases for all the oscillators in the one dimensional lattice. It becomes evident that such disordered snapshots are characterized by a larger fraction of peaked motifs $\{(1,-1),(-1,1)\}$ than other motifs. Thus, peaked motifs are a hallmark of disorder and we consider the presence of at least one peaked motif in a snapshot as an indicator that some amount of disorder is present in the system.

Similarly, we can identify the presence of order by looking for flat motifs $\{(0,0)\}$. Flat motifs can also happen by chance in disordered states, Figure 5.6(b). Therefore we consider that there is order present in the system only if there is at least one domain with a minimum amount m_0 of consecutive zeros. To calibrate this parameter, we study the distribution of consecutive zeros in disordered states, Figure 5.6(c,d). The number of consecutive zeros that could appear in a disordered state decays exponentially. We consider as a reference the value of m for which the exponential falls to a value of 1% of its maximum for $m = 2$. A linear fit shows this happens roughly for $m > 5$, Figure 5.6(d). Then, we consider that if at least $m_0 = 6$ consecutive zeros (i.e. three consecutive flat motifs) are present in a snapshot of the system state, the snapshot presents an ordered domain. This domain could have the size of the system or could coexist with other motifs.

With the described procedure, we are able to locally distinguish the presence of order and disorder in a snapshot of the system state by looking at flat and peaked motifs, Figure 5.7(a-f) bottom panels. When domains with at least m_0 consecutive zeros coexist with at least one peaked motif, our approach identifies a chimera state. Other motifs, black in Figure 5.6, are not used by our classification scheme. Domain walls, characterized by $\{(1,1),(-1,-1)\}$ motifs are thus naturally excluded in our scheme and we are able to distinguish states with coexisting in-phase and antiphase domains from chimera states. In-phase and

anti-phase ordered domains can be distinguished by evaluating the mean value of the phase differences within the domains. In conclusion, our approach is capable of distinguishing between the totality of the dynamical states mentioned in previous sections, Figure 5.7.

5.3 Discussion

In this chapter we addressed the problem of classification of dynamical states that arises from the necessity of distinguishing between a variety of very different patterns that appear in the system of mobile delayed-coupled oscillators. The main issue comes from the fact that these patterns include chimera states, with coexisting domains of order and disorder. Chimera states are complex patterns that have been widely studied in several systems, showing different characteristics depending on the system. In the next chapter we give some context about these intriguing states, Figure 6.1. Identifying and classifying chimera states posses a challenge, and has led to the development of several methods [87–93]. The problem of having a universal way of defining chimera states was highlighted in recent works [90–92]. While these recent works propose classification schemes that are useful in several systems, they fail to distinguish chimeras in the context of mobile delayed-coupled oscillators where noisy local order states and states that include domain walls are also present. The many methods proposed in the literature have their pros and cons depending on the characteristics of the dynamical states that the systems to which they are applied show. Developing tools for systematically and reliably detecting and classifying chimera states is still an opened problem in the field.

Here we devised a computational method based on phase-difference motifs that reliably distinguishes chimera states from a wide repertoire of other dynamical states, Figure 5.7. Furthermore, as we show in the next chapter, the method allows to identify new kinds of chimera states that, to the best of our knowledge, have not been reported so far. Our method improves the performance of other methods for noisy states and could be applied to other systems such as experimental designs where noise is unavoidable.

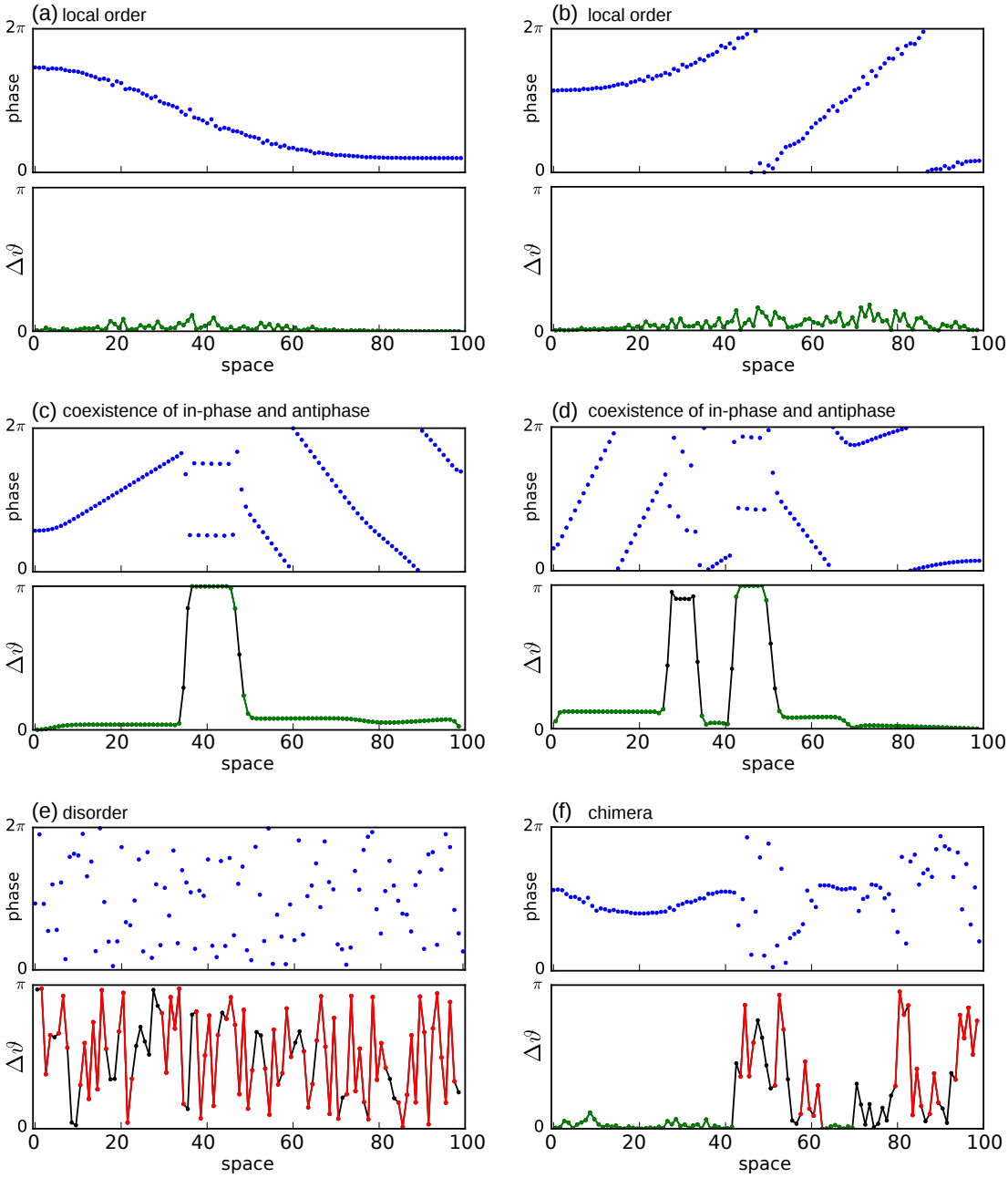

Figure 5.7: Examples of how the devised classification method works for the repertoire of dynamical states. For each of the states, top and bottom panels show a snapshot of phases and the spatial profile for phase differences, respectively. Parameters of the classification method: $\delta = 0.15\pi$ and $m_0 = 6$: peaked motifs are marked in red and ordered domains are green. Other motifs in black are not used by the classification method.

Chapter 6

Mobility-induced persistent chimera states

In Chapter 4 we studied the dynamics of the system of mobile delayed-coupled oscillators exploring parameter space for values of the delay that lay outside the multistability regions of in-phase and antiphase order for non-mobile oscillators. We now explore these other regions of parameter space, where chimera states spontaneously emerge. Additionally to the well known chimera states with coexisting domains of in-phase order and disorder, we find novel kinds of chimera states that blend coherent in-phase and antiphase domains with incoherent domains in different combinations. These chimera states are dynamic and can persist for long times for intermediate mobility values. We employ the method devised in the previous chapter to study where the different kinds of chimera states occur in parameter space. We discuss the mechanisms leading to the formation of these chimera states in different mobility regimes. Some of the results presented in this chapter have been included in the publication *Mobility-induced persistent chimera states* [86]. We first make a brief intermission on chimera states to contextualize our results.

6.1 Brief intermission on chimera states

As explained in previous sections, systems of coupled identical oscillators are usually expected to display stable homogeneous solutions such as completely synchronized states. For more than twenty five years, it was thought that either

these completely synchronized solutions or completely incoherent solutions were the only possible behaviour that these systems could show. There was no reason to expect that identical oscillators coupled in identical ways to their neighbours could display other kind of solutions. However it is now known that, intriguingly, under certain conditions systems of identical oscillators can also exhibit states of broken symmetry. In such states the population spontaneously splits into two distinct groups of oscillators, some oscillating in synchrony with a unique collective frequency and the others drifting around with distributed phases and frequencies. These states of broken symmetry where first noticed by Kuramoto and Battogtokh in 2002 [84] and subsequently named *chimera states* [85]. It is important to notice that partial synchronization was not new, but until 2002 it was thought to occur only when non-identical units where considered, emerging from some heterogeneity in the frequencies that made some oscillators impossible to follow the mean-field forcing, Section 2.1. Chimera states are conceptually different from this as they occur in systems of identical oscillators. In Greek mythology, a chimera was a monstrous fire-breathing hybrid creature, composed of parts of different animals, typically a lion, a goat and a snake, Figure 6.1(a). In non-linear dynamics, chimeras are monstrous spatio-temporal patterns composed of synchronous and asynchronous domains that coexist within the same state in networks of identical coupled oscillators, Figure 6.1(b-g). Below, we provide some important examples of chimera states reported both in theoretical and experimental systems.

In 2002 Kuramoto and Battogtokh noticed for the first time that the system of identical units can develop peculiar patterns where one group of oscillators oscillate together with the same phase and a collective frequency Ω, whereas other group of oscillators drift incoherently with their phases spread, Figure 6.1(b). This finding demonstrated that identical oscillators could show a much richer behavior than what it was expected and opened a whole new avenue of research for non-linear dynamics [94]. In their original work, they considered the dynamics of a ring of non-locally coupled identical oscillators with the phase equations in the continuum limit

$$\frac{\partial}{\partial t}\theta(x,t) = \omega - \int G(x-x')\,\sin\left(\theta(x,t) - \theta(x',t) + \alpha\right) dx' \tag{6.1}$$

where ω is the natural frequency of the oscillators, α is a phase shift in the coupling function and x is the one-dimensional spatial dimension. The non-locality of the

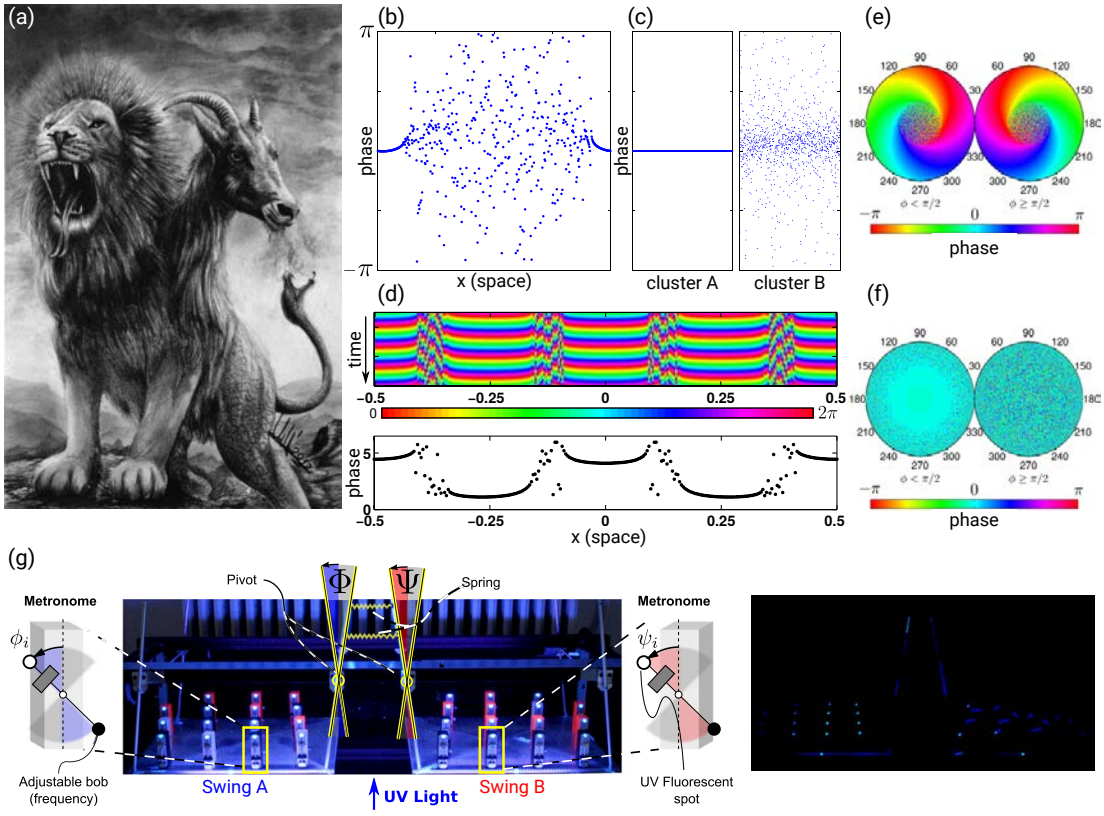

Figure 6.1: (a) Chimera creature in greek mythology, (b-f) chimera states in theoretical systems of coupled oscillators, (g) chimera state in two populations of coupled mechanical oscillators. In (g), swing and metronome displacements are measured by digital tracking of UV fluorescent spots placed on the pendula and swings. Figure adapted from [94] and [95].

coupling is provided by an exponentially decaying kernel

$$G(x - x') = A\,\kappa e^{-\kappa d_{x,x'}}, \tag{6.2}$$

with $d_{x,x'}$ the shortest distance between x and x' in the ring and A a normalization constant. In subsequent years, results in this first work were generalized for a more tractable non-local kernel [85] and also for a simpler system consisting of two populations of oscillators with all-to-all coupling, provided that the coupling strength is weaker between populations than within each population [96], Figure 6.1(c).

A few years later, chimeras where also reported for the delayed version of the

original Kuramoto-Battoghtok system [97]

$$\frac{\partial}{\partial t}\theta(x,t) = \omega - \int G(x-x')\,\sin\left(\theta(x,t) - \theta(x', t-\tau_{x,x'}) + \alpha\right) dx', \qquad (6.3)$$

in which the time delay in the coupling $\tau_{x,x'} = d_{x,x'}/v$ accounts for the time that the interaction signal needs to travel the shortest distance in the ring $d_{x,x'}$, with v the signal propagation speed. In the absence of delay, the above equation reduces to Eq. (6.1). Interestingly, the characteristics of the chimera state in the delayed system are different from known chimeras for systems without coupling delays. Unlike two groups of oscillators separated in space, they consist of several groups of synchronized oscillators forming domains in space separated by other small domains of incoherent oscillators, Figure 6.1(d). Furthermore, adjacent synchronized domains are found to be in antiphase with respect to each other.

After these first findings, chimera states were reported in a multiplicity of network topologies, all of which had some sort of non-local coupling and include time-delays and/or phase shifts [98–103]. Depending on the system considered and on the coupling schemes, chimera states show different characteristics. For example, they can present multiple or traveling coherent domains [103, 104]. Chimeras have also been encountered in two-dimensional systems, with oscillators distributed along an infinite plane [105–107], a torus [108, 109] and a sphere [110]. In two dimensions, chimeras are visualized either as spots or spiral waves, Figure 6.1(e,f).

During more than a decade, chimeras where predicted by theory in numerous systems but it was not known whether they were robust enough to be observed in experiments. It was not until 2012 that chimera states were reported in two almost simultaneous experiments, one working with optical oscillators and the second one working with chemical oscillators [111–113]. These experiments were carefully designed to look for chimera states based on previous theoretical work, and required of computational algorithms for achieving the non-local coupling between oscillators. These two were the first of several experiments that observed chimera states in optical and chemical systems [93, 114–116]. Remarkably, many of the theoretically predicted chimeras with different characteristics where observed experimentally in these systems, including chimeras with multiple and traveling domains that could vary in time [115] or spiral wave chimeras [116].

In 2013, chimera states as predicted in [96] where shown to appear in a system

of mechanical oscillators where the coupling does not rely on computational algorithms [95]. The system consisted in two populations of identical metronomes placed on two platforms that can swing freely on a plane and are coupled between them through springs, Figure 6.1(g). Oscillators within one population are coupled strongly by the motion of the platform onto which they are attached. Coupling between populations via the springs is weaker and is tunable, with an effective coupling strength κ. Starting from chimera-like initial conditions (with either of the two populations synchronized and the other desynchronized), the dynamics of the system show different states depending on the effective coupling strength. For low κ, oscillators within the two swings synchronize and each swing remains in antiphase with respect to the other. For intermediate coupling strength a chimera state occurs, where oscillators within one swing synchronize while in the other swing oscillators remain unsynchronized, Figure 6.1(g) right panel.

In summary, since they where first noticed, chimera states have been studied on a plethora of theoretical systems with very different couplings and network topologies and have even demonstrated to be robust enough to be observed in experiments in a variety of different systems [94]. In spite of the huge number of quite distinct systems where they appear, or because of it, it is still not clear where these states come from. How can a population of oscillators that are identical to each other develop a state in which one group behaves radically different from another? What are the sources of heterogeneity that are breaking the symmetry in each system? By looking for common elements and differences between systems, progress has been made in understanding what are the necessary conditions for chimera states to emerge, yet this is still one of the most intriguing open questions in the field.

Above we reviewed some of the first works on chimera states. Over the basis of these first works, and for more than ten years, it was believed that non-local/non-global coupling and an accurately tuned phase lag or time-delay were necessary conditions for the emergence of chimera states. However, chimera states were later reported in systems with global coupling [117–122] and, more recently, even with local coupling [123–126]. Thus no clue of the necessary conditions for their formation can be conclusively extracted from the network topology or the range of the coupling. In globally coupled systems the role of multistability in providing a

mechanism for splitting the population in coherent and incoherent groups is highlighted in several works [93, 121, 127]. However, other works reported chimeras without multistability in globally coupled systems [128]. How exactly multistability is linked with the formation of chimera states is not fully understood. In systems with local coupling, chimeras have been first shown to appear in different one-dimensional networks with a diffusive-like coupling with two timescales, and the interplay of timescales was spotted as a key element for the emergence of chimera states [123]. In other locally coupled systems, nonlinearity in the coupling function and bistability were alternatively stated as necessary requirements for the system to admit chimera states [124, 125]. Other apparently important elements for chimera states to arise are well-tuned phase shifts or coupling delays. In addition, initial conditions can be determinant for the formation of chimera states. For many years, chimeras where found in regions of parameter space where the synchronized state is linearly stable and initial conditions had to be carefully prepared to observe chimeras. Later, chimeras were found to emerge spontaneously out of disordered initial conditions in some systems. The role of initial conditions in the formation of chimera states is not yet clear and seems to depend on each system.

In recent years, chimera states continued to be observed in experiments with photo- and electro- chemical [115, 116, 119, 129], optical [93, 112] and mechanical systems [95, 130]. Together, all these experimental observations conclusively indicate that chimera states can be hosted by real systems. Nevertheless, all the experimental setups where chimeras have been observed were carefully designed produce this kind of states. Whether chimera states can appear in non-designed systems is still not known. Despite these intriguing dynamical states were hypothesized to play a role in some natural phenomena like unihemispheric sleep [131] and in psychophysical experiments [132], the observation of chimeras in natural systems outside the laboratory remains elusive.

We next describe chimera states that spontaneously emerge in the system of mobile delayed-coupled oscillators. The emergence of chimeras in this system provides a new mechanism for the formation of chimera states that arises from the interplay between mobility and coupling delays. This could be relevant for looking for chimera states in natural systems where both mobility and coupling delays are present like the vertebrate segmentation clock.

6.2 Chimera states in the system of mobile delayed-coupled oscillators

We consider the dynamics of the system of mobile delayed-coupled oscillators described in Chapter 3. We start by considering only the time delay τ_{in} , which accounts for the time to process a received signal, and neglect the time that each oscillator needs to prepare and send the signal $\tau_{\text{out}} = 0$[1]. In this situation, Eq. (3.1) becomes

$$\dot{\theta}_i(t) = \omega + \frac{\kappa}{n_i} \sum_{j \in V_i(t-\tau_{\text{in}})} \sin\left(\theta_j(t-\tau_{\text{in}}) - \theta_i(t)\right) \tag{6.4}$$

with

$$V_i(t) = \{j \text{ such that } |x_j(t) - x_i(t)| = 1\}\,.$$

We employ the classification method developed in the previous chapter to identify the different kinds of patterns that the system exhibits depending on parameters. We find that for some values of mobility and coupling delays chimera states appear. Remarkably, in addition to the well-known chimera states where in-phase order coexists with disorder we find other kinds: *antichimera* states where antiphase order coexists with disorder and *dual-chimera* states where both types of order coexist with disorder. From now on we call the first ones *in-phase chimera states* to distinguish them from these other two kinds.

6.2.1 In-phase chimera states

In-phase chimera states for the system of mobile delayed-coupled oscillators display a variety of shapes, Figure 6.2. For example, they can either consist of multiple ordered and disordered domains or they could include only one domain of in-phase order. Coherent in-phase ordered domains within chimeras have variable sizes and can occur at any place in the lattice. For larger mobility rates, ordered domains could be more or less noisy, with small phase differences among the oscillators, Figure 6.2(c,d). The classification method developed in Chapter 5, is capable to distinguishing chimera states, despite the variability in domain sizes, positions and noise, Figure 6.2(a-d) bottom panels.

[1]Note that this case is different of what we did in Chapter 4, where we took $\tau_{\text{in}} = 0$ and $\tau_{\text{out}} \neq 0$. Later in this chapter we show that results are similar for this other time delay.

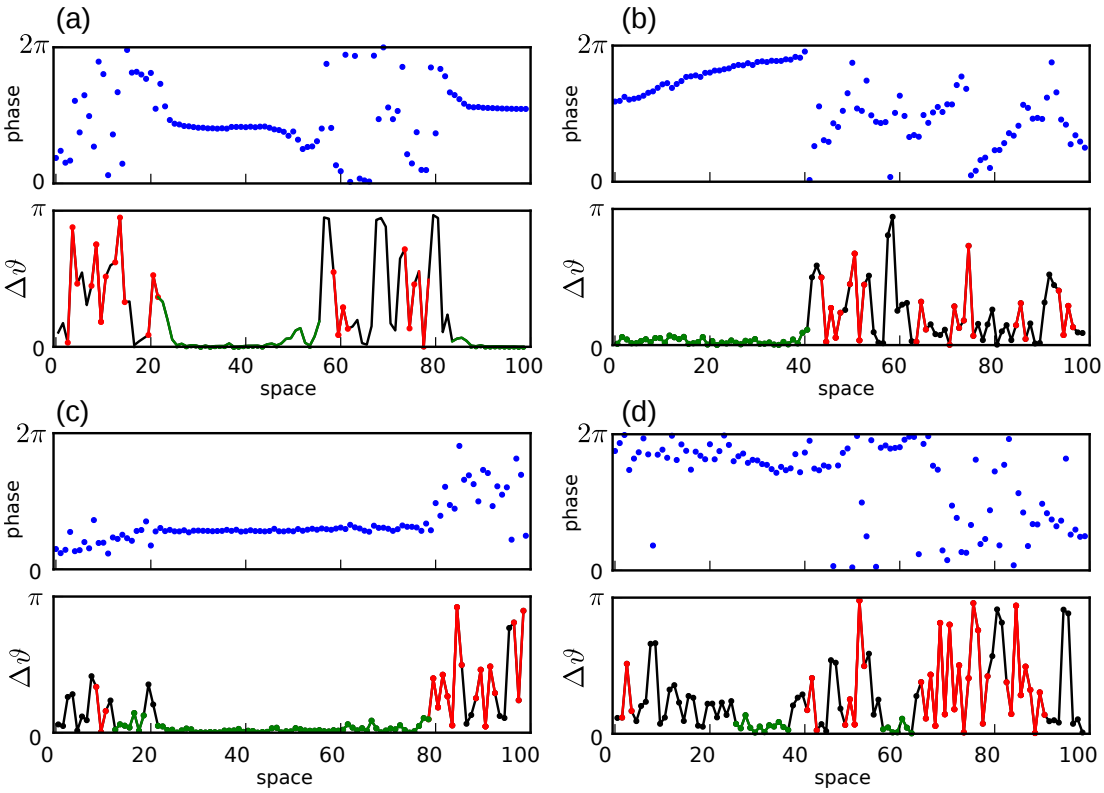

Figure 6.2: Examples of the variety of shapes of in-phase chimera states. Parameter values are: (a,b) $\lambda/\kappa = 1$, $\tau = 1.2$, (c) $\lambda/\kappa = 10$, $\tau = 1.36$ and (d) $\lambda/\kappa = 10$, $\tau = 1.4$. Bottom panels ilustrate how the classification method devised in Chapter 5 works for $\delta = 0.15\pi$, $m_0 = 6$. Other parameters: $\omega = 1$, $N = 100$.

We observe that chimera states are long-lived and dynamic, Figure 6.3(a). Coherent domains spontaneously form out of incoherence, change their sizes and die out while other domains may be born in a different place in the lattice (movies S1 and S2 [86]). However, the formed pattern can persist for many oscillation cycles, Figure 6.3(a) bottom panel.

Instantaneous and averaged phase velocities at each lattice site show that oscillators within coherent domains have the same frequency, Figure 6.3(c). The value of the collective frequency within coherent domains coincides with the well-known value of the collective frequency Ω of in-phase solutions of Eq. (6.4) for non-mobile oscillators, Eq. (2.14). In contrast, frequencies are not locked between lattice sites in disordered domains. To visualize a smoother transition between the domains it is useful to look at averaged frequencies over a time window ΔT, gray lines in Figure 6.3(c). In the example figure we chose a time window

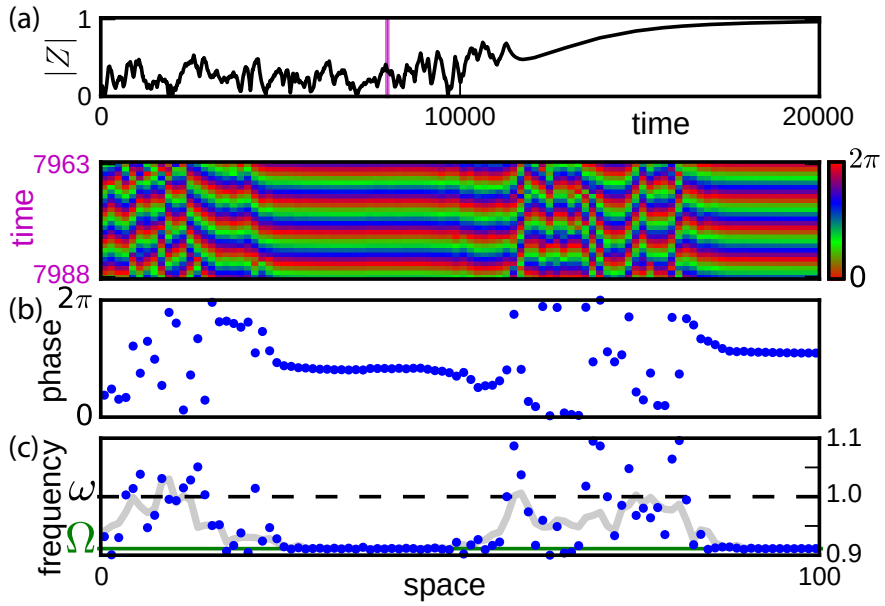

Figure 6.3: In-phase chimera states. (a) Modulus $|Z|$ of the order parameter vs. time for one realization in which the system exhibits chimera states (top panel). Space-time plot of the phases (bottom panel). The pink vertical bar in the top panel shows the time window expanded in the bottom panel. (b) Snapshot of a chimera state for the last frame of the time window above. (c) Instantaneous frequencies of oscillators (blue dots) and averaged frequencies at each lattice site (solid gray line) at the same time as in (b). Dashed black line is the autonomous frequency ω and solid green line is collective frequency of the in-phase state Ω. Parameter values are $\lambda/\kappa = 1$, $\tau = 1.2$, $\omega = 1$, $N = 100$. Averaged frequencies were computed with $\Delta T\,\omega/2\pi \approx 20$.

of $\Delta T \sim 20$ oscillation cycles. However, chimera states are dynamic, forming, disassembling and moving across the lattice. A larger value of ΔT will result in a smoother average frequency profile, but at the cost of blurring the boundaries between ordered and disordered domains. Small coherent domains which may form and disassemble faster may not be visible in this way.

6.2.2 Novel kinds of chimera states: antichimeras and dual-chimeras

Besides in-phase chimera states where in-phase order coexists with disorder, for low mobility we also find other kinds, Figure 6.4. We call *antichimera states* to a novel kind of chimera where synchronous domains display antiphase order. Antichimeras are characterized by coexisting antiphase domains and disorder

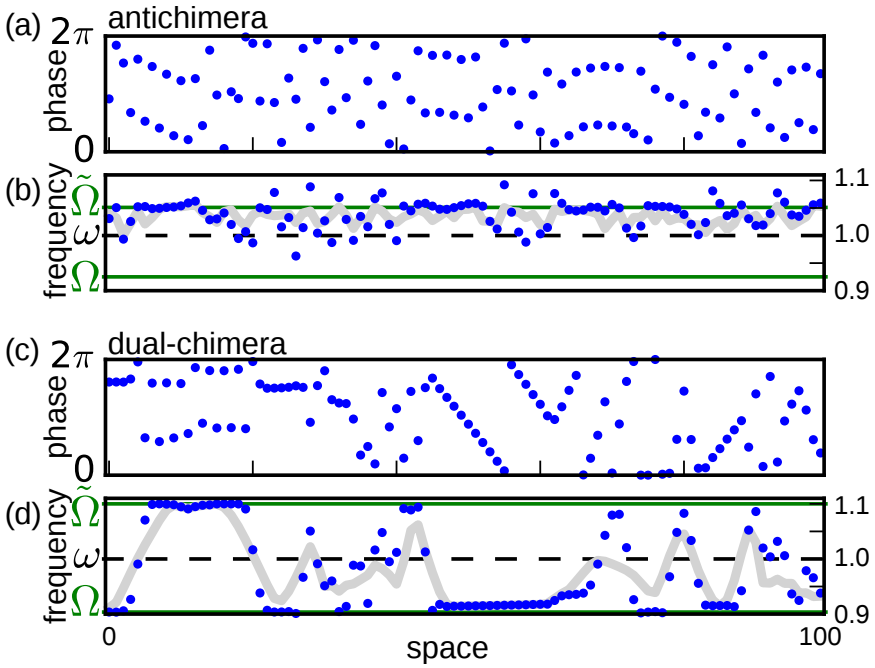

Figure 6.4: Anti-chimera and dual-chimera states. Snapshots and instantaneous frequencies for (a,b) an anti-chimera state and (c,d) a dual-chimera state. (b,d) Instantaneous frequencies of oscillators (blue dots) and averaged frequencies at each lattice site (solid gray line) at the same time as in (a,c) respectively. Dashed black line is the autonomous frequency ω and solid green lines are the collective frequencies of the in-phase state Ω and the antiphase state $\tilde{\Omega}$. Parameter values are (a,b) $\lambda/\kappa = 0.1$ and $\tau = 2.48$ and (c,d) $\lambda/\kappa = 0.001$ and $\tau = 1.44$. Averaged frequencies were computed with $\Delta T\,\omega/2\pi \approx 20$. Snapshots taken after at least $t = 4000$.

domains, Figure 6.4(a,b). In addition, coexistence of domains with both types of order and disorder are also observed. We call *dual-chimera states* to this third kind of chimera consisting of alternating domains of in-phase order, antiphase order and disorder, Figure 6.4(c,d).

Similar to what is observed for in-phase chimeras, instantaneous and averaged phase velocities for antichimeras and dual-chimeras show that oscillators within coherent domains have the same frequency, Figure 6.4(b,d). The value of the frequency within coherent domains of each type of order coincides with the known collective frequency of in-phase Ω and antiphase $\tilde{\Omega}$ solutions, respectively, Eqs. (2.14) and (2.20). In contrast, frequencies of oscillators in disordered domains are not locked.

It is worth noticing that without the classification method devised in Chapter 5, it is difficult to systematically identify and distinguish between the different

kinds of chimera states. By means of the phase difference motifs, the devised method can locally tell apart in-phase order from antiphase order and from disorder. Thus, the classification method developed here is a key tool to identify and properly characterize the variety of dynamical states that appear in this system. We highlight the ability of the method to distinguish between the three different kinds of chimeras, two of which, to the best of out knowledge, have not been reported so far. In summary, in the system considered here, a diversity of dynamical states are present together with chimera states, Figure 6.5(a-g) top panels:

(a) disorder

(b) in-phase local order

(c) anti-phase local order

(d) coexistence of in-phase and anti-phase

(e) in-phase chimera states (χ_+)

(f) anti-chimera states (χ_-)

(g) dual-chimera states (χ_{+-})

6.2.3 Chimeras for periodic boundaries

We have also observed chimera states for periodic boundary conditions (for an example see Figure 6.6 and supplementary movie S3). Hence, although an open boundary condition breaks translation invariance at boundaries, this is not crucial for the formation of chimera states. Therefore, we employ open boundary conditions in the rest of the Thesis. As already mentioned, this choice of open boundary conditions avoid the formation of stable twisted states and also keeps an eye on biological systems, which have open boundaries.

6.3 Fraction of chimera states in time

We next study how the likelihood of observing chimera states changes with time, Figure 6.8. We define the fraction f_χ at any given time t as the number of realizations in which chimera states are detected by the classification method, divided by the total number of realizations. We start the simulations from *random initial conditions*, i. e. disorder states, where the phases of all the oscillators in

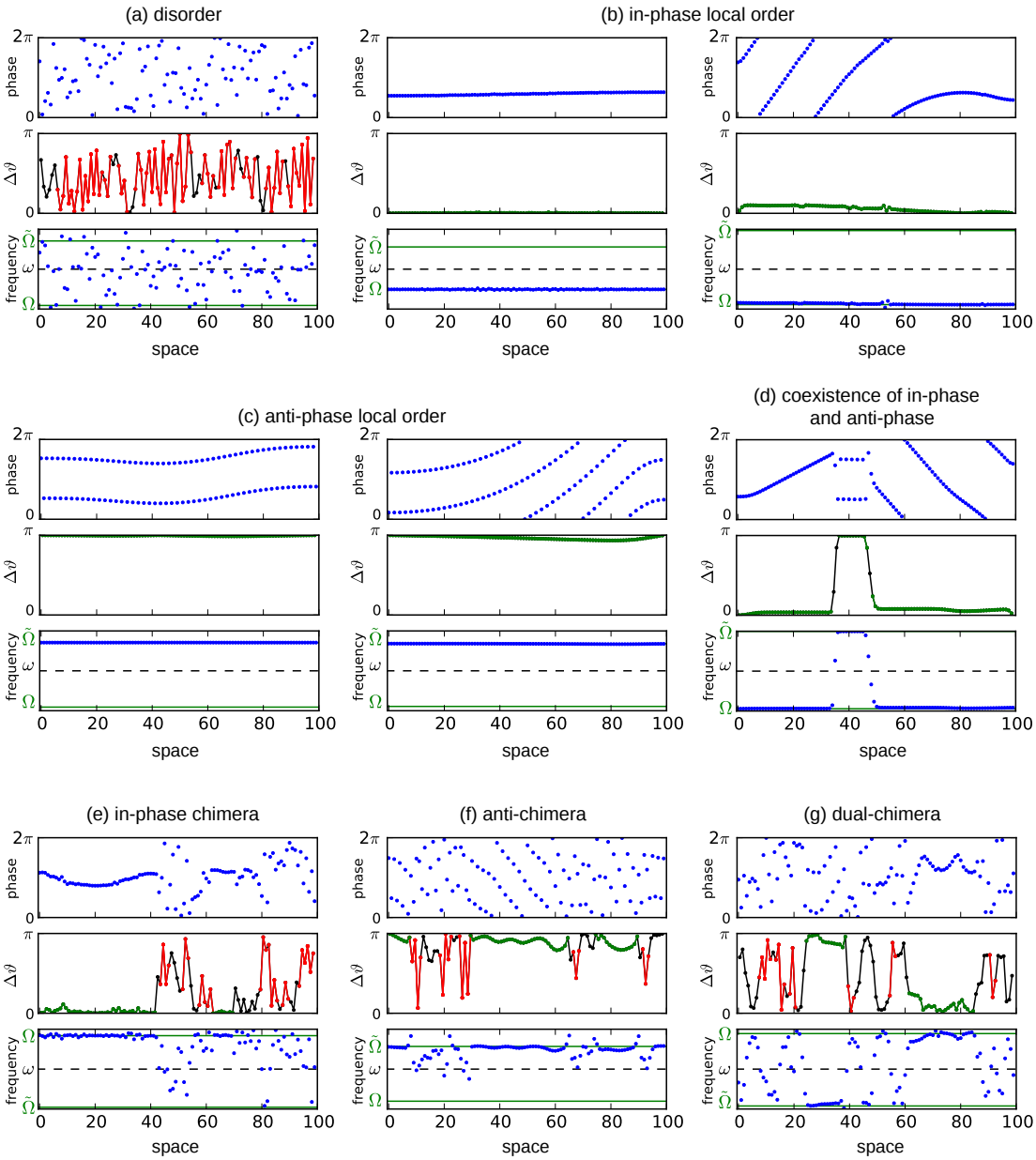

Figure 6.5: Examples of the variety of dynamical states that the system can visit depending on parameters. For each of the states, top, middle and bottom panels show a snapshot of phases, the spatial profile for phase differences, and instantaneous phase velocities, respectively. Middle panel illustrates how the classification method works for $\delta = 0.15\pi$ and $m_0 = 6$: peaked motifs are marked in red and ordered domains are green. Solid green lines in the bottom panel show the in-phase Ω and antiphase $\tilde{\Omega}$ collective frequencies. Parameters: (a) $\lambda/\kappa = 10^2$ and $\tau = 2.2$, (b) $\lambda/\kappa = 10$ and $\tau = 0.56$ (left), $\lambda/\kappa = 0.01$ and $\tau = 1.2$ (right), (c) $\lambda/\kappa = 0$ and $\tau = 2.2$ (left), $\lambda/\kappa = 0$ and $\tau = 2.24$ (right), (d) $\lambda/\kappa = 0$ and $\tau = 1.36$, (e) $\lambda/\kappa = 1$ and $\tau = 4.88$, (f) $\lambda/\kappa = 0.01$ and $\tau = 2.4$, (g) $\lambda/\kappa = 0.01$ and $\tau = 4.76$.

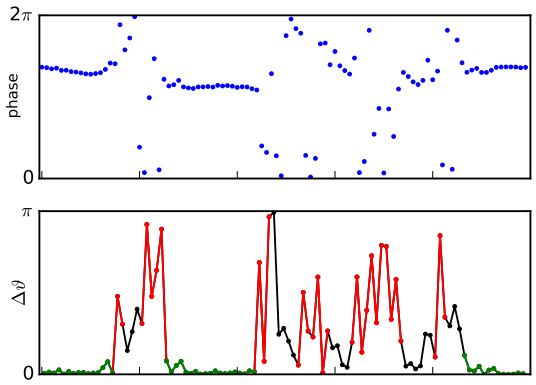

Figure 6.6: Example of an in-phase chimera state for periodic boundary conditions. $\lambda/\kappa = 1$, $\tau_{\text{in}} = 1.2$.

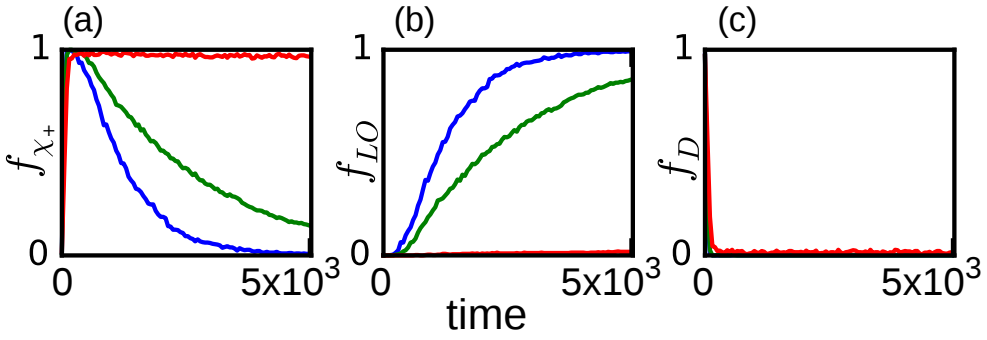

Figure 6.7: Transient and persistent in-phase chimera states. Fraction of (a) in-phase chimera states (b) local order states and (c) disorder states vs. time for mobility to coupling ratio $\lambda/\kappa = 1$ and $\tau = 1.081$ (blue line), $\tau = 1.131$ (green line) and $\tau = 1.244$ (red line). The fraction was obtained over 512 realizations for random initial conditions. Other parameters: $\omega = 1$, $N = 100$. Parameters of the classification method: $\delta = 0.15\pi$, $m_0 = 6$, $m_p = 1$.

the lattice are drawn from a uniform distribution in $[0, 2\pi)$. We study how the fraction of the different kinds of chimeras evolves in time for different mobility rates and delay values, in simulations that last up to $t \sim 5000$ time units. We find that the fraction f_{χ_+} of in-phase chimera states increases rapidly, as the fraction of disorder states f_D quickly decays, Figure 6.7(a,c). For some coupling delay values the fraction of in-phase chimera states decays for longer times, as some of them evolve into local order states, Figure 6.7(a,b). Remarkably, there are other delay values for which in-phase chimera states persist within the time window studied, red line in Figure 6.7(a).

Persistent antichimeras and dual-chimeras are also found. The fraction f_{χ_-} of antichimera states quickly increases for some coupling delay values and persists

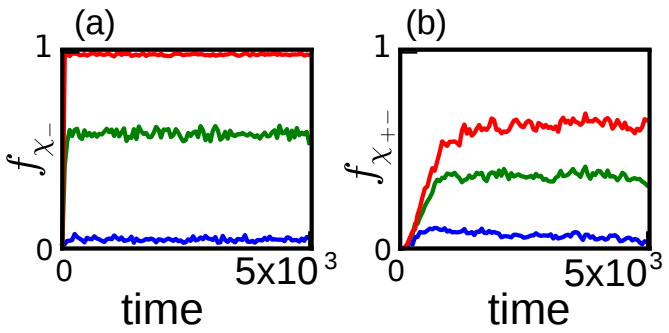

Figure 6.8: Persistent antichimeras and dual-chimeras. Fraction of (a) anti-chimera and (b) dual-chimera states vs. time. Mobility to coupling ratio and delay values are (a) $\lambda/\kappa = 0.1$ and $\tau = 1.6$ (blue line), $\tau = 1.88$ (green line) and $\tau = 2.48$ (red line); and (b) $\lambda/\kappa = 0.001$ and $\tau = 1.36$ (blue line), $\tau = 1.44$ (green line) and $\tau = 1.6$ (red line). The fraction is obtained over 512 realizations for random initial conditions. Other parameters: $\omega = 1$, $N = 100$. Parameters of the classification method: $\delta = 0.15\pi$ and $m_0 = 6$.

with $\lambda/\kappa = 10^{-1}$, Figure 6.8(a). The fraction $f_{\chi_{+-}}$ of dual-chimera states grows slower, yet stays larger than zero for some coupling delay values with $\lambda/\kappa = 10^{-3}$, indicating their persistence, Figure 6.8(b).

6.4 Statistics for chimera states from random initial conditions

We have shown that in the system of mobile delayed-coupled oscillators three kinds of chimera states can spontaneously emerge out of disorder, Figures 6.3 and 6.4. For some mobility and delay values, these chimera states can persist in time, Figures 6.7 and 6.8. We now address the statistics of these states when exploring mobility and delay values. Starting from random initial conditions, i.e. disorder states, we ask whether the fraction of the different dynamical states persists after a transient time has past, Figure 6.9.

For the time window studied in the previous section, we find that chimera states may persist even for no mobility, Figure 6.9(I). Most of these chimeras are dual-chimera states and appear in the bi-stability region, where in-phase and antiphase order are both stable for non-mobile oscillators. However, for very long times $t \sim 10^5$ chimeras for non-mobile oscillators are not present, Figure 6.9(II). This seems to indicate that dual-chimeras appearing for non-mobile oscillators at

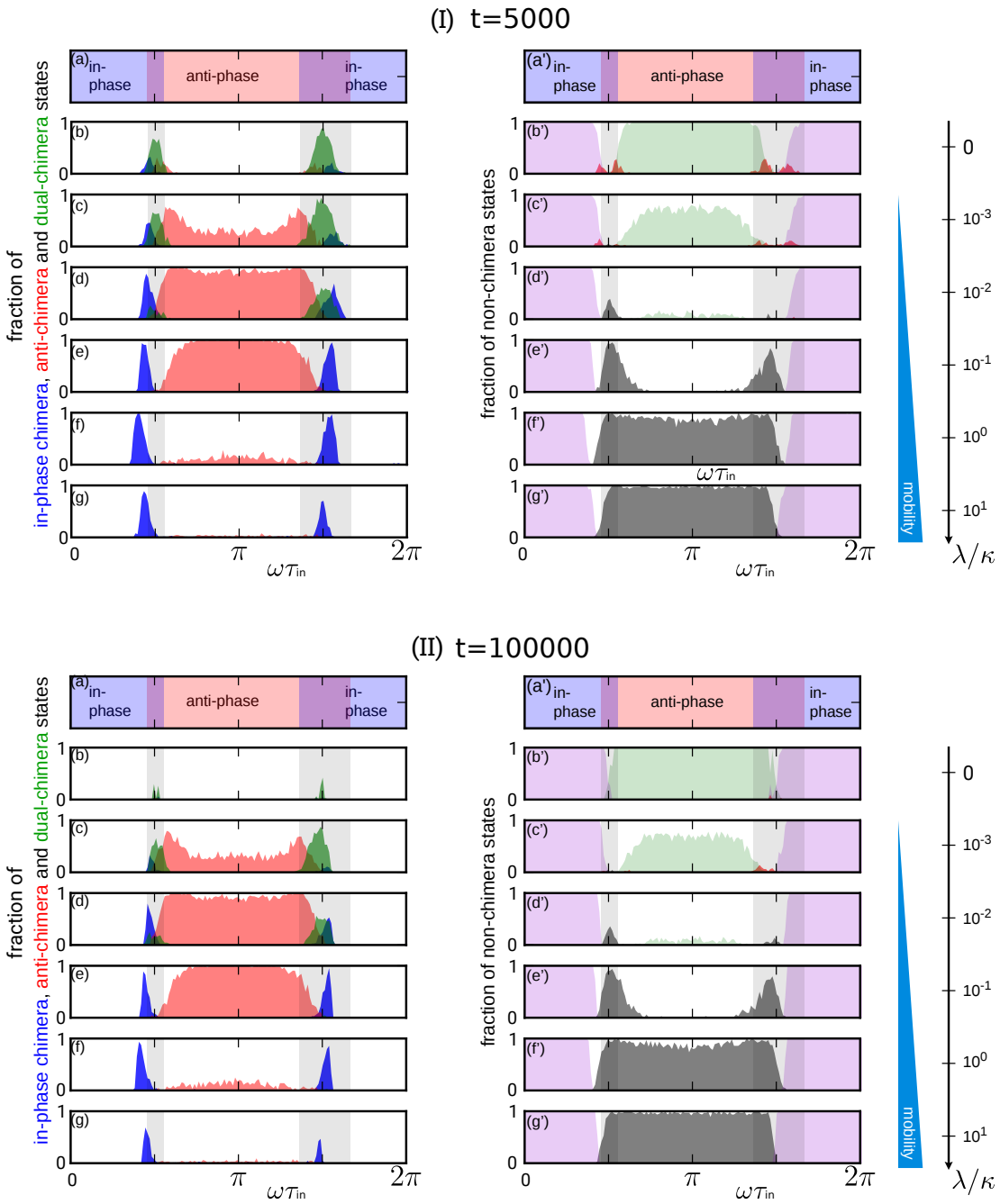

Figure 6.9: Fraction of dynamical states after (I) $t = 5000$ and (II) $t = 100000$ starting from random initial conditions. (a),(a') Regions in which in-phase and antiphase order states are stable for non-mobile oscillators. Bi-stability regions of in-phase and antiphase order states in panel (a) are replicated in the next panels as light grey bands. (b)-(g) Fraction of in-phase chimera (blue), anti-chimera (red) and dual-chimera states (green) as a function of coupling delay $\tau = \tau_{\text{in}}$ (in this simulations $\tau_{\text{out}} = 0$). (b')-(g') Fraction of in-phase local order (lilac), antiphase local order (light green), coexistence of in-phase and antiphase (dark red) and disordered states (dark grey) as a function of coupling delay τ_{in} . Fraction is computed over 64 realizations of initial conditions for each set of parameters. See examples of all dynamical states in Figure 6.5.

previous times belong to a long transient in which some oscillators still did not manage to revert their initial phase differences and synchronize. The fact that this long transient is longer in the bi-stability regions reflects that in-phase and antiphase synchronization compete within that region. Panel 6.9(II,b') shows that after this long transient dual-chimera states end either in in-phase or antiphase states. Interestingly, this is a different route towards synchronization for non-mobile oscillators than the one that involves forming local patterns described in previous sections.

In contrast, for these long times for which chimera states finally synchronize for non-mobile oscillators, chimera states for mobile oscillators persist, 6.9(II, c-g). We find persistent chimera states within an intermediate range of mobility. Without mobility persistent chimeras are not observed, Figure 6.9(II,b). Instead, the system exhibits in-phase and antiphase local order, Figure 6.9(II,b'). With increasing mobility, the three different kinds of chimera states occur. The fraction of in-phase chimera states peaks near the bi-stability regions and within the regions where in-phase order is stable. These peaks become largest around $\lambda/\kappa = 1$ and seem to gradually decrease for larger mobility, Figure 6.9(II,g). Anti-chimera states form for small λ/κ in the region where antiphase order is stable, and disappear for $\lambda/\kappa \sim 1$, Figure 6.9(II,c-e). Larger mobility disorganizes antiphase structures and leads the system into disordered states, Figure 6.9(II,f'-g'). Dual-chimera states exist in the very small mobility regime, for coupling delay values around $\pi/2$ and $3\pi/2$, Figure 6.9(II,c,d). Interestingly, all kinds of chimera states form below the onsets of the mobile regime for all the delay values explored, see values of λ/κ in Figures 6.9 and 6.12 and vertical lines in 4.7(a). Comparing Figure 6.9(I) with 6.9(II), we conclude that it is the interplay between mobility and coupling delays which makes chimera states long-lived.

6.5 Statistics for chimera states from ordered initial conditions

Persistent in-phase chimera states occur near the regions of delay values for which the known in-phase and antiphase synchronization solutions for non-mobile oscillators overlap and exchange stability, Section 2.3.2. In the bi-stability regions, violet in Figure 6.11(a), non-mobile oscillators visit transient states where domains of in-phase and antiphase order coexist, Figure 5.1(c). When mobility

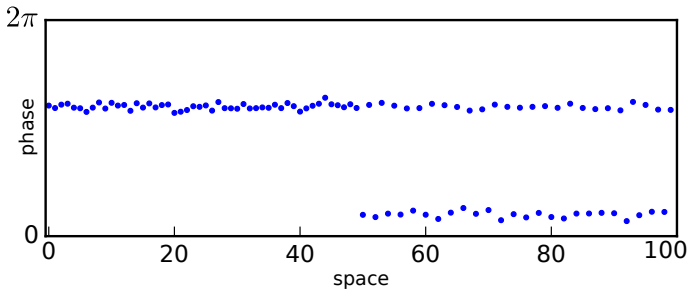

Figure 6.10: Prepared initial states without disorder. Half of the oscillators in the lattice show in-phase order while the other half shows antiphase order, with added Gaussian noise $\sigma = 0.1\pi/4$.

is added to the system, persistent chimera states occur in the vicinity of these regions of parameter space. Chimera states occurring near these regions motivated us to start from initial conditions that consist of separate domains of in-phase and antiphase order.

We prepare initial conditions where half of the lattice is in-phase and the other half in antiphase, with added Gaussian noise $\sigma = 0.1\pi/4$, Figure 6.10. Such initial states do not include any disordered domains, and we can examine whether mobility induces persistent disordered domains from ordered initial conditions, which would lead the system into chimera states.

We determine the fraction of chimera states that persist after a transient, starting from these initial conditions, Figure 6.11. Importantly, the evolution from these ordered initial conditions has a shorter transient and it is sufficient to look at the statistics at $t = 5000$. This significantly reduces the computational time, and we are able to (i) make a fraction over a larger number of realizations and (ii) explore larger mobility values[2]. After the transient, we find similar results to those described in the previous section, with persistent chimera states occurring for intermediate mobility values, Figure 6.11. When exploring larger mobility values, we observe that the peaks of in-phase chimeras that are largest around $\lambda/\kappa = 1$ gradually reduce when increasing mobility until almost disappearing for large mobility, Figure 6.11(h). Interestingly, chimera states disappear before the onsets of the mean field regime, see values of λ/κ in Figure 6.11 and vertical lines in 4.8(a). Large mobility does not allow the formation of in-phase chimera states, but it rather promotes in-phase local order or disordered states depending

[2]As explained in appendix A, realizations with large mobility have smaller integration step δt and are thus computationally expensive.

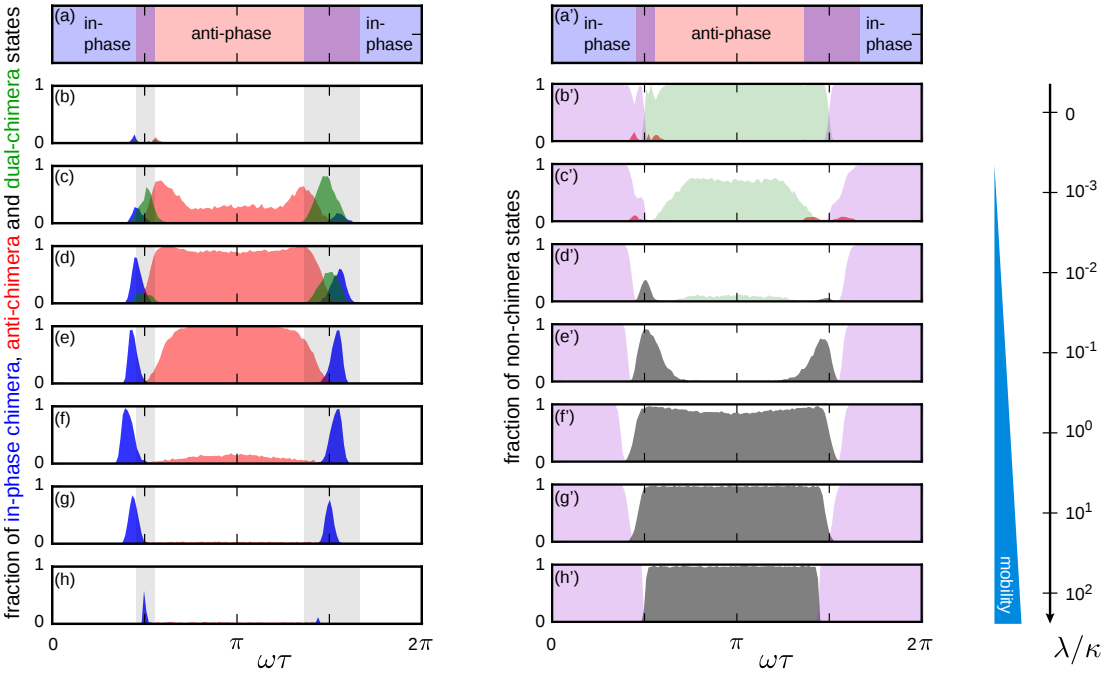

Figure 6.11: Mobility induces chimera states from neighboring in-phase and antiphase domains. Fraction of dynamical states at time $t = 5000$, starting from initial conditions with half the lattice with in-phase order and the other half with antiphase order, and added Gaussian noise, Figure 6.10. Fraction is computed over 512 realizations of initial conditions for each set of parameters.

on coupling delay values, Figure 6.11(h'). We conclude that mobility induces persistent chimera states when starting from conditions that include only ordered domains.

6.6 Chimera states with the signal-sending delay

So far in this chapter we only considered the incoming delay τ_{in} that accounts for signal processing time. In addition to their different interpretations, one difference between this and the outgoing time delay that could be mathematically relevant is that τ_{in} causes a dependence of the model equations (3.1) on a delayed neighborhood $V(t - \tau_{\text{in}})$. In every other model described in Section 2.3, the considered delayed coupling do not include any delayed neighborhood. This raised the question of whether this delayed neighborhood is necessary for the chimera states to form and persist. To address this question we consider the system

studied in Chapter 4, which corresponds to the general model but keeping only the delay τ_{out} , Eq. (4.2)

$$\dot{\theta}_i(t) = \omega + \frac{\kappa}{n_i} \sum_{j \in V_i(t)} \sin\left(\theta_j(t - \tau_{\text{out}}) - \theta_i(t)\right) \tag{6.5}$$

We already anticipated the result at the end of that Chapter 4. We find that the three kinds of chimera states appear for this system, indicating that the delayed neighborhood is not crucial for their occurrence. Similar results for their persistence in parameter space are encountered, Figure 6.12.

We examine the correlation of chimera fractions shown in Figures 6.9(II) and 6.12(II), to compare the statistics of chimera states for the two delays τ_{in} and τ_{out} . For each value of τ, we plot the fraction f_{out} of each kind of chimera state for τ_{out} against the fraction f_{in} obtained for the delay τ_{in} , Figure 6.13. The values lay near the identity line, reflecting the similarity of the results obtained for the two delays. As we carefully explained in Chapter 3, these two time delays represent different molecular processes in the biological problem and are thus conceptually different. Mathematically, the delay τ_{in} is included in the equations not only in the sinusoidal coupling function but in providing a delayed neighborhood. These differences do not seem to affect the statistics of chimera states. Still, it might be possible that the two delays have distinct effects on the temporal evolution of the system that is not captured when looking at the long term states. Similar to this, while phase shifts and coupling delays have similar effects on steady states, they display different transient dynamics towards synchronization [68]. Besides, the two delays may have distinct effects on the dynamics of the individual oscillators that are not captured when looking at the collective behavior. Whether the conceptual and mathematical differences between τ_{in} an τ_{out} can be noticed in the relevant features of the dynamics of the system is an intriguing question. We leave this for future work.

6.7 Discussion

We have shown that in the presence of coupling delay, mobility can induce the formation of persistent chimera states that blend disorder with in-phase and antiphase order in different combinations, Figure 6.11. In contrast to the expectation that mobility favors the relaxation to homogeneous states [47, 60, 133],

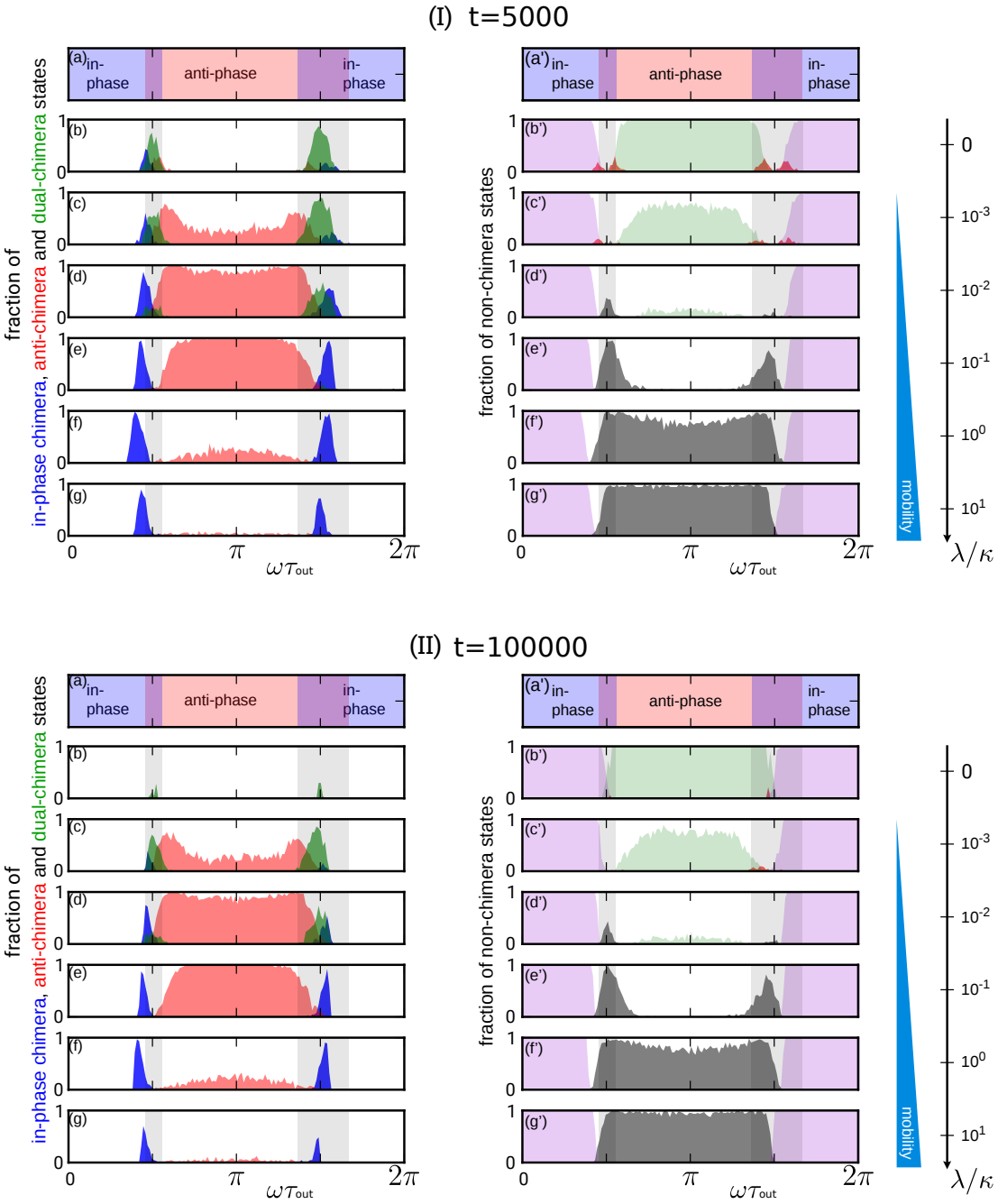

Figure 6.12: Fraction of dynamical states after (I) $t = 5000$ and (II) $t = 100000$ starting from random initial conditions. In this simulations $\tau_{\text{in}} = 0$ and the x axis in the plots corresponds to τ_{out} . Fraction is computed out of 64 realizations. Results are similar to Figure 6.9, where the x axis corresponds to τ_{in} and $\tau_{\text{out}} = 0$.

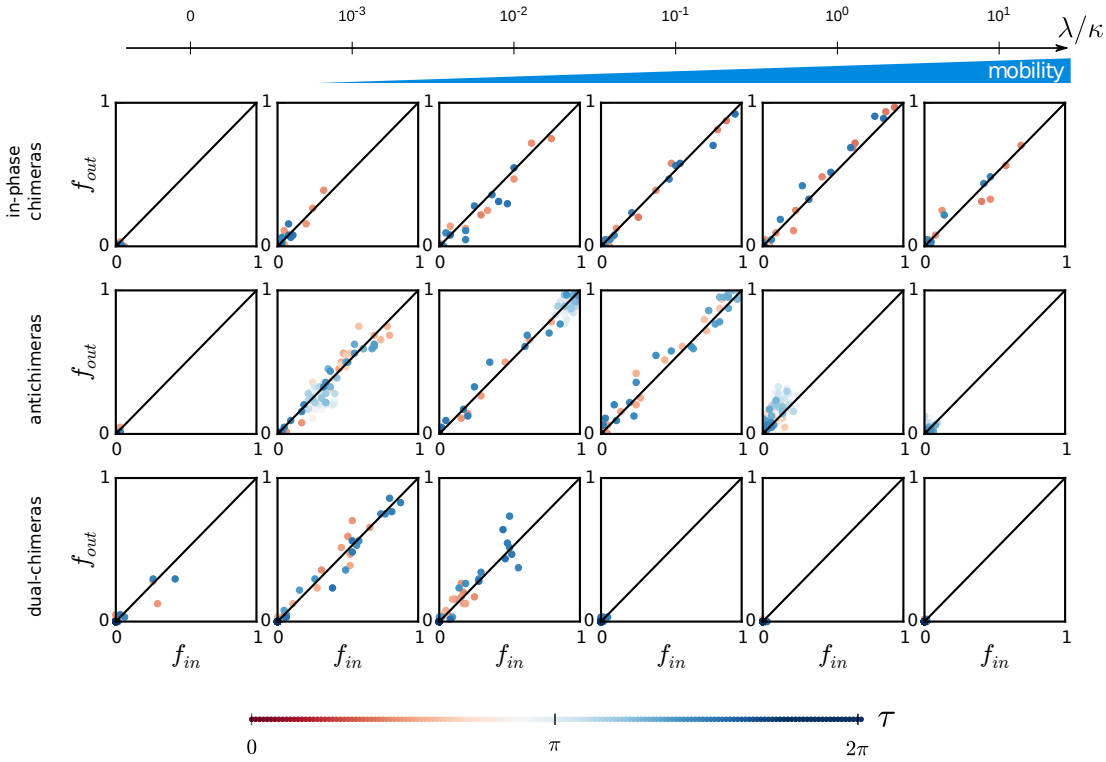

Figure 6.13: The fraction of chimera states in the long term is similar for τ_{in} and τ_{out} . Each panel is a plot of the fraction f_{out} of chimera states obtained for τ_{out} vs. the fraction f_{in} of chimera states obtained for the same values of τ_{in} . Each value of the delay is represented by a color. Each row corresponds to one kind of chimera. Each column corresponds to one value of λ/κ. The x axes is the fraction shown in Figure 6.9(II) and the y axes is the data shown in Figure 6.12(II).

here we show that mobility can also drive the system into heterogeneous states with complex long-lived patterns. These chimera states represent a paradigm of dynamic symmetry breaking as the symmetry present in the equations of motion of the system of coupled identical oscillators is not present in these solutions.

The conditions required for chimera states to form are still matter of debate [94]. Chimera states were first observed in systems with some form of non-local coupling [84, 85, 97, 104], and for some time this was thought to be a condition for chimera states to occur. Later, chimera states were also spotted in systems with global coupling [117–119, 122]. Chimera states in systems with local coupling have only been reported recently [123–126]. Here coupling is local, yet oscillators can exchange neighbors and interact with others originally far away [60].

Phase diagrams for systems of coupled mechanical oscillators reveal that

chimera states appear in between regions where in-phase and antiphase synchronization exchange stability [95]. Besides, chimera states are thought to occur near the stability boundaries of order and disordered states in systems with delayed coupling [100, 134]. Here we observe in-phase chimera states near the bi-stability region of in-phase and antiphase states. For the very low mobility regime, in-phase chimera states form between regions where in-phase or antiphase states dominate, Figure 6.11(b')-(c'). For larger mobility, in-phase chimera states form between regions where in-phase order or disorder dominate, Figure 6.11(d')-(h'). Thus, our results are consistent with both scenarios described above.

Analytical results for the stability of chimera states are scarce [96, 134, 135]. Here we find that chimera states appear either as transient or persistent states, Figure 6.8. Even the most persistent chimera states we observe are dynamic, with ordered domains that form and disappear in a background of disorder. Because mobility affects distinctly the different forms of order and disorder, there may be more than one mechanism at play. For example mobility introduces disorder into antiphase domains, while it favors order within in-phase domains. The interplay of these mechanisms could underlie the different kinds of chimera states reported here.

Our work suggests an unexpected avenue of research to look for chimera states in engineered and natural systems. Technological applications featuring mobile coupled oscillators have motivated recent theoretical studies [62, 136] and might give rise to chimera states provided that communication delays are present [137]. Our results could be relevant to the vertebrate segmentation clock, the biological system that initially motivated the theory, Eq. (3.1). As carefully explained in Section 1, the vertebrate segmentation clock is thought to be a population of coupled oscillators where significant coupling delays [50–52] occur together with cell mixing [18, 42–46, 138]. Therefore, both key ingredients in the theory are present in this system and it is possible that perturbations to delays or mobility could induce the formation of chimera states. In the case of coupling delays, it is possible to generate mutants in which the dynamics of the genetic oscillations in the PSM is consistent with a change in the value of the coupling delay [51], Figure 2.7(c). Chemically induced changes in the coupling strength that do not affect the delay, Figure 2.7(a), could also affect the dynamical states shown by the biological system as they would alter the multistability regions. Perturbations of the mobility rate of cells in the PSM is challenging but possible [44]. Further-

more, there is a natural gradient of mobility that could be taken advantage of to explore different mobility regimes [43, 44, 46], see Section 1. These experimental setups may provide a way to probe for the occurrence of chimera states in the segmentation clock.

Chapter 7

Measures for synchronization timescales

In Chapter 4, we studied a system of mobile delayed-coupled oscillators as it approaches the completely synchronized state. We analysed a characteristic time T_c in the linear regime, where the system is close to the synchronized state. In biological systems, however, noise hampers synchronization. Noise present in biological systems can push them away from synchronization, into states that are far from the completely synchronized state. Furthermore, some assays designed to determine the effects of noise and measure coupling strength consist of driving the system away from the synchronized state, sometimes almost to complete desynchronization. Thus, it is biologically relevant to quantify the time that the system needs to recover synchronization when it is still far from this state. In this chapter, we ask to what extent the characteristic time T_c is representative of the dynamics far from the synchronized state. We define measures to quantify these other timescales and look at the correlations between these measures and the characteristic time T_c previously analyzed. For simplicity in this chapter we consider the system of mobile oscillators without coupling delays $\tau_{in} = \tau_{out} = 0$.

7.1 Synchronization dynamics far away from synchrony

In Chapter 4 we characterized the synchronization dynamics of mobile delayed coupled oscillators in the exponential regime, where the system is close to the syn-

chronized state. In that regime, it is possible to define a characteristic relaxation time T_c that can be considered as a measure of how fast the system approaches synchronization. Because it describes the dynamics close to synchronization, T_c can be related to the relaxation of small perturbations to the synchronized state. This strategy is often used because it allows to linearize the equations and make analytical calculations that are otherwise not possible. This is the main reason why this linear regime is broadly considered in the literature. Similarly, a characteristic time is usually defined for the initial exponential grow from the incoherent state, in the short-time regime [139]. In particular, defining T_c permits us to relate our work with previous works that considered synchronization relaxation times in systems with either mobility or coupling delays separately [60, 68].

In biological systems, genetic oscillations are subjected to different sources of noise [140]. These include environmental changes like temperature variations and also intracellular fluctuations. Examples of the latter are cell divisions and the stochastic nature of the transcription processes generating the oscillations in each cell [141]. For these reasons, biological systems usually display states with some degree of partial synchronization that keep some distance from the completely synchronized state and from the completely incoherent state. We already introduced a complex order parameter $Z = re^{i\psi}$, Eq. (2.7), as a macroscopic quantity to measure the degree of global synchronization in the system, Figure 2.1. In terms of order parameters, these states where the relevant dynamics for biology occurs correspond to intermediate values $0 < r < 1$ [142]. In the vertebrate segmentation clock Delta-Notch coupling competes with noise to synchronize the oscillations, Figure 1.3. When the coupling is weak, noise can lead the system into states with rather small values of the order parameter. The relevant dynamics of the system during recovery of synchronization occurs within these intermediate values of r, Figure 1.4. This raises the question of whether the characteristic time in the regime close to complete synchronization T_c is adequate to describe the relevant synchronization timescales for the biological system.

To address this question, in this chapter we consider the system of mobile coupled identical oscillators with nearest neighbor coupling but without coupling delays

$$\dot{\theta}_i(t) = \omega + \frac{\kappa}{n_i} \sum_{j \in V_i(t)} \sin\left(\theta_j(t) - \theta_i(t)\right) \tag{7.1}$$

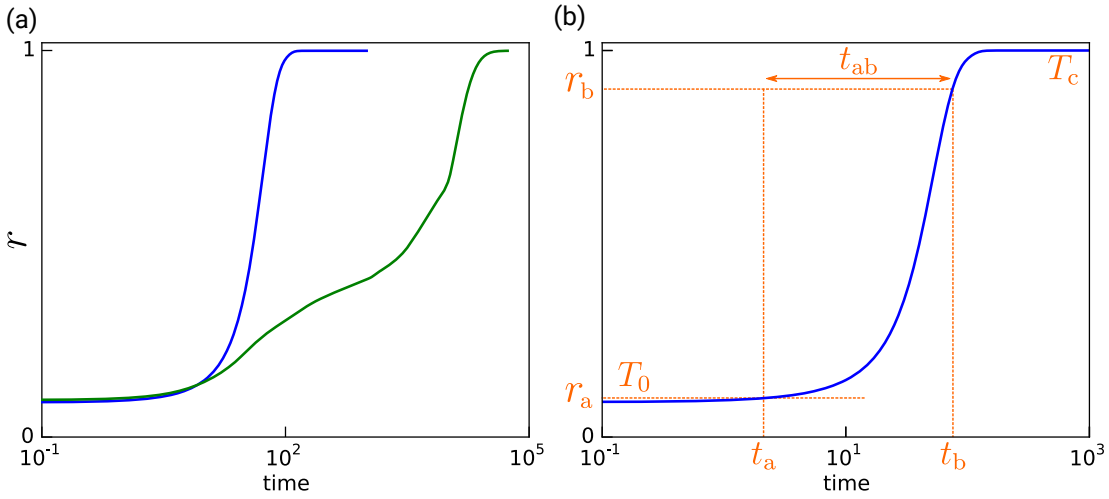

Figure 7.1: Time evolution of the order parameter as the system goes from disorder to order states. (a) Synchronization is faster for larger mobility, $\lambda/\kappa = 1000$ (blue) and $\lambda/\kappa = 1$ (green). (b) Definition of the different time measures. t_a and t_b measure the time in which the system goes through intermediate values of the order parameter. T_c and T_0 are the characteristic times for the last and first exponential regimes, respectively. Curves shown are averages over 128 realizations.

with

$$V_i(t) = \{j \text{ such that } |x_j(t) - x_i(t)| = 1\}\,.$$

7.2 Different quantitative measures characterize different synchronization regimes

Previous analysis of the system described by Eq. (7.1) showed that mobility reduces the time the system needs to achieve synchronization [60], Chapter 2.2. In terms of the order parameter, this result can be visualized comparing the temporal evolution of r when mobility is increased, Figure 7.1(a). We next define alternative quantities to the relaxation time T_c that aim to measure the intermediate timescales where oscillators are on their way to synchronization but far from the completely synchronized state, Figure 7.1(b). An interesting question is how these timescales are related to the usually considered timescales of the linear regimes, T_c and its analogous close to the incoherent state T_0.

We characterize synchronization timescales within intermediate values of the

order parameter r defining two quantities t_a and t_b , Figure 7.1(b). We define t_a as the value of time for which the absolute value of the order parameter transverses a threshold value $r_a = r(t_a)$. Definition of t_b is analogous, $r_b = r(t_b)$, with threshold $r_b > r_a$. The quantity t_a sets the time in which the system has moved away from the initial incoherent state at least by an amount r_a . Similarly, t_b sets the time in which the system starts to be close to the synchronized state, at least by an amount $1-r_b$. The intermediate range, in which the system goes from r_a to r_b represents the regime in which relevant dynamics for biological systems occur. The timescale of this intermediate regime is defined by $t_{ab} \equiv t_b$ -t_a . All these timescales are illustrated in Figure 7.1(b) for a typical time evolution of the order parameter. Interestingly, we can define similar timescales for the spatial correlations $\rho_d(t)$ analysed in Chapter 4, Eq. (4.6). We next study the dependence of the different timescales with mobility.

7.3 Effects of mobility on the different synchronization regimes

Previously, the characteristic time T_c was defined from the spatial correlations ρ_d [60], Chapter 4. It was shown that T_c is the same for all correlations ρ_d with $d = 1, \ldots, N-1$ and that its value decreases with increasing mobility. The characteristic time T_c can be defined as well for the order parameter in the regime where $1 - r \sim e^{-t/T_c}$. The value of T_c for the Kuramoto order parameter r decreases for increasing mobility and it coincides with the values obtained for the spatial correlations, Figure 7.2(a).

Analogous plots for t_a and t_{ab} show that, while the characteristic time T_c does not depend on the correlation length d, the curves for both times t_a and t_{ab} are different for different correlation lengths, Figure 7.2(b,c). For low mobility, the different values of t_{ab} for the different correlation lengths reflect the fact that, for intermediate times, several spatial modes are present with different lifetimes. Similar to T_c , the value of t_{ab} decreases with increasing mobility, Figure 7.2(b). This happens for all the correlations ρ_d with the exception of ρ_1. Remarkably, ρ_1 takes similar values for all the range of mobility, suggesting that the timescale in which the local correlations between first neighbors grows is independent of mobility. Moreover, for large mobility the value of t_{ab} is the same for all correlations ρ_d and coincides with its value for ρ_1. The value of λ/κ for which t_{ab} for a certain

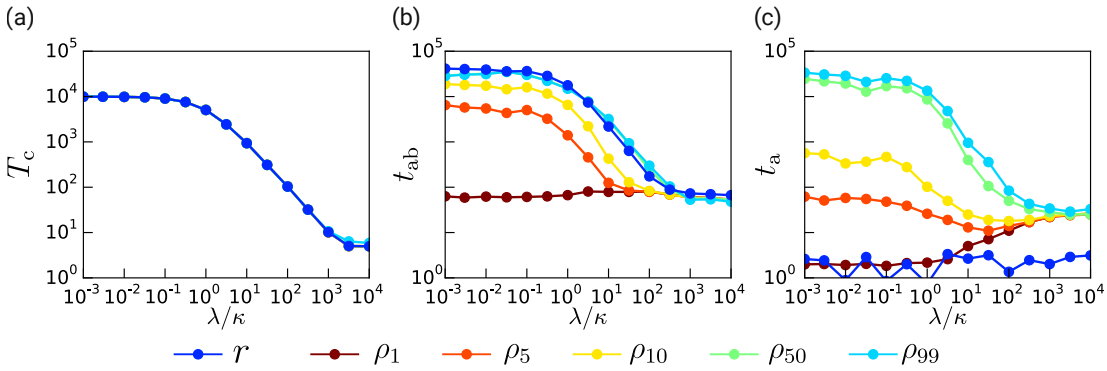

Figure 7.2: Dependence of the different measures of synchronization timescales with mobility. Threshold values are $r_a = 0.1$ and $r_b = 0.9$ for all the magnitudes considered (order parameter and correlations). Measures where computed from an average over 128 realizations for each parameter set.

correlation starts to coincide with t_{ab} for ρ_1 depends on the correlation length d. For short correlations like ρ_5 and ρ_{10}, the value of t_{ab} collapses to its value for ρ_1 at lower values of λ/κ. This reflects the fact that, at intermediate times, larger mobility leads to spatial patterns composed of modes of longer wavelengths. With increasing d, curves become more similar to the one for the order parameter. This curve for r seems to be an upper limit to the curves for the correlations.

The behavior of t_a is quite different, Figure 7.2(c). For very short correlations like ρ_1, t_a increases with increasing mobility. In contrast, for long correlations t_a shows the opposite behavior, decreasing with increasing mobility. The fact that the time t_a is different for different correlations reflects that short correlations start to increase earlier than long correlations, as already observed in Figure 4.2(a,b). The values of t_a for all correlations collapse for sufficiently large mobility $\lambda/\kappa > 10^3$, Figure 4.2(c). For the order parameter r, the behaviour of t_a is quite noisy. This reflects the fact that t_a depends on initial conditions, and the average over random initial conditions still gives a value of the order parameter that starts very close to r_a . Fluctuations near $r \sim 0$ depend on the system size N and we expect smaller fluctuations for bigger systems. It should be interesting to look at how this time t_a relates to a more robust characteristic time like the one of the initial exponential take off T_0. We leave this for future work.

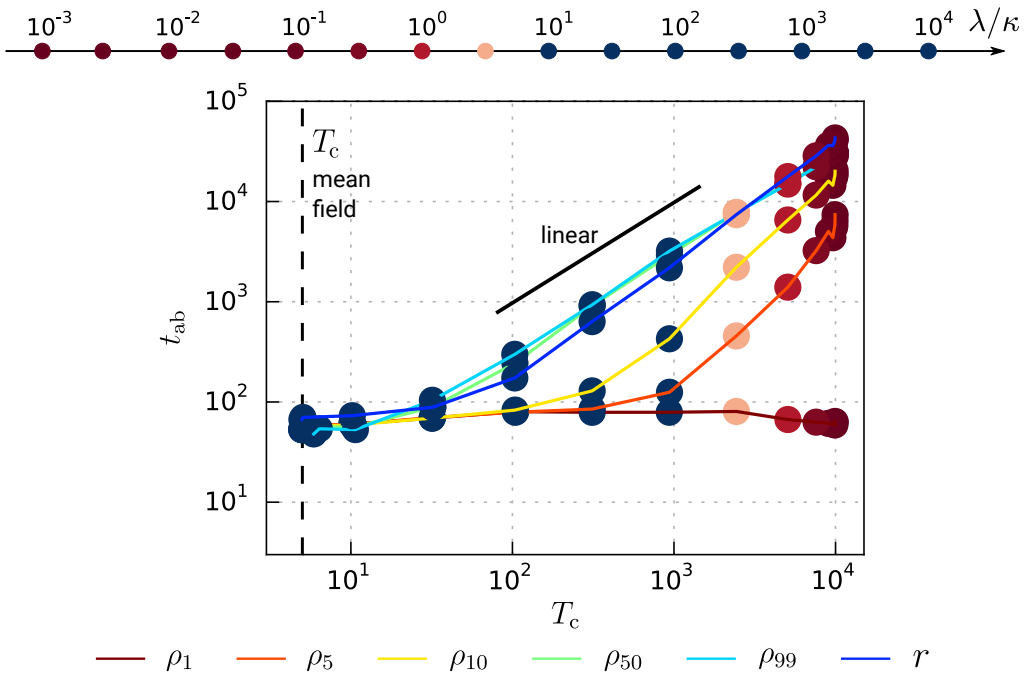

Figure 7.3: Correlations between synchronization timescales for the intermediate regime t_{ab} and for exponential relaxation T_c . Coloured lines correspond to different correlation distances d while coloured dots correspond to different values of the mobility to coupling ratio λ/κ. A black solid line corresponding to linear correlation is drawn for reference. Both timescales are computed from an average over 128 realizations.

7.4 Relation between the different measures

We study how the usually considered characteristic relaxation time T_c correlates with the intermediate timescale t_{ab} , Figure 4.2. Interestingly, we find that the correlation between t_{ab} and T_c is a power law. The exponent of the power law is close to one for the long range correlations, see for example ρ_{50} and ρ_{99} in Figure 4.2, and also for the order parameter. This almost linear relationship between the two timescales supports the idea that we can use T_c as an informative proxy of what happens in the intermediate regime.

7.5 Discussion

We proposed different quantitative measures that characterize different timescales for synchronization. In particular, we defined two quantities t_a and t_{ab} that describe distinct regimes of the evolution of the system from disorder to synchro-

nization. On the one hand, t_{a} characterizes the regime close to the incoherent state. When applied to spatial correlations ρ_d, this is a measure of how early the system starts to generate local correlations of range d. When applied to the order parameter, t_{a} indicates how early the system separates from the incoherent state and produces some degree of coherence. However, the value of t_{a} strongly depends on the initial conditions. On the other hand, t_{ab} quantifies the time that the system spends within intermediate values of the relevant order parameters. Because how we define this quantity, we expect this timescale to reflect an intrinsic property of the system, that does not depend on initial conditions. We compared this timescale with the usually employed timescale T_{c} of the linear regime near the synchronized state. The almost linear correlation between t_{ab} and T_{c} for long correlations and the order parameter positively supports the idea that T_{c} can be used as a measure of the time the system needs to recover synchronization even when it is originally far from the synchronized state. This provides an important link between theoretically tractable timescale measures and biologically relevant timescales.

Several interesting aspects of the dynamics of the system remain to be explored. First, in the same way as we consider correlations between the intermediate timescale t_{ab} and the characteristic relaxation time towards synchronization T_{c} , it would be interesting to explore how the time t_{a} correlates with the usually defined characteristic time T_0 of the linear take off from the incoherent state. Second, the behavior of the quantities defined here constitute a first step in understanding the relation between different measures quantifying different synchronization regimes, and could be system dependent. In this sense, it would be interesting to explore the behaviour of these measures in other systems of coupled oscillators. In particular, the effects of coupling delays on the timescales defined in this chapter will be interesting future work. Finally, the fact that $t_{\mathrm{ab}}\,(\lambda/\kappa)$ is almost constant for ρ_1, Figure 7.2(b), suggests that this timescale could be derived analytically. To this end, we have attempted to derive an analytical expression for $\rho_1(t)$. The expression for $\rho_1(t)$ is coupled to higher order moments and to longer range correlations in a hierarchy that does not seem trivial to close consistently. We plan to find a moment closure strategy that allows to derive a consistent expression for ρ_1.

Chapter 8

Summary and outlook

In this Thesis we proposed a theoretical framework to study the dynamics of mobile delayed-coupled oscillators. The theory is motivated by the biological process of embryonic segment formation. The vertebrate body is provided with a repetitive structure of segments that originate sequentially -one by one- during embryonic development, with a precise rhythm. This rhythm is controlled by a biological clock, known as the vertebrate segmentation clock. Proper segment formation relies on the coherence of the rhythm produced by the many cells that form the clock tissue. An intriguing question is how these cells self-organize and maintain this collective rhythm. In zebrafish it is thought that each cell in the tissue behaves as a noisy autonomous oscillator. Synchronization of noisy single cell oscillators is achieved through intercellular communication via Delta-Notch signaling. Intercellular communication via Delta-Notch signaling is local, as cells need to be close enough to allow for mechanical contact between transmembrane ligands and receptors. This local signaling involves a cascade of complex events that include synthesis and transport of macromolecules. This cascade introduces communication delays which may alter collective dynamics and patterning. Besides this delayed local communication mechanism, cells move within the posterior zone of the tissue exchanging neighbors over time. This mobility is expected to affect information flow in the tissue and pattern formation.

Both communication delays and cell mobility had been separately described in theories of the segmentation clock. Theories consisting of coupled oscillators that include explicit delays in the coupling have demonstrated to capture the complexity of Delta-Notch communication. Theories that describe cell movement

as an exchange of neighbors in a lattice may account for the mobility observed in segmentation clock tissue. In more general theoretical works, both the presence of coupling delays and mobility of oscillators had been addressed separately, showing these aspects have distinct effects on the collective dynamics. However, the combined effect of coupling delays and mobility on the dynamics of coupled oscillators had not been addressed before this work due to its complexity. The presence of delays in the coupling causes neighboring oscillators to exchange information about their phases at a previous time point. If in addition there is also mobility, it could happen that these neighboring oscillators were not neighbors at that previous time point. Thus, it was unclear how mobility affects dynamics in the presence of coupling delays. In this Thesis, we address this problem through a theoretical description that brings together coupling delays and mobility.

We considered a system of coupled phase oscillators on a one dimensional lattice, where mobility was described as a stochastic exchange of positions in the lattice. In between position exchanges produced by mobility, the dynamics of the phases was described with a system of differential equations with delayed local coupling. In Chapter 3 we carefully explained the theoretical description and motivated its components from the biology. The description includes two different contributions to the total time delay $\tau = \tau_{\text{in}} + \tau_{\text{out}}$ that represent different aspects of the communication mechanism. Splitting the delay in this way is important in the context with mobility. We considered alternatively each contribution τ_{in} or τ_{out} depending on what aspect of the system we aimed to consider in each chapter. To study the evolution of the system, we developed numerical methods to solve the delayed differential equations in the context of the stochastic exchange of positions. When possible, we complemented the computational implementation of the theory with analytical calculations.

In Chapter 4 we examined synchronization timescales, motivated fundamentally on the biological system. We considered only the time delay that accounts for sending the signals τ_{out} , linked with the synthesis and transport of the Delta ligands from the nucleus to the cell membrane. We argued that in the biological system this signal-sending delay may be larger than the signal-processing one and therefore set $\tau_{\text{in}} = 0$. We explored values of the delay in the first and second stable branches for synchronization, the latter being the region where the value of τ_{out} in the biological system was estimated [51]. We showed that mobility can speed up synchronization even in the presence of coupling delays. In addition to

the numerical results, we used analytical calculations to show that mobility and delays drive the system into different dynamical regimes towards synchronization. Analytical results were in good agreement with numerical simulations. Results presented in Chapter 4 were summarized in a manuscript that will be sent for publication soon [143].

Results presented in Chapter 4 show that mobility has a role on the dynamics of synchronization also when coupling delays are present. Moreover, delays seem to favor this role by extending the range of the mobile regime. This results should be relevant to understand the mechanisms underlying synchronization timescales in the biological system, where both mobility and delays are present. Perturbations to coupling delay in the biological system are possible with loss-of-function Notch mutants and with novel transgenic lines that overexpress Delta ligands [51,53]. Disturbing mobility is challenging but also possible with chemicals such as blebbistatin [44]. Therefore, experimental tools for perturbing both key elements of the theory presented here are available and, in principle, the results presented could be tested in experiments.

In chapters 5 and 6 we showed that in the presence of coupling delay, mobility can induce the formation of persistent chimera states. Chimera states are complex spatio-temporal patterns in which order and disorder coexist within the same state in systems of identical oscillators. Since their discovery in 2002, they have demonstrated to be broadly encountered in multiple systems, both theoretically and in experiments. Due to the different dynamical properties that chimera states present depending on the system where they appear, different quantitative measures have been proposed to characterize them. Still, the mixed nature of these states entails a difficulty in developing measures capable to reliably detect and classify chimera states.

In Chapter 5 we proposed a new method for the classification of dynamical states that succeeds to distinguish chimera states from a variety of other states appearing in the system. The main idea of the method is to locally detect order and disorder based on three-node motifs in the phase differences between neighboring oscillators. The proposed method improves the reliability on identifying chimeras with respect to previous methods proposed in the literature. In particular, it allows to classify a wide repertoire of dynamical states with very different characteristics between them such as noisy states or states including twists and domain walls. This method is a valuable new tool that could be relevant to

identify chimera states in other contexts.

In Chapter 6 we employed the classification method devised to analyse the occurrence and persistence of chimera states in the system of mobile delayed-coupled oscillators. We found three kinds of chimera states, two of which are novel kinds of chimeras previously unreported. In addition to well-known chimera states where in-phase order coexists with disorder, with the devised method we identified antichimera states where antiphase order coexists with disorder and dual-chimera states where both in-phase and anti-phase order coexist with disorder. We showed that the three kinds of chimera states are dynamic and can persist for long times for intermediate mobility values. Despite the great progress that had been made in understanding chimera states, the mechanisms and conditions for their existence are still not clear. The unexpected appearance of chimera states in the system with mobility and delays reveals a new mechanism for their formation and constitutes an important contribution to our understanding of these intriguing broken symmetry patterns. In addition, although chimera states are thought to play a role in natural systems, most of the experimental evidence is found in carefully designed laboratory setups. Our work suggests an avenue of research to look for chimera states in engineered and natural systems where mobility occurs together with coupling delays. In particular, both key ingredients in the theory are present in the vertebrate segmentation clock and it is possible that perturbations to delays or mobility could induce the formation of chimera states. The main results reported in chapters 5 and 6 were recently published in Physical Review E [86].

In Chapter 7 we went back to synchronization dynamics in a simplified system without coupling delays to address the question of how to characterize different synchronization regimes. In Chapter 4 we had quantified the characteristic time that the system needed to approach synchronization in the last exponential regime. This corresponds to the exponential relaxation to synchronization, when the order parameter is already near its synchronization value of $r \approx 1$. It is advantageous to consider this exponential relaxation because it allows to make analytical calculations that broaden our understanding of synchronization dynamics, as we showed in Chapter 4. However, biological systems usually work in intermediate regimes, far from complete synchrony $r \approx 1$ and from complete incoherence $r \approx 0$. In order to compare our results with experimental evidence on synchronization timescales in biological systems and test the theory, it is neces-

sary to have a quantification that can be related to these timescales. In Chapter 7 we defined other quantities t_{ab} to study the evolution of the system in these intermediate regimes. We analysed the dependence of these quantities with mobility and their relationship with the previously defined characteristic time T_{c} of the exponential regime. Correlations in the two main quantities t_{ab} and T_{c} representing the intermediate and final regimes respectively, suggest that the characteristic time T_{c} addressed in Chapter 7 could be well representing the tendency of the biologically relevant regimes. We note however that these results could be model dependent and a more extensive analysis needs to be done to extract conclusive results. It would also be interesting to study how these results change when including coupling delays.

In brief, in the present Thesis we theoretically addressed the interplay between mobility and coupling delays in a system of coupled oscillators, motivated by the vertebrate segmentation clock. By means of numerical and analytical methods we carefully analysed two main aspects of the dynamics, synchronization and chimera states. Synchronization is one of the fundamental features in the vertebrate segmentation clock, as it has the functional relevance of generating a collective rhythm necessary to make correct segments. Chimera states are intriguing broken symmetry patterns and the appearance of this states in the biological system could disturb segment formation. In a broader context, this Thesis constitutes one step forward in the quantitative understanding of how collective dynamics emerge from the behaviour of individual units in biological systems.

Appendix A

Numerical methods

As described in Chapter 3 we consider a system of N phase oscillators with phases θ_i, with $i = 1, \ldots, N$, placed at discrete positions $x_i = 0, \ldots, N-1$ in a one dimensional lattice of N sites. The phases of the oscillators evolve according to Eqs. (3.1), which we integrate numerically using an integration scheme with a time step δt that is fixed within each simulation. Additionally, oscillators are able to move through the lattice by exchanging positions with their nearest-neighbors. This stochastic exchange of oscillators positions is described as a Poisson process. We introduce a mobility rate λ so that each pair of neighboring oscillators has a probability $\lambda/2$ of exchanging positions per unit time. Together with the two contributions to the coupling delay τ_{in} and τ_{out} , the mobility rate λ is a relevant parameter of our description. In this Thesis we explore different values of the mobility rate and coupling delays. Importantly, the values of these relevant parameters can be set independently from each other. To obtain numerical solutions for the dynamics of the system, we developed a computational algorithm that solves the delayed differential equations (3.1) in the context with mobility. We next describe the algorithm, which is written in C programming language and receives the relevant parameter values for each simulation via the command line.

To simulate the Poisson process we use an approximation of the Gillespie algorithm for discrete time intervals. The distribution of waiting times t_e for the next exchange event in the lattice of N oscillators is

$$P(t_e) = a_0 \, \exp\left(-a_0 \, t_e\right) \tag{A.1}$$

where $a_0 = (N-1)\,\lambda/2$ is the propensity for an exchange event [82]. We generate a discrete set of random waiting times $\{t_e\}$ drawn from this distribution. We approximate each of the waiting times t_e in this set by the closest larger integer multiple of δt. As a result we obtain a discretized waiting time t_{ed}

$$t_e \to t_{ed} = n_e\,\delta t \quad \text{with} \quad n_e = \text{ceil}(t_e/\delta t). \tag{A.2}$$

Therefore, exchange events occur at time points that are integer multiples of the integration step. This discretization of the waiting times introduces a perturbation from the Poissonian statistics. For this perturbation to be negligible, this approximation requires small enough δt compared to the average time interval between two successive exchange events $\langle t_e \rangle = 1/a_0$, that is $\delta t \ll 1/a_0$. Thus, to obtain accurate realizations of exchange events we set

$$\delta t \leqslant \langle t_e \rangle / 10 \tag{A.3}$$

in all simulations [48]. Thus, the time step δt for numerical integration is fixed within each simulation and is the same for simulations with the same parameter values.

Eqs. (3.1) include a delayed coupling between first neighbors in the lattice. From a mathematical point of view, these are delayed differential equations (DDEs) [74, 78, 79]. To integrate DDEs, it is necessary to know the value of the variables at past times [77]. We already ilustrate this with a simple example in Chapter 2.3. To go from $t \to t + \delta t$ in the equation for the oscillator $\theta_i(t)$, we need to know the value of the variables θ_j at a previous time $t - \tau$. Thus, we need to make sure that we possess those values $\theta_j(t - \tau)$ at each time t to make the following integration step. For the first steps of integration up to $t = \tau$, these are given by fixing the initial history of the variables in the interval $[-\tau, 0]$. For the subsequent integration steps, these values are the ones previously computed by the integration method. Because numerical integration conceives discrete time steps of size δt, the values of the variables that we have are only the ones at time points belonging to the grid of discrete times $t_n = n\,\delta t$ with n a natural number. Thus, to have computed the needed values of the variables at time $t - \tau$ for each time step, we always fix the delay value to an integer number of time steps

$$\tau = n_\tau\,\delta t \tag{A.4}$$

where n_τ is a natural number. The delay τ includes the two contributions to the coupling delay $\tau = \tau_{\text{in}} + \tau_{\text{out}}$. As we sometimes put one of these to zero, we additionally ask that each of the contributions is also an integer number of time steps

$$\tau_{\text{in}} = n_{\text{in}}\,\delta t \tag{A.5}$$

$$\tau_{\text{out}} = (n_\tau - n_{\text{in}})\,\delta t \tag{A.6}$$

with n_{in} a natural number. Eq. (A.4) ensures that the previous times in which we need to evaluate the variables to proceed with the integration coincide with grid points. Then, at the moment we need it, we had already computed the state of the system at those previous times.

At each time t_n, we save the phase state for all the oscillators at previous times in the complete interval $[t_n - n_\tau\,\delta t, t_n]$. In the algorithm, we save these values in an array of $n_\tau + 1$ places for each oscillator. At each new time step t_{n+1}, we replace in these arrays i the value that we will not longer need $\theta_i(t_n - n_\tau \delta t)$ with the value just computed that we will need in the future. To this end, the code includes an index whose value we update at each time step to make it point to the place in the arrays where the value of the phases at the present time are. This index runs circularly in from 0 to n_τ ($ind = 0, \ldots, n_\tau, 0, \ldots$) and allows us to track where in each array the phase that we want to replace is. In addition, to integrate the equations we need to evaluate the neighborhoods in past times $V_i(t - \tau_{\text{in}})$. We track the neighborhoods of all the oscillators in the interval $[t_n - n_{\text{in}}, t_n]$ storing the positions $x_i(t_n)$ for t_n in that interval in arrays i of $n_{\text{in}} + 1$ places each. We replace the values not longer needed at each new time step with the help of a second index $ind_2 = 0, \ldots, n_{\text{in}}$ that points at the places in the arrays where current positions are. The indexes in the code have a double role. On the one hand, they avoid storing in memory the whole evolution of the system, which would be prohibitively expensive numerically. On the other hand, at each time step the indexes allow to track the place in the array where the new value of each variable should be stored. This considerably saves computational time, as it permits to store information in convenient places in the array and thus avoids scrolling the values already saved to leave the last place free for the new value.

In summary, the theoretical model described here is implemented numerically as follows. Given a mobility rate λ we fix a time step δt as stated before. Next we

set the delay value τ as in Eq. (A.5) by choosing a number n_τ of time steps. We then choose the initial phases $\theta_i(t=0)$ and positions $x_i(t=0)$ for the oscillators $i = 1, \dots N$ and set their history for t in $[-\tau, 0)$. No exchange events occur before $t = 0$, so $x_i(t) = x_i(t=0)$ for t in $[-\tau, 0)$ and $\forall i$. Finally, we iterate the following steps:

1. Generate the time for the next exchange event t_e from the distribution in Eq. (A.1) and also randomly choose which pair of oscillators will exchange positions from a uniform distribution in the amount of nearest-neighbor pairs $\mathcal{U}(N-1)$.

2. Integrate n_e time steps of Eq. (3.1), with fixed positions for all the oscillators in the lattice.

3. Update positions and neighborhoods affected by the exchange event and go back to step 1.

On the integration scheme employed. Even when the delay is chosen to be an integer multiple of the time step, some integration schemes like for example Runge Kutta methods need evaluation of the equation functions at intermediate points in between grid points. When using this methods, interpolation is needed to obtain the values of the variables at those time points. In this Thesis, a Runge Kutta fourth order (RK4) was utilized in chapters 5 and 6. Instead of interpolating, we approximate the values of the variables in between grid points by the value they had at the closest previous grid point. This approximation can affect the order of the error in the RK4 method, but does not affect the results presented. To confirm this we have reproduced the main results in Chapter 6 with an Euler scheme. In Chapter 4 we utilized an Euler integration scheme. The time step δt employed is set as explained above, Eq. (A.3). For the Runge Kutta scheme, when the value obtained that way is $\delta t > 0.01$ we set $\delta t = 0.01$. For the Euler scheme, when the value obtained that way is $\delta t > 0.0001$ we set $\delta t = 0.0001$.

Bibliography

[1] C. Gomez, E. M. Özbudak, J. Wunderlich, D. Baumann, J. Lewis, and O. Pourquié, "Control of segment number in vertebrate embryos," *Nature*, vol. 454, no. 7202, pp. 335–339, 2008.

[2] L. Wolpert, J. Smith, T. Jessell, P. Lawrence, E. Robertson, and E. Meyerowitz, *Principles of development*. Oxford University Press, 3rd ed., 2006.

[3] M. P. Bulman, K. Kusumi, T. M. Frayling, C. McKeown, C. Garrett, E. S. Lander, R. Krumlauf, A. T. Hattersley, S. Ellard, and P. D. Turnpenny, "Mutations in the human delta homologue, dll3, cause axial skeletal defects in spondylocostal dysostosis," *Nat. genet.*, vol. 24, no. 4, p. 438, 2000.

[4] O. Pourquié, "Vertebrate segmentation: from cyclic gene networks to scoliosis," *Cell*, vol. 145, no. 5, pp. 650–663, 2011.

[5] C. Schröter, L. Herrgen, A. Cardona, G. J. Brouhard, B. Feldman, and A. C. Oates, "Dynamics of zebrafish somitogenesis," *Developmental Dynamics*, vol. 237, no. 3, pp. 545–553, 2008.

[6] A. Hubaud and O. Pourquié, "Signalling dynamics in vertebrate segmentation," *Nat. Rev. Mol. Cell Biol.*, vol. 15, no. 11, pp. 709–721, 2014.

[7] J. Cooke and E. C. Zeeman, "A clock and wavefront model for control of the number of repeated structures during animal morphogenesis," *Journal of theoretical biology*, vol. 58, no. 2, pp. 455–476, 1976.

[8] Y. Saga and H. Takeda, "The making of the somite: molecular events in vertebrate segmentation," *Nature Reviews Genetics*, vol. 2, no. 11, p. 835, 2001.

[9] D. Roellig, L. G. Morelli, S. Ares, F. Jülicher, and A. C. Oates, "Enhanced snapshot: The segmentation clock," *Cell*, vol. 145, no. 5, pp. 800–800, 2011.

[10] A. C. Oates, L. G. Morelli, and S. Ares, "Patterning embryos with oscillations: structure, function and dynamics of the vertebrate segmentation clock," *Development*, vol. 139, no. 4, pp. 625–639, 2012.

[11] R. Kageyama, Y. Niwa, A. Isomura, A. González, and Y. Harima, "Oscillatory gene expression and somitogenesis," *Wiley Interdisciplinary Reviews: Developmental Biology*, vol. 1, no. 5, pp. 629–641, 2012.

[12] Y. Saga, "The mechanism of somite formation in mice," *Current opinion in genetics & development*, vol. 22, no. 4, pp. 331–338, 2012.

[13] I. Palmeirim, D. Henrique, D. Ish-Horowicz, and O. Pourquié, "Avian hairy gene expression identifies a molecular clock linked to vertebrate segmentation and somitogenesis," *Cell*, vol. 91, no. 5, pp. 639–648, 1997.

[14] Y. Masamizu, T. Ohtsuka, Y. Takashima, H. Nagahara, Y. Takenaka, K. Yoshikawa, H. Okamura, and R. Kageyama, "Real-time imaging of the somite segmentation clock: revelation of unstable oscillators in the individual presomitic mesoderm cells," *Proceedings of the National Academy of Sciences*, vol. 103, no. 5, pp. 1313–1318, 2006.

[15] D. Soroldoni and A. C. Oates, "Live transgenic reporters of the vertebrate embryo's segmentation clock," *Current opinion in genetics & development*, vol. 21, no. 5, pp. 600–605, 2011.

[16] E. A. Delaune, P. François, N. P. Shih, and S. L. Amacher, "Single-cell-resolution imaging of the impact of notch signaling and mitosis on segmentation clock dynamics," *Dev. Cell*, vol. 23, pp. 995–1005, 2012.

[17] D. Soroldoni, D. J. Jörg, L. G. Morelli, D. L. Richmond, J. Schindelin, F. Jülicher, and A. C. Oates, "A doppler effect in embryonic pattern formation," *Science*, vol. 345, no. 6193, pp. 222–225, 2014.

[18] K. Uriu and L. G. Morelli, "Determining the impact of cell mixing on signaling during development," *Development, growth & differentiation*, 2017.

[19] A. J. Krol, D. Roellig, M.-L. Dequéante, O. Tassy, E. Glynn, G. Hattem, A. Mushegian, A. C. Oates, and O. Pourquié, "Evolutionary plasticity of segmentation clock networks," *Development*, vol. 138, pp. 2783–2792, 2011.

[20] J. Lewis, "Autoinhibition with transcriptional delay: a simple mechanism for the zebrafish somitogenesis oscillator," *Curr. Biol.*, vol. 13, no. 16, pp. 1398–1408, 2003.

[21] B. Novák and J. J. Tyson, "Design principles of biochemical oscillators," *Nature reviews Molecular cell biology*, vol. 9, no. 12, pp. 981–991, 2008.

[22] C. Schröter, S. Ares, L. G. Morelli, A. Isakova, K. Hens, D. Soroldoni, M. Gajewski, F. Jülicher, S. J. Maerkl, B. Deplancke, and A. C. Oates, "Topology and dynamics of the zebrafish segmentation clock core circuit," *PLoS Biology*, vol. 10, p. e1001364, 2012.

[23] A. Hanisch, M. V. Holder, S. Choorapoikayil, M. Gajewski, E. M. Özbudak, and J. Lewis, "The elongation rate of rna polymerase ii in zebrafish and its significance in the somite segmentation clock," *Development*, vol. 140, no. 2, pp. 444–453, 2013.

[24] A. B. Webb, I. M. Lengyel, D. J. Jörg, G. Valentin, F. Jülicher, L. G. Morelli, and A. C. Oates, "Persistence, period and precision of autonomous cellular oscillators from the zebrafish segmentation clock.," *eLife*, vol. 5, pp. 1–17, jan 2016.

[25] J. Dubrulle, M. J. McGrew, and O. Pourquié, "Fgf signaling controls somite boundary position and regulates segmentation clock control of spatiotemporal hox gene activation," *Cell*, vol. 106, no. 2, pp. 219–232, 2001.

[26] A. Sawada, M. Shinya, Y.-J. Jiang, A. Kawakami, A. Kuroiwa, and H. Takeda, "Fgf/mapk signalling is a crucial positional cue in somite boundary formation," *Development*, vol. 128, no. 23, pp. 4873–4880, 2001.

[27] L. Bajard, L. G. Morelli, S. Ares, J. Pécréaux, F. Jülicher, and A. C. Oates, "Wnt-regulated dynamics of positional information in zebrafish somitogenesis," *Development*, vol. 141, no. 6, pp. 1381–1391, 2014.

[28] K. Wahi, M. S. Bochter, and S. E. Cole, "The many roles of notch signaling during vertebrate somitogenesis," in *Seminars in cell & developmental biology*, vol. 49, pp. 68–75, Elsevier, 2016.

[29] B.-K. Liao and A. C. Oates, "Delta-notch signalling in segmentation," *Arthropod structure & development*, 2016.

[30] E. C. Lai, "Notch signaling: control of cell communication and cell fate," *Development*, vol. 131, no. 5, pp. 965–973, 2004.

[31] R. Kopan and M. X. G. Ilagan, "The canonical notch signaling pathway: unfolding the activation mechanism," *Cell*, vol. 137, no. 2, pp. 216–233, 2009.

[32] U. Koch, R. Lehal, and F. Radtke, "Stem cells living with a notch," *Development*, vol. 140, no. 4, pp. 689–704, 2013.

[33] M. Boareto, D. Iber, and V. Taylor, "Differential interactions between notch and id factors control neurogenesis by modulating hes factor autoregulation," *Development*, vol. 144, no. 19, pp. 3465–3474, 2017.

[34] N. Guisoni, R. Martinez-Corral, J. Garcia-Ojalvo, and J. de Navascues, "Diversity of fate outcomes in cell pairs under lateral inhibition," *Development*, vol. 144, no. 7, pp. 1177–1186, 2017.

[35] J. C. Luna-Escalante, P. Formosa-Jordan, and M. Ibañes, "Redundancy and cooperation in notch intercellular signaling," *Development*, pp. dev–154807, 2017.

[36] S. C. Manrubia, A. S. Mikhailov, and D. H. Zanette, *Emergence of dynamical order: synchronization phenomena in complex systems*. World Scientific, 1st ed., 2004.

[37] Y.-J. Jiang, B. L. Aerne, L. Smithers, C. Haddon, D. Ish-Horowicz, and J. Lewis, "Notch signaling and the synchronization of the somite segmentation clock.," vol. 408, pp. 475–479, 2000.

[38] I. H. Riedel-Kruse, C. Müller, and A. C. Oates, "Synchrony dynamics during initiation, failure, and rescue of the segmentation clock," *Science*, vol. 317, no. 5846, pp. 1911–1915, 2007.

[39] K. Horikawa, K. Ishimatsu, E. Yoshimoto, S. Kondo, and H. Takeda, "Noise-resistant and synchronized oscillation of the segmentation clock.," vol. 441, pp. 719–723, 2006.

[40] E. M. Özbudak and J. Lewis, "Notch signalling synchronizes the zebrafish segmentation clock but is not needed to create somite boundaries.," vol. 4(2), p. e15, 2008.

[41] C. Soza-Ried, E. Öztürk, D. Ish-Horowicz, and J. Lewis, "Pulses of notch activation synchronise oscillating somite cells and entrain the zebrafish segmentation clock," *Development*, vol. 141, no. 8, pp. 1780–1788, 2014.

[42] A. Mara, J. Schroeder, C. Chalouni, and S. A. Holley, "Priming, initiation and synchronization of the segmentation clock by deltaD and deltaC.," *Nat. Cell Biol.*, vol. 9, pp. 523–30, may 2007.

[43] M. C. Delfini, J. Dubrulle, P. Malapert, J. Chal, and O. Pourquié, "Control of the segmentation process by graded mapk/erk activation in the chick embryo," *Proc. Natl. Acad. Sci. USA*, vol. 102, pp. 11343–11348, 2005.

[44] B. Bénazéraf, P. Francois, R. E. Baker, N. Denans, C. D. Little, and O. Pourquié, "A random cell motility gradient downstream of fgf controls elongation of an amniote embryo," *Nature*, vol. 466, no. 7303, pp. 248–252, 2010.

[45] A. Lawton, A. Nandi, and M. Stulberg, "Regulated tissue fluidity steers zebrafish body elongation," *Development*, vol. 140, pp. 573–582, 2013.

[46] K. Uriu, R. Bhavna, A. C. Oates, and L. G. Morelli, "A framework for quantification and physical modeling of cell mixing applied to oscillator synchronization in vertebrate somitogenesis," *Biology open*, pp. bio–025148, 2017.

[47] K. Uriu, Y. Morishita, and Y. Iwasa, "Random cell movement promotes synchronization of the segmentation clock," *Proc. Natl. Acad. Sci. USA*, vol. 107, pp. 4979–4984, 2010.

[48] K. Uriu, S. Ares, A. C. Oates, and L. G. Morelli, "Optimal cellular mobility for synchronization arising from the gradual recovery of intercellular interactions," *Phys. Biol.*, vol. 9, p. 036006, 2012.

[49] S. F. Heuss, D. Ndiaye-Lobry, E. M. Six, A. Israël, and F. Logeat, "The intracellular region of notch ligands dll1 and dll3 regulates their trafficking and signaling activity," *Proceedings of the National Academy of Sciences*, vol. 105, no. 32, pp. 11212–11217, 2008.

[50] L. G. Morelli, S. Ares, L. Herrgen, C. Schröter, F. Jülicher, and A. C. Oates, "Delayed coupling theory of vertebrate segmentation," *HFSP*, vol. 3, pp. 55–66, 2009.

[51] L. Herrgen, S. Ares, L. G. Morelli, C. Schröter, F. Jülicher, and A. C. Oates, "Intercellular coupling regulates the period of the segmentation clock," vol. 20, pp. 1244–1253, 2010.

[52] S. Ares, L. G. Morelli, D. J. Jörg, A. C. Oates, and F. Jülicher, "Collective modes of coupled phase oscillators with delayed coupling," *Phys. Rev. Lett.*, vol. 108, p. 204101, 2012.

[53] B.-K. Liao, D. J. Jörg, and A. C. Oates, "Faster embryonic segmentation through elevated delta-notch signalling," *Nature communications*, vol. 7, 2016.

[54] W. Kim, T. Matsui, M. Yamao, M. Ishibashi, K. Tamada, T. Takumi, K. Kohno, S. Oba, S. Ishii, Y. Sakumura, *et al.*, "The period of the somite segmentation clock is sensitive to notch activity," *Molecular biology of the cell*, vol. 22, no. 18, pp. 3541–3549, 2011.

[55] Y. Kuramoto, *Chemical Oscillations, Waves, and Turbulence.* Berlin: Springer-Verlag, 1984.

[56] A. S. Pikovsky, M. G. Rosenblum, and J. Kurths, *Synchronization: a Universal Concept in Nonlinear Sciences.* Cambridge: Cambridge University Press, 2001.

[57] J. A. Acebrón, L. L. Bonilla, C. J. P. Vicente, F. Ritort, and R. Spigler, "The kuramoto model: A simple paradigm for synchronization phenomena," *Reviews of modern physics*, vol. 77, no. 1, p. 137, 2005.

[58] F. A. Rodrigues, T. K. D. Peron, P. Ji, and J. Kurths, "The kuramoto model in complex networks," *Phys. Rep.*, vol. 610, pp. 1–98, 2016.

[59] Y. Kuramoto, *Self-entrainment of a population of coupled non-linear oscillators*. 1975.

[60] K. Uriu, S. Ares, A. C. Oates, and L. G. Morelli, "Dynamics of mobile coupled phase oscillators," *Phys. Rev. E*, vol. 87, no. 3, p. 032911, 2013.

[61] F. Peruani, E. M. Nicola, and L. G. Morelli, "Mobility induces global synchronization of oscillators in periodic extended systems," *New J. Phys.*, vol. 12, p. 093029, 2010.

[62] N. Fujiwara, J. Kurths, and A. Díaz-Guilera, "Synchronization in networks of mobile oscillators," *Phys. Rev. E*, vol. 83, no. 2, p. 025101, 2011.

[63] K. Uriu and L. G. Morelli, "Collective cell movement promotes synchronization of coupled genetic oscillators.," *Biophys. J.*, vol. 107, pp. 514–26, jul 2014.

[64] S. Yeung and S. H. Strogatz, "Time Delay in the Kuramoto Model of Coupled Oscillators," *Phys. Rev. Lett.*, vol. 82, pp. 648–651, jan 1999.

[65] S. Yeung, *Time Delay in the Kuramoto Model of Coupled Oscillators*. PhD thesis, Cornell University, 1999.

[66] H. G. Schuster and P. Wagner, "Mutual entrainment of two limit cycle oscillators with time delayed coupling," *Progress of Theoretical Physics*, vol. 81, no. 5, pp. 939–945, 1989.

[67] E. Niebur, H. G. Schuster, and D. M. Kammen, "Collective frequencies and metastability in networks of limit-cycle oscillators with time delay.," *Phys. Rev. Lett.*, vol. 67, pp. 2753–2756, 1991.

[68] D. J. Jörg, L. G. Morelli, S. Ares, and F. Jülicher, "Synchronization Dynamics in the Presence of Coupling Delays and Phase Shifts," *Phys. Rev. Lett.*, vol. 112, p. 174101, apr 2014.

[69] M. G. Earl and S. H. Strogatz, "Synchronization in oscillator networks with delayed coupling: A stability criterion," *Phys. Rev. E*, vol. 67, no. 3, p. 036204, 2003.

[70] Y. Nakamura, F. Tominaga, and T. Munakata, "Clustering behavior of time-delayed nearest-neighbor coupled oscillators," *Phys. Rev. E*, vol. 49, no. 6, p. 4849, 1994.

[71] L. Wetzel, *Effect of distributed delays in systems of coupled phase oscillators*. PhD thesis, TU Dresden, 2012.

[72] M. Kaern, M. Menzinger, and A. Hunding, "Segmentation and somitogenesis derived from phase dynamics in growing oscillatory media," *Journal of theoretical biology*, vol. 207, no. 4, pp. 473–493, 2000.

[73] J. Jaeger and B. C. Goodwin, "A cellular oscillator model for periodic pattern formation," *Journal of theoretical biology*, vol. 213, no. 2, pp. 171–181, 2001.

[74] H. L. Smith, *An introduction to delay differential equations with applications to the life sciences*, vol. 57. Springer New York, 2011.

[75] N. MacDonald, *Time lags in biological models*. Berlin: Springer-Verlag, 1978.

[76] N. MacDonald, *Biological delay systems*. Cambridge University Press, 1989.

[77] A. Bellen and M. Zennaro, *Numerical methods for delay differential equations*. Oxford university press, 2013.

[78] R. D. Driver, *Ordinary and delay differential equations*, vol. 20. Springer Science & Business Media, 2012.

[79] P. Amster, "Ecuaciones diferenciales con retardo," 2017.

[80] F. M. Atay, *Complex time-delay systems: theory and applications*. Springer, 2010.

[81] D. A. Wiley, S. H. Strogatz, and M. Girvan, "The size of the sync basin," *Chaos*, vol. 16, no. 1, p. 015103, 2006.

[82] D. T. Gillespie, "A general method for numerically simulating the stochastic time evolution of coupled chemical reactions," *J. Comput. Phys.*, vol. 22, pp. 403–434, dec 1976.

[83] A. Hubaud, I. Regev, L. Mahadevan, and O. Pourquie, "Excitable dynamics and yap-dependent mechanical cues drive the segmentation clock," *Cell*, vol. 171, no. 3, pp. 668–682, 2017.

[84] Y. Kuramoto and D. Battogtokh, "Coexistence of coherence and incoherence in nonlocally coupled phase oscillators," *Nonlinear Phenom. Complex Syst.*, vol. 5, no. 4, pp. 380–385, 2002.

[85] D. M. Abrams and S. H. Strogatz, "Chimera states for coupled oscillators," *Phys. Rev. Lett.*, vol. 93, no. 17, p. 174102, 2004.

[86] G. Petrungaro, K. Uriu, and L. G. Morelli, "Mobility-induced persistent chimera states," *Phys. Rev. E*, vol. 96, no. 6, p. 062210, 2017.

[87] M. Shanahan, "Metastable chimera states in community-structured oscillator networks," *Chaos*, vol. 20, no. 1, p. 013108, 2010.

[88] M. Wolfrum, O. E. Omel'chenko, S. Yanchuk, and Y. L. Maistrenko, "Spectral properties of chimera states," *Chaos*, vol. 21, no. 1, p. 013112, 2011.

[89] P. Ashwin and O. Burylko, "Weak chimeras in minimal networks of coupled phase oscillators," *Chaos*, vol. 25, no. 1, p. 013106, 2015.

[90] F. P. Kemeth, S. W. Haugland, L. Schmidt, I. G. Kevrekidis, and K. Krischer, "A classification scheme for chimera states," *Chaos*, vol. 26, p. 094815, sep 2016.

[91] R. Gopal, V. K. Chandrasekar, A. Venkatesan, and M. Lakshmanan, "Observation and characterization of chimera states in coupled dynamical systems with nonlocal coupling," *Phys. Rev. E*, vol. 89, no. 5, pp. 1–8, 2014.

[92] R. Gopal, V. K. Chandrasekar, D. V. Senthilkumar, A. Venkatesan, and M. Lakshmanan, "Effect of asymmetry parameter on the dynamical states of nonlocally coupled nonlinear oscillators," *Phys. Rev. E*, vol. 91, no. 6, p. 062916, 2015.

[93] J. D. Hart, K. Bansal, T. E. Murphy, and R. Roy, "Experimental observation of chimera and cluster states in a minimal globally coupled network," *Chaos*, vol. 26, no. 9, p. 094801, 2016.

[94] M. J. Panaggio and D. M. Abrams, "Chimera states: coexistence of coherence and incoherence in networks of coupled oscillators," *Nonlinearity*, vol. 28, no. 3, pp. R67–R87, 2015.

[95] E. A. Martens, S. Thutupalli, A. Fourrière, and O. Hallatschek, "Chimera states in mechanical oscillator networks," *Proc. Natl. Acad. Sci.*, vol. 110, no. 26, pp. 10563–10567, 2013.

[96] D. M. Abrams, R. Mirollo, S. H. Strogatz, and D. A. Wiley, "Solvable model for chimera states of coupled oscillators," *Phys. Rev. Lett.*, vol. 101, no. 8, p. 084103, 2008.

[97] G. C. Sethia, A. Sen, and F. M. Atay, "Clustered chimera states in delay-coupled oscillator systems," *Phys. Rev. Lett.*, vol. 100, no. 14, pp. 1–4, 2008.

[98] E. Omel'chenko, Y. L. Maistrenko, and P. A. Tass, "Chimera states: The natural link between coherence and incoherence," *Phys. Rev. Lett.*, vol. 100, no. 4, p. 044105, 2008.

[99] J. H. Sheeba, V. Chandrasekar, and M. Lakshmanan, "Globally clustered chimera states in delay-coupled populations," *Physical Review E*, vol. 79, no. 5, p. 055203, 2009.

[100] J. H. Sheeba, V. Chandrasekar, and M. Lakshmanan, "Chimera and globally clustered chimera: Impact of time delay," *Phys. Rev. E*, vol. 81, no. 4, p. 046203, 2010.

[101] E. A. Martens, "Chimeras in a network of three oscillator populations with varying network topology," *Chaos*, vol. 20, no. 4, p. 043122, 2010.

[102] Y. Zhu, Y. Li, M. Zhang, and J. Yang, "The oscillating two-cluster chimera state in non-locally coupled phase oscillators," *EPL (Europhysics Letters)*, vol. 97, no. 1, p. 10009, 2012.

[103] N. Yao, Z.-G. Huang, C. Grebogi, and Y.-C. Lai, "Emergence of multicluster chimera states," *Sci. Rep.*, vol. 5, 2015.

[104] E. Omel'chenko, M. Wolfrum, and Y. L. Maistrenko, "Chimera states as chaotic spatiotemporal patterns," *Physical Review E*, vol. 81, no. 6, p. 065201, 2010.

[105] Y. Kuramoto and S.-i. Shima, "Rotating spirals without phase singularity in reaction-diffusion systems," *Progress of Theoretical Physics Supplement*, vol. 150, pp. 115–125, 2003.

[106] S.-i. Shima and Y. Kuramoto, "Rotating spiral waves with phase-randomized core in nonlocally coupled oscillators," *Phys. Rev. E*, vol. 69, no. 3, p. 036213, 2004.

[107] E. A. Martens, C. R. Laing, and S. H. Strogatz, "Solvable model of spiral wave chimeras," *Phys. Rev. Lett.*, vol. 104, no. 4, p. 044101, 2010.

[108] O. E. Omel'chenko, M. Wolfrum, S. Yanchuk, Y. L. Maistrenko, and O. Sudakov, "Stationary patterns of coherence and incoherence in two-dimensional arrays of non-locally-coupled phase oscillators," *Physical Review E*, vol. 85, no. 3, p. 036210, 2012.

[109] M. J. Panaggio and D. M. Abrams, "Chimera states on a flat torus," *Physical review letters*, vol. 110, no. 9, p. 094102, 2013.

[110] M. J. Panaggio and D. M. Abrams, "Chimera states on the surface of a sphere," *Physical Review E*, vol. 91, no. 2, p. 022909, 2015.

[111] A. G. Smart, "Exotic chimera dynamics glimpsed in experiments," *Physics Today*, vol. 65, no. 10, p. 17, 2012.

[112] A. M. Hagerstrom, T. E. Murphy, R. Roy, P. Hövel, I. Omelchenko, and E. Schöll, "Experimental observation of chimeras in coupled-map lattices," *Nat. Phys.*, vol. 8, no. 9, pp. 658–661, 2012.

[113] M. R. Tinsley, S. Nkomo, and K. Showalter, "Chimera and phase-cluster states in populations of coupled chemical oscillators," *Nat. Phys.*, vol. 8, no. 9, pp. 662–665, 2012.

[114] S. Nkomo, M. R. Tinsley, and K. Showalter, "Chimera states in populations of nonlocally coupled chemical oscillators," *Phys. Rev. Lett.*, vol. 110, no. 24, p. 244102, 2013.

[115] S. Nkomo, M. R. Tinsley, and K. Showalter, "Chimera and chimera-like states in populations of nonlocally coupled homogeneous and heterogeneous chemical oscillators," *Chaos*, vol. 26, no. 9, p. 094826, 2016.

[116] J. F. Totz, J. Rode, M. R. Tinsley, K. Showalter, and H. Engel, "Spiral wave chimera states in large populations of coupled chemical oscillators," *Nat. Phys.*, p. 1, 2017.

[117] A. Yeldesbay, A. Pikovsky, and M. Rosenblum, "Chimeralike states in an ensemble of globally coupled oscillators," *Phys. Rev. Lett.*, vol. 112, p. 144103, Apr 2014.

[118] G. C. Sethia and A. Sen, "Chimera states: The existence criteria revisited," *Phys. Rev. Lett.*, vol. 112, p. 144101, Apr 2014.

[119] L. Schmidt, K. Schönleber, K. Krischer, and V. García-Morales, "Coexistence of synchrony and incoherence in oscillatory media under nonlinear global coupling," *Chaos*, vol. 24, no. 1, p. 013102, 2014.

[120] A. Yeldesbay, A. Pikovsky, and M. Rosenblum, "Chimeralike states in an ensemble of globally coupled oscillators," *Physical review letters*, vol. 112, no. 14, p. 144103, 2014.

[121] F. Böhm, A. Zakharova, E. Schöll, and K. Lüdge, "Amplitude-phase coupling drives chimera states in globally coupled laser networks," *Physical Review E*, vol. 91, no. 4, p. 040901, 2015.

[122] L. Schmidt and K. Krischer, "Clustering as a prerequisite for chimera states in globally coupled systems," *Phys. Rev. Lett.*, vol. 114, p. 034101, Jan 2015.

[123] C. R. Laing, "Chimeras in networks with purely local coupling," *Phys. Rev. E*, vol. 92, p. 050904, nov 2015.

[124] B. K. Bera and D. Ghosh, "Chimera states in purely local delay-coupled oscillators," *Phys. Rev. E*, vol. 93, no. 5, p. 052223, 2016.

[125] M. G. Clerc, S. Coulibaly, M. A. Ferré, M. A. García-Ñustes, and R. G. Rojas, "Chimera-type states induced by local coupling," *Phys. Rev. E*, vol. 93, no. 5, pp. 1–5, 2016.

[126] B.-W. Li and H. Dierckx, "Spiral wave chimeras in locally coupled oscillator systems," *Phys. Rev. E*, vol. 93, no. 2, p. 020202, 2016.

[127] A. Pikovsky and M. Rosenblum, "Dynamics of globally coupled oscillators: Progress and perspectives," *Chaos*, vol. 25, no. 9, p. 097616, 2015.

[128] A. Röhm, F. Böhm, and K. Lüdge, "Small chimera states without multistability in a globally delay-coupled network of four lasers," *Physical Review E*, vol. 94, no. 4, p. 042204, 2016.

[129] K. Schönleber, C. Zensen, A. Heinrich, and K. Krischer, "Pattern formation during the oscillatory photoelectrodissolution of n-type silicon: turbulence, clusters and chimeras," *New J. Phys.*, vol. 16, no. 6, p. 063024, 2014.

[130] J. Wojewoda, K. Czolczynski, Y. Maistrenko, and T. Kapitaniak, "The smallest chimera state for coupled pendula," *Scientific Reports*, vol. 6, 2016.

[131] N. C. Rattenborg, C. J. Amlaner, and S. L. Lima, "Behavioral, neurophysiological and evolutionary perspectives on unihemispheric sleep," *Neurosci. Biobehav. Rev.*, vol. 24, no. 8, pp. 817–842, 2000.

[132] E. Tognoli and J. S. Kelso, "The metastable brain," *Neuron*, vol. 81, no. 1, pp. 35–48, 2014.

[133] T. Reichenbach, M. Mobilia, and E. Frey, "Mobility promotes and jeopardizes biodiversity in rock–paper–scissors games," *Nature*, vol. 448, no. 7157, p. 1046, 2007.

[134] O. E. Omel'chenko, "Coherence–incoherence patterns in a ring of non-locally coupled phase oscillators," *Nonlinearity*, vol. 26, no. 9, p. 2469, 2013.

[135] E. A. Martens, M. J. Panaggio, and D. M. Abrams, "Basins of attraction for chimera states," *New J. Phys.*, vol. 18, no. 2, p. 022002, 2016.

[136] D. Levis, I. Pagonabarraga, and A. Díaz-Guilera, "Synchronization in dynamical networks of locally coupled self-propelled oscillators," *Phys. Rev. X*, vol. 7, p. 011028, 2017.

[137] F. Perez-Diaz, R. Zillmer, and R. Groß, "Control of synchronization regimes in networks of mobile interacting agents," *Phys. Rev. Appl.*, vol. 7, p. 054002, 2017.

[138] K. Uriu, "Genetic oscillators in development," *Dev. Growth Differ.*, vol. 58, no. 1, pp. 16–30, 2016.

[139] S. H. Strogatz and R. E. Mirollo, "Stability of incoherence in a population of coupled oscillators," *Journal of Statistical Physics*, vol. 63, no. 3-4, pp. 613–635, 1991.

[140] L. S. Tsimring, "Noise in biology," *Reports on Progress in Physics*, vol. 77, no. 2, p. 026601, 2014.

[141] M. B. Elowitz, A. J. Levine, E. D. Siggia, and P. S. Swain, "Stochastic gene expression in a single cell," *Science*, vol. 297, no. 5584, pp. 1183–1186, 2002.

[142] A. Isomura, F. Ogushi, H. Kori, and R. Kageyama, "Optogenetic perturbation and bioluminescence imaging to analyze cell-to-cell transfer of oscillatory information," *Genes & development*, vol. 31, no. 5, pp. 524–535, 2017.

[143] G. Petrungaro, K. Uriu, and L. G. Morelli, "Synchronization dynamics of mobile oscillators in the presence of coupling delays," *in preparation*.